Harmonic Mixer Analysis and Design

Marius van der Merwe

Thesis presented in partial fulfilment of the requirements for the degree of Master of Science (Engineering) at the University of Stellenbosch.

Promoter : Prof. JB De Swardt

March 2002

Declaration

I, the undersigned, hereby declare that the work contained in this thesis is my own original work and that I have not previously in its entirety or in part submitted it at any university for a degree.

Marius van der Merwe : Date :

Summary

Harmonic mixers are capable of extended frequency operation by mixing with a harmonic of the LO (local oscillator) signal, eliminating the need for a high frequency, high power LO. Their output spectra also have certain characteristics that make them ideal for a variety of applications. The operation of the harmonic mixer is investigated, and the mixer is analyzed using an extension of the classic mixer theory. The synthesis of harmonic mixers is also investigated, and a design procedure is proposed for the design and realization of a variety of harmonic mixers. This design procedure is evaluated with the design and realization of two harmonic mixers, one in X-band and the other in S-band. Measurements suggest that the procedure is successful for the specific applications.

Opsomming

Harmoniese mengers kan by hoër frekwensies gebruik word as gewone mengers deurdat hulle gebruik maak van 'n harmoniek van die LO. 'n Hoë-frekwensie, hoë-drywing LO word dus nie benodig nie. Die mengers se uittreespektra het ook 'n aantal karakteristieke wat hulle goeie kandidate maak vir 'n verskeidenheid van toepassings. Die werking van die harmoniese menger word ondersoek deur uit te brei op die klassieke menger-teorie. Die ontwerp van die harmoniese menger word vervolgens ondersoek, waarna 'n ontwerpsprosedure voorgestel word vir die ontwerp van 'n verskeidenheid van harmoniese mengers. Hierdie prosedure word getoets met die ontwerp en realisering van twee harmoniese mengers, een in X-band en die ander in S-band. Vanuit die metings is dit duidelik dat die ontwerpsprosedure geslaagd is vir die spesifieke geval.

Acknowledgements / Erkenning

Verskeie mense het deur die verloop van hierdie tesis verskillende bydraes gelewer. Dit is vir my 'n voorreg om vir hulle kortliks hier dankie te sê :

My studieleier, Johann de Swardt, vir sy planne, bemoediging, leiding en vertroue in my, selfs as bladsy 6 en 7 wegraak – dis vir my 'n konstante bron van inspirasie.

Wessel Croukamp en Ashley Cupido van SED, vir die vervaardiging van die mengers, meer as een keer onder druk…

My vriende, vir die konstante bemoediging, kuiers, hulp en laataand sms'e.

My ouers en broer, vir hul opregte belangstelling en aanmoediging.

My verloofde, Martinette Müller, nie net vir die laat nagte se geduld en hulp nie, maar omdat jy in my glo.

Contents

List of Figures and Tables **1**

Introduction **5**

1) Microwave Diode Mixers **8**

1.1 Fundamental Mixer Theory 8

1.1.1 Generalized Frequency Mixing 8

1.1.2 The Diode as Nonlinear Element 9

1.2 Diode Mixer Topologies 11

1.2.1 Single Diode Mixers 11

1.2.2 Balanced Mixers 13

1.2.2.1 Single Balanced Mixer 14

1.2.2.2 Double Balanced Mixer 15

1.2.2.3 Higher-Level Balanced Mixers 18

1.2.2.4 Subharmonic Mixers 18

1.3 Mixer Characteristics 20

1.3.1 Conversion Loss 21

1.3.2 Noise 22

1.3.2.1 Inherent Noise 22

1.3.2.2 Signal Noise 23

1.3.3 Conversion Compression 24

1.3.4 Intermodulation Distortion 25

1.3.5 Reflection (VSWR) 26

2) Diode Harmonic Mixers **30**

2.1 The Schottky-Barrier Diode 30

2.1.1 Junction Characteristics 31

2.1.2 Intrinsic Model 33

2.1.2.1 Large-Signal Model 34

2.1.2.2 Small-Signal Model 34

2.1.3 The Complete Diode Model 36

2.2 The Antiparallel Diode Pair 37
2.2.1 Single Diode Fundamentals 38
2.2.2 The Antiparallel Configuration 38
2.2.3 Two-Tone Analysis 41
2.2.4 IF Frequency Spectrum 43
2.3 Analysis 44
2.3.1 Large-Signal Analysis 45
2.3.2 Harmonic Balance for Single Diode 46
2.3.3 Harmonic Balance for Antiparallel Diode Pair 50
2.3.3.1 Multiport Network 51
2.3.3.2 Equivalent Diode 53
2.4 Small-Signal Diode Parameters 55
2.4.1 Conversion Matrix for Junction Conductance 55
2.4.2 Conversion Matrix for Junction Capacitance 56
2.4.3 Mixer Conversion Matrix 57
2.4.4 Input Impedance 60
2.4.5 Conversion Loss 61
2.5 Noise 63
2.5.1 Thermal Noise 64
2.5.2 Shot Noise 64
2.5.3 Noise Correlation 65
2.5.3.1 Shot Noise 66
2.5.3.2 Thermal Noise 66
2.5.4 Signal Noise 67
2.6 Diode Unbalance 68
2.6.1 Theory 68
2.6.2 Analysis 69
2.7 The Antiparallel Diode Pair – A Quantitative Analysis 70
2.7.1 LO Excitation 70
2.7.2 Large-Signal Input Impedance 71
2.7.3 Model 74

3) Design Considerations 76
3.1 "The Design Requirement" 77
3.1.1 Frequency Allocation 77
3.1.2 Optimum Conversion Loss 78
3.1.3 Port Isolation 78
3.2 Choice of Diode 79
3.3 Design Topologies 81
3.3.1 Series Topologies 81
3.3.1.1 Isolated Series Topology 82
3.3.1.2 Non-Isolated Series Topology 82
3.3.2 Shunt Topology 82
3.3.3 Additional topologies 83
3.4 Design Overview 83
3.4.1 Specifications 84
3.4.2 Choice of Frequencies 84
3.4.3 Topology 84
3.4.4 Choice of Diodes 84
3.4.5 Basic Design 84
3.4.6 Extended Design 85
3.4.7 Simulation 85

4) Implementation and Measurements 86
4.1 S-Band Mixer 86
4.1.1 Specifications 86
4.1.2 Choice of Frequencies 86
4.1.3 Topology 87
4.1.4 Choice of Diodes 88
4.1.5 Basic Design 88
4.1.6 Extended Design 90
4.1.6.1 IF Low-Pass Filter 91
4.1.6.2 RF Band-Pass Filter 92
4.1.6.3 IF Matching Network 93
4.1.6.4 RF Matching Network 94
4.1.6.5 LO Isolation 95
4.1.7 Microstrip Simulation 96

4.1.8 Realization 99
4.1.9 Measurements 100
4.1.10 Comments 102
4.2 X-Band Mixer 102
4.2.1 Specifications 102
4.2.2 Choice of Frequencies 103
4.2.3 Topology 103
4.2.4 Choice of Diodes 104
4.2.5 Basic Design 104
4.2.6 Extended Design 106
4.2.6.1 IF Low-Pass Filter 106
4.2.6.2 RF Band-Pass Filter 107
4.2.6.3 IF Matching Network 108
4.2.6.4 RF Matching Network 108
4.2.6.5 LO Isolation 109
4.2.7 Microstrip Simulation 111
4.2.8 Realization 113
4.2.9 Measurements 114
4.2.10 Comments 115

Conclusion 116

Appendix A 119

Appendix B 122

Appendix C 126

References 130

List of Figures and Tables

Figure 1.1 Topology for Single Diode Mixer 11
Figure 1.2 Frequency Spectrum of Single Diode Mixer 12
Figure 1.3 Single Balanced Mixer using a 180°-Hybrid 14
Figure 1.4 Frequency Spectrum at the IF port of typical Single Balanced Mixer 15
Figure 1.5 Double Balanced Mixer using three baluns 16
Figure 1.6 Typical IF Frequency Spectrum of Double Balanced Mixer 17
Figure 1.7 Basic topology for Antiparallel Diode Pair Subharmonic Mixer 20
Figure 1.8 Typical Characteristic for Conversion Compression 25
Figure 1.9 Typical downconversion spurious response chart 26
Figure 1.10 Output Spectrum for fRF = 8 GHz and fRF = 8.25 GHz 27
Figure 1.11 Typical Diode Input Impedance for different LO power levels 29

Figure 2.1 The Schottky diode junction 31
Figure 2.2 Intrinsic Schottky-Barrier Diode Model 34
Figure 2.3 Small- and Large-signal calculation of g(V) 35
Figure 2.4 Complete Schottky-Barrier Diode Model 36
Figure 2.5 Conductance Waveform g(t) for a single diode 38
Figure 2.6 Antiparallel diode configuration 38
Figure 2.7 Junction Conductance g for Antiparallel Diode Pair 40
Figure 2.8 Output Spectrum of Antiparallel Diode Pair 43
Figure 2.9 LO Noise Rejection in Antiparallel Diode Pair 44
Figure 2.10 Diagram of Generalized Mixer Analysis 45
Figure 2.11 Equivalent Circuit of Mixer with Single Diode 47
Figure 2.12 Division of diode circuit in Linear and Nonlinear parts 48
Figure 2.13 Large-Signal circuit of a mixer with an antiparallel diode pair 51
Figure 2.14 Equivalent circuit of Antiparallel diode pair driven by LO 54
Figure 2.15 Equivalent Mixer Circuits at harmonics of the LO 54
Figure 2.16 Small-Signal equivalent model for mixer with antiparallel diode pair 58
Figure 2.17 Alternative Small-signal representation of Diode Mixer 63
Figure 2.18 Adaptation of the Schottky Diode model to include the effects of shot noise and thermal noise 65

Figure 2.19 Antiparallel diode pair LO time-Waveform....70
Figure 2.20 Spectrum of Antiparallel Diode Pair LO Waveform....70
Figure 2.21 Antiparallel Diode Pair Capacitance modulated by LO....71
Figure 2.22 Antiparallel Diode Pair Conductance modulated by LO....71
Figure 2.23 Input Impedance of Antiparallel Diode Pair as function of LO Power....72
Figure 2.24 Input Impedance of Single Diode as function of LO power....72
Figure 2.25 Junction Capacitance as a function of Junction Voltage Vj for single diode and the Antiparallel diode pair....72
Figure 2.26 Input Impedance of the Antiparallel Diode Pair for swept LO Power at 5 GHz....73
Figure 2.27 Real part of the Antiparallel Diode Pair Junction Impedance....73
Figure 2.28 Imaginary part of the Antiparallel Diode Pair Junction Impedance....73
Figure 2.29 Simulated Reflection Coefficient for the HSMS-8202 diode pair....74
Figure 2.30 Final Model for HSMS-8202 Antiparallel Diode Pair....75

Figure 3.1 IF Output Power for variation in Junction Capacitance....80
Figure 3.2 IF Output Power for variation in Series Resistance....80
Figure 3.3 IF Output Power for variation in Diode Non-Ideality....80
Figure 3.4 IF Output Power for variation in Series Inductance....80
Figure 3.5 Isolated Series Topology....81
Figure 3.6 Non-Isolated Series Topology....81
Figure 3.7 Shunt Topology....83

Figure 4.1 Intended topology for S-band 2nd harmonic mixer....87
Figure 4.2 MWO layout of the Basic Design....89
Figure 4.3 Impedance on the Small-Signal port....89
Figure 4.4 Output Spectrum of the Small-Signal Port....90
Figure 4.5 Intended Topology showing Matching Circuits and Filters....91
Figure 4.6 Low-Pass Filter Frequency Response....92
Figure 4.7 Band-Pass Filter Frequency Response for realized microstrip filter....92
Figure 4.8 RF port Input Impedance....93
Figure 4.9 IF port Input Impedance....93
Figure 4.10 RF port Input Impedance (after the addition of the IF matching network)....94
Figure 4.11 IF port Input Impedance (after the addition of the IF matching network)....94
Figure 4.12 Final RF port Input Impedance (after the addition of the IF and RF matching networks)....95

Figure 4.13 Final IF port Input Impedance (after the addition of the IF and RF matching networks) 95
Figure 4.14 Frequency Spectrum at LO port (before isolation) 96
Figure 4.15 Frequency Response of implemented LO LPF 96
Figure 4.16 Simulated IF power as a function of LO power for the S-band Harmonic Mixer 97
Figure 4.17 Simulated Output Spectrum at the IF Port 98
Figure 4.18 Simulated plot of RF frequency vs IF power 98
Figure 4.19 Final S-band mixer layout 99
Figure 4.20 The Manufactured S-band Harmonic Mixer 100
Figure 4.21 Measured LO power vs IF power for S-band harmonic mixer 101
Figure 4.22 Measured RF-sweep for S-band harmonic mixer showing IF amplitude against IF frequency 101
Figure 4.23 Measured LO power vs IF power for X-band harmonic mixer 103
Figure 4.24 Input Impedance on the Small-Signal port 105
Figure 4.25 Small-Signal Port Output Spectrum 105
Figure 4.26 Low-Pass Filter Frequency Response 107
Figure 4.27 Band-Pass Filter Frequency Response for realized microstrip filter 107
Figure 4.28 IF port Input Impedance (after the addition of the IF matching network) 108
Figure 4.29 RF port Input Impedance (after the addition of the IF matching network) 108
Figure 4.30 Final RF port Input Impedance (after the addition of the IF and RF matching networks) 109
Figure 4.31 Final IF port Input Impedance (after the addition of the IF and RF matching networks) 109
Figure 4.32 Frequency Spectrum at LO port (before isolation) 110
Figure 4.33 Frequency Response of implemented LO BPF 110
Figure 4.34 Simulated LO power against IF Power of the X-band Harmonic Mixer 111
Figure 4.35 Simulated Output Spectrum at the IF Port 112
Figure 4.36 Simulated plot of RF frequency against IF power for the X-band mixer 112
Figure 4.37 Layout of finalized X-band mixer 113
Figure 4.38 The Manufactured X-band Mixer 113
Figure 4.39 Measured LO power vs IF power for X-band harmonic mixer 114
Figure 4.40 Measured RF-sweep of X-band harmonic mixer 115

Figure A.1 Large-Signal Circuit used for the Reflection Algorithm....119
Figure A.2 The division of the mixer circuit into equivalent circuits for use with the Reflection Algorithm....120
Figure B.1 S-Band Harmonic Mixer Layout....122
Figure B.2 Lumped Topology for the IF low-pass filter....123
Figure B.3 Response for the IF low-pass filter....123
Figure B.4 Microstrip Topology for LO low-pass filter....124
Figure B.5 Response for the LO low-pass filter....124
Figure B.6 Microstrip Topology for RF band-pass filter....125
Figure B.7 Response for the RF low-pass filter....125
Figure C.1 X-Band Harmonic Mixer Layout....126
Figure C.2 Topology for the IF low-pass filter....127
Figure C.3 Response for the IF low-pass filter....127
Figure C.4 Microstrip Topology for LO band-pass filter....128
Figure C.5 Response for the LO low-pass filter....128
Figure C.6 Microstrip Topology for RF band-pass filter....129
Figure C.7 Response for the RF band-pass filter....129

Table 1.1 Summary of Characteristics for Single Diode Mixer....13
Table 1.2 Summary of Characteristics for Single Balanced Mixer....15
Table 1.3 Summary of Characteristics for Double Balanced Mixer....17
Table 2.1 Selected Diode parameters for HSMS-820x-series....37
Table 2.2 Comparison of Mixer Performance for Diode Unbalance caused by variation of Diode Parameters....69

Introduction

Frequency mixers are used to achieve frequency conversion of an input signal. A nonlinear device, most commonly a diode or transistor, is used for this purpose. The nonlinear device generates the necessary integer multiples, or *harmonics*, of the signals that are necessary for the process of frequency conversion. This process can be described by the following general equation

$$\omega_{m,n} = m\omega_s + n\omega_p$$

where ω_s is the input signal, ω_p is the signal driving the mixer, and $\omega_{m,n}$ is the output signal. Here m and n are integers denoting the harmonic of the input signal and driving signal respectively. For conventional mixers $|m| = 1$ and $|n| = 1$. Conventional mixers therefore use the fundamental frequencies of the input and driving signals to perform the frequency conversion, and are subsequently collectively called *fundamental mixers*. These mixers require a driving signal ω_p with a frequency of the same order as the frequency of the input signal ω_s to produce an output signal.

With the upper frequency barrier of communication systems continuously creeping upwards (with the occasional leap), it becomes increasingly difficult to realize stable, powerful and cost effective driving sources for the fundamental mixers. A mixer topology utilizing an easily realizable driving source of lower frequency, while still taking a higher frequency input signal would provide a solution to the problem.

The *harmonic mixer* is such a topology. Harmonic mixers, while still obeying the above equation, require $|m| = 1$ and $|n| > 1$. A harmonic of the lower frequency driving signal is therefore utilized in order to produce an output signal of the same frequency as a fundamental mixer. Apart from the ability to utilize a lower frequency driving signal, the harmonic mixer provides the additional advantage of rejecting certain frequency components associated with conventional mixers. The operation of diode multipliers is in some aspects very similar to that of harmonic mixers, and it is not surprising that the multipliers incorporate similar structures as the harmonic mixer.

Harmonic mixers were first introduced in 1975 [1]. Initially conversion losses of 5 to 8 dB worse than equivalent fundamental mixers were obtained [2]. However, harmonic mixers have evolved to provide very competitive conversion losses at lower frequencies, while they are an established technology at higher frequencies [41, 42, 43]. Using 2^{nd}-order mixers, 5 dB conversion loss at 100 GHz has been achieved [3], while 10dB loss at 230 GHz demonstrates the power of this technology [38].

Harmonic mixers can utilize the higher order even harmonics of the driving signal, with a corresponding increase in conversion loss. Examples include a 6^{th}-order mixer producing 24 dB loss at 26 GHz, a 10^{th}-order mixer producing 28 dB loss at 50 GHz, and a 18^{th}-order mixer producing 46 dB loss at 110 GHz [4]. The harmonic mixer therefore provides a convenient method of achieving acceptable conversion loss, without the need for a specialized source producing driving signal of adequate power at high frequencies.

The purpose of this thesis was to investigate the properties and implementation possibilities of the harmonic mixer. Its aim is to characterize the harmonic mixer adequately in terms of existing mixer properties. The operation and performance of the harmonic mixer were to be explored by means of design examples, and the minimization of conversion loss was chosen to be an important design criteria. Due to its extensive nature, noise analysis was restricted to the basics.

The thesis is divided into two main parts : the first part explores the analysis of the harmonic mixer with reference to conventional mixer theory. In many instances it is possible to extend existing mixer theory to accommodate the harmonic mixers. The second part explores the synthesis of the harmonic mixer, setting out to create a comprehensive design procedure which to date is not readily available in literature. The aim was to create a design procedure which considers the as many as possible of options offered by harmonic mixers, and then provide a step-by-step method for realizing a variety of harmonic mixers. Such a procedure was created and evaluated by designing two harmonic mixers. The procedure proved adequate and repeatable, producing a mixer at X-band with a conversion loss of 7.8 dB.

Chapter 1 provides a general overview of the basic structures employed for frequency conversion. The harmonic mixer is introduced, and an overview of its properties is given. The chapter concludes with an overview of the general properties used to describe mixer operation.

Chapter 2 is a detailed description of the diode harmonic mixer. The operation of the diode harmonic mixer is considered, and the antiparallel diode pair is introduced as a fundamental building block of the harmonic mixer. The analysis of the mixer is subsequently discussed, with emphasis on the large-signal and small-signal analysis. Conversion loss, noise and other mixer properties are then related to the harmonic mixer. The chapter concludes with a comprehensive discussion on the analysis, paving the way for mixer synthesis.

Chapter 3 contains a detailed discussion of the various design considerations of the harmonic mixer. The mixer properties of Chapter 2 are related to various design methods. The chapter concludes with a proposed design procedure for harmonic mixers.

Chapter 4 contains two implementations of the design procedure proposed in Chapter 3. Both S-band and X-band harmonic mixers are designed and realized, and their performance is discussed. This discussion is carried over to the Conclusion, where a few final ideas are presented.

The Appendix contains discussions and design procedures omitted from the text.

Chapter 1 : *Microwave Diode Mixers*

Out of all the different mixer classes, diode mixers are the most versatile tool to perform frequency conversion. Although they have been around since 1939, the simplicity and yet versatility have preserved their usefulness. In the mm-wave region and beyond, they are still utilized almost exclusively due to the limitations of active devices. In the RF and microwave region they constantly compete with newer technology, and are still often preferred to more complex circuits.

This chapter will investigate the usefulness of the diode mixer in the microwave region. It starts with a mathematical description of the process of frequency conversion, or mixing. Thereafter the diode is introduced as a nonlinear element capable of performing frequency conversion. Once the role of the diode as a tool for frequency conversion has been defined, its application in standard mixer circuits and topologies for the microwave region is investigated. The harmonic mixer is introduced, and the basics of operation are considered. The chapter is concluded with a discussion of the terminology and properties used to characterize mixers.

1.1) Fundamental Mixer Theory

Frequency conversion, or mixing, is achieved when a periodic signal of frequency ϖ_s is modulated by a periodic conductance waveform with frequency ϖ_p. The periodic signal is called the RF signal (*radio frequency*), while the periodic conductance is a result of an applied LO signal (*local oscillator*). The current resulting from the RF signal being modulated by the LO signal contains the generated frequency products, otherwise known as the *sum and difference products*.

1.1.1 Generalized Frequency Mixing

A frequency mixer is essentially a multiplier. Any nonlinear device can be used to perform the frequency mixing, as will be demonstrated. A voltage v (the independent variable) is applied across such an element with a nonlinear transfer function, with the current i_d (the dependent variable) flowing through the element as a result of the applied voltage.

This current-voltage, or I-V, characteristic of the nonlinear device can be described by a power series of the form

$$i_d = a_0 + a_1 v + a_2 v^2 + a_3 v^3 + \ldots \quad \ldots\ldots\ldots\ldots (1.1)$$

where a_0, a_1, a_2, ... are suitable coefficients [5]. Equation (1.1) summarizes the general relation for the currents and voltages associated with a nonlinear device.

1.1.2 The Diode as Nonlinear Element

The I-V relationship of the general diode provides the required mechanism for frequency conversion. The diode is not the only nonlinear element exhibiting this relationship – the I-V curves of various families of transistors also obey the relationship in equation (1.1), and they are consequently employed as frequency mixers.

In general there will be two voltages applied across the nonlinear diode :

1) The periodic RF signal v_s, which is generally of the form

$$v_s(t) = V_s \cos(\omega_s t)$$

2) The periodic LO signal v_p, which is generally of the form

$$v_p(t) = V_p \cos(\omega_p t)$$

The phase angles ω_s and ω_p of the RF and LO signal respectively are ignored for the purpose of this qualitative discussion. When these two signals are applied across a diode simultaneously, the nonlinear current i_d from equation (1.1) flowing in the diode as a result of the applied voltages is given by

$$i_d(t) = i_a(t) + i_b(t) + i_c(t) + \ldots \quad \ldots\ldots\ldots\ldots (1.2)$$

The general trigonometric identities were used to obtain

$$i_a(t) = \quad i_a(t) = aV_s\cos(\omega_s t) + aV_p\cos(\omega_p t) \qquad \text{.....(1.3)}$$

$$\begin{aligned} i_b(t) = \quad & \tfrac{1}{2}b\left[\, V_s^2 + V_p^2 + V_s^2\cos(2\omega_s t) + V_s^2\cos(2\omega_p t)\right. \\ & \left. + 2V_sV_p\left\{\cos\left((\omega_s+\omega_p)t\right) + \cos\left((\omega_s-\omega_p)t\right)\right\}\,\right] \end{aligned} \qquad \text{.....(1.4)}$$

$$\begin{aligned} i_c(t) = \quad & \tfrac{1}{2}c\left[\, V_s^3\cos(3\omega_s t) + V_p^3\cos(3\omega_p t)\right. \\ & + 3V_s^2V_p\left\{\cos\left((2\omega_s+\omega_p)t\right) + \cos\left((2\omega_s-\omega_p)t\right)\right\} \\ & + 3V_sV_p^2\left\{\cos\left((2\omega_p+\omega_s)t\right) + \cos\left((2\omega_p-\omega_s)t\right)\right\} \\ & + 3\left(V_s^3 + 2V_sV_p^2\right)\cos(\omega_s t) \\ & \left. + 3\left(V_p^3 + 2V_s^2V_p\right)\cos(\omega_p t)\,\right] \end{aligned} \qquad \text{.....(1.5)}$$

where *a, b, c,...* are general coefficients. What is important to note, is that frequencies *other* than those of the original signals are created. A closer inspection of equations (1.3) – (1.5) reveals that all the generated frequency products are a linear combination of the two excitation frequencies, or

$$\omega_{m,n} = m\omega_s + n\omega_p \qquad \text{.....(1.6)}$$

where *m,n* = ..., *-2, -1, 0, +1, +2,* ... The fundamental mixing product with m = 1 and n = -1 is in most cases the desired *intermediate frequency*, or IF, while the second order mixing product with m = -1 and n = 2 is termed the *image*. The *order* of the mixing product is given by $|m|$. Mixing products with orders greater than one are called *intermodulation products, IM products* or *spurs* [6, 37].

Although not formally, the output spectrum of the mixer provides an additional means of characterization for the different types of frequency mixers. Apart from aspects such as physical diode topology, conversion loss, frequency range of operation etc., a given type of mixer (e.g. a "double balanced mixer") always implies a certain frequency content of the output spectrum.

In mixer selection and design it is fundamental to have a knowledge of the output spectrum of a specific frequency mixer. Standard considerations include the amount of LO power "leaking through" to the IF, how much of the power available to the IF is lost to the image, and how the

output filters need to be designed in order to filter out the intermodulation products. In the following sections the classic topologies for diode frequency mixers will be considered with reference to their output spectra.

1.2) Diode Mixer Topologies

Diode frequency converters are primarily classified by the number of diodes they employ, and by the manner in which these diodes are arranged in the circuit. The mixers can further be classified by their frequency band of operation (e.g. X-band), the medium used for wave-propagation (e.g. stripline), or a special function the mixer performs (e.g. image enhancement). An overview of the most common topologies with a brief description of their operation is given.

1.2.1 Single Diode Mixers

Single diode mixers (or single-ended mixers) provide the simplest way of frequency conversion. A single diode mixer essentially comprises a diode *embedded* in two matching networks : one combined network for the LO and RF, and one network for the IF. Figure 1.1 shows the standard topology for a single diode mixer.

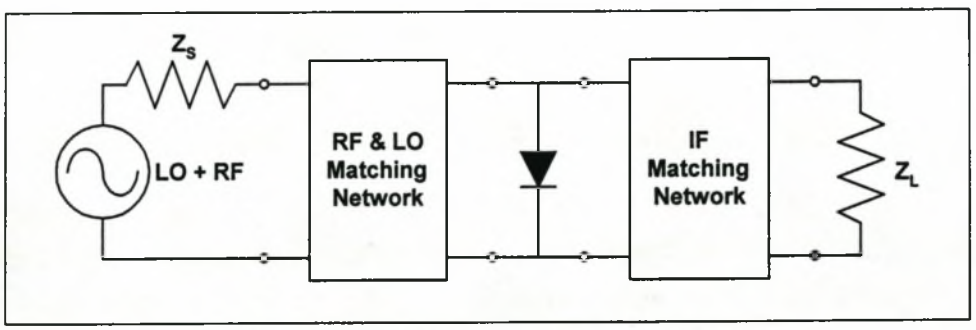

Figure 1.1 : Topology for Single Diode Mixer

Single diode mixers are rarely used at frequencies below the millimeter-wave region. Their simplicity and minimal components make them the only truly effective mixers at higher frequencies, but at lower frequencies they are outperformed by improved configurations. As it might have been expected, the analysis and synthesis of single diode mixers provide the "building blocks" for most multi-diode mixers. Multi-diode mixers can essentially be reduced to equivalent single diode mixers [7].

The typical frequency spectrum of the current flowing through the diode is shown below. Although the graph only shows mixing products up to the 3rd order, it is clear that the lower order mixing products are generally those of interest, since the amplitude of these lower order mixing products makes it necessary to consider them when designing input and output filter networks. Also note the "tapering" of the amplitudes as the frequency increases; as it can be expected, the majority of the power lies at the mixing products of the *fundamental* RF and LO frequencies, while less power is available at the higher frequencies.

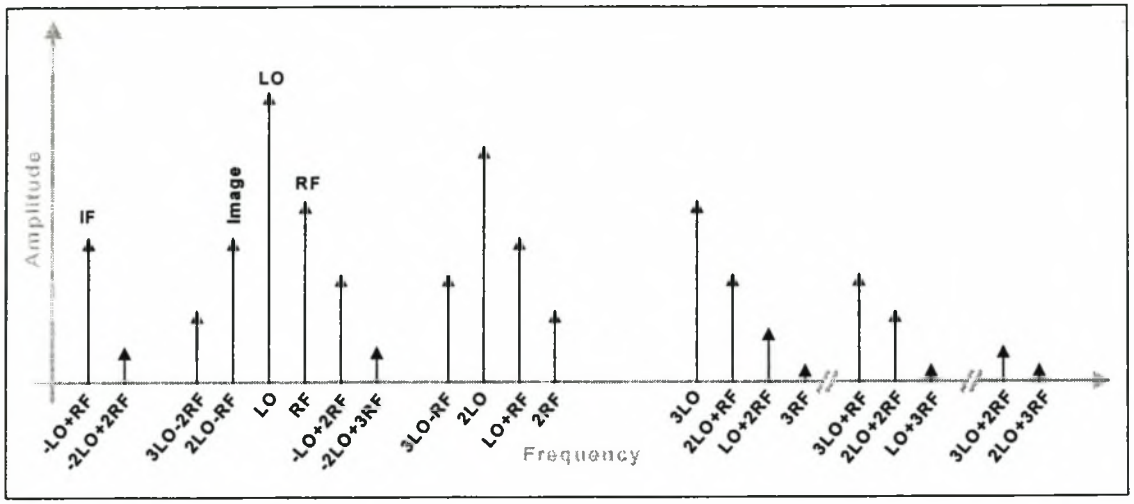

Figure 1.2 : Frequency Spectrum of Single Diode Mixer (up to 3rd order mixing products)

The frequency content of the current through the single diode mixer is typical for any general nonlinear element. The various frequency components described by equations (1.3) – (1.5) can be graphically identified above. Specific frequencies to note are as follows :

- The RF and LO, with their harmonics
- The IF : {-LO + RF}
- The Image Frequency : {2LO – RF}
- Even-order IM products : {-LO + RF}, {2LO + 2RF}, etc.
- Odd-order IM : {2LO – RF}, {-2LO – 3RF}, etc.

As a measure of comparison to the topologies of the following sections, it is noted that the frequency spectrum of the current through the single diode contains the LO and RF signals, and all their harmonics. There is consequently no inherent *isolation* of these signals from the IF port. Removing these signals from the IF port is a task that must be done completely by means of filtering. It is also noted that the spectrum contains both the even-order and odd-order IM products. The single diode mixer therefore provides no *spurious-response rejection*; a task that must once again be done entirely by filtering.

Finally, it is noteworthy that any amplitude or phase noise present in the LO will be directly "translated" to the IF signal – therefore there is no *noise-rejection*.

To conclude, single diode mixers have the following general characteristics :

Characteristic	Performance
Isolation	No isolation between LO, RF and IF
Spurious-response rejection	No rejection of even- or odd-order IM products
Noise-rejection	No rejection of LO amplitude or phase noise
Frequency Range	Classic mixer for higher GHz-region

Table 1.1 : Summary of Characteristics for Single Diode Mixer

Although the single diode mixer is predominantly used in the mm-wave region and beyond, more complex topologies generally outperform this mixer at lower frequencies. These topologies will briefly be discussed in the following section.

1.2.2 Balanced Mixers

In addition to single diode mixers, balanced mixers provide a further dimension to frequency conversion. Their multi-diode configurations allow for certain very attractive characteristics, as will be shown shortly. Balanced mixers usually employ diodes in groups of 2, 4 or 8, and are characterized accordingly. The harmonic mixer has often been characterized as a sub-division of balanced mixers, since its operation is in some ways similar to that of a balanced mixer. The operation of the balanced mixer will briefly be presented here in order to verify and explore this classification of the harmonic mixer.

Apart from utilizing more than one diode, balanced mixers make use of *hybrids* and *baluns* [8]. A hybrid circuit has an isolated port, and provides a phase difference (usually 90° or 180°, depending on the design). When the LO and RF signals are applied as unbalanced signals at the input ports, the hybrid produces a balanced signal consisting of a combination of the LO and RF signal on each of its output ports. A balun simply converts a balanced transmission line to an unbalanced line. Single balanced mixers utilize one hybrid or balun, while double balanced mixers use more than one. At lower frequencies the baluns are realized using transformers, while distributed elements are used at GHz-frequencies.

1.2.2.1 Single Balanced Mixer

Figure 1.3 shows the typical topology for a single balanced mixer. The circuit essentially utilizes a 180° hybrid and two diodes. The LO voltage over the diodes is out of phase by 180°, while the RF voltage appearing over the diodes is in phase. These phase differences are characteristic of the specific hybrid, and they determine the harmonic content of the IF.

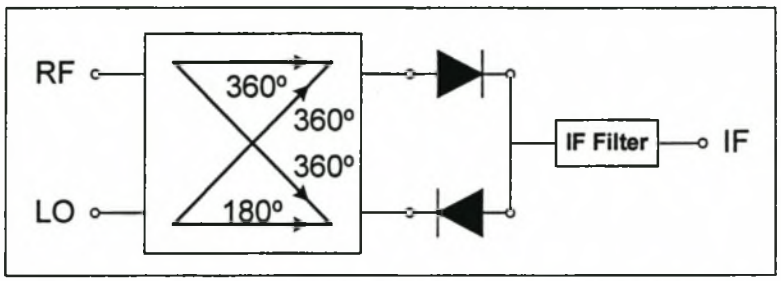

Figure 1.3 : Single Balanced Mixer using a 180°-Hybrid

The method of analysis in the current text for determining the frequency content at the IF port is qualitative, and general to all the types of balanced mixers that are presented in the following sections [9].

For the LO : It can be shown that each diode contains frequency components at all the harmonics of the LO. However, the *pair* of diodes produces *no* frequency components at any of the LO harmonics. The respective diode currents at the harmonics of the LO must therefore be equal but opposite, cancelling at the IF port.

For the RF : It can also be shown that each diode contains frequency components at all the harmonics of the RF. The *pair* of diodes, however, only has frequency components at the *odd* harmonics of the RF. The respective diode currents at the even harmonics of the RF must therefore be equal but opposite in phase, cancelling at the IF port.

Although all the frequency components of the LO are confined to the loop containing the diodes and the hybrid, the mixing products containing these components (e.g. {2LO – RF}, {LO + 3RF}) are not limited to the loop, and appear at the IF port where they can be filtered out by the IF Filter. Figure 1.4 below shows a typical output spectrum for a single balanced mixer, with mixing products to the 3rd order. The frequency components characteristic of the single diode mixer that are not present (i.e. rejected) in the single balanced mixer have been grayed.

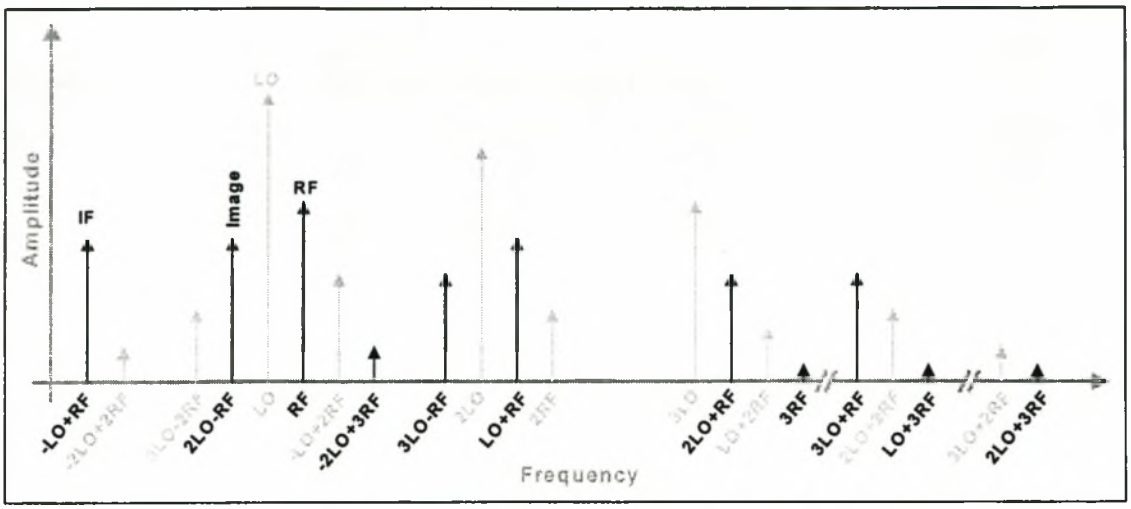

Figure 1.4 : Frequency Spectrum at the IF Port of typical Single Balanced Mixer

The single balanced mixer also has the property of rejecting LO amplitude noise (or AM noise) at IF frequencies. The noise voltage V_n that enters the mixer at the LO port, is 180° out of phase through the diodes, and cancels at the IF port. As can be expected, the IF has much improved isolation from the LO signal (limited mainly by the *degree of balance* in the circuit, which is in turn determined by the quality of the hybrid, and the similarity of the two diodes).

To conclude, single balanced mixers have the following general characteristics :

Characteristic	Performance
Isolation	Good isolation between LO and IF No isolation between RF and IF
Spurious-response rejection	(1) All $\{m\omega_s + n\omega_p\}$ mixing products with m **and** n even are eliminated (e.g. {–2LO + 2RF}) (2) All $\{m\omega_s + n\omega_p\}$ mixing products with m even **and** n odd are eliminated (e.g. {–LO + 2RF})
Noise-rejection	Rejection of LO amplitude noise
Frequency Range	MHz-range (baluns) and low GHz-range (hybrids)

Table 1.2 : Summary of Characteristics for Single Balanced Mixer

1.2.2.2 Double Balanced Mixer

A double balanced mixer typically uses four diodes and three baluns. Figure 1.5 shows a configuration for displaying the operation of the double balanced mixer. (In practice the mixers are rarely realized in this way. A ring- or star-configuration, described later, is often used.)

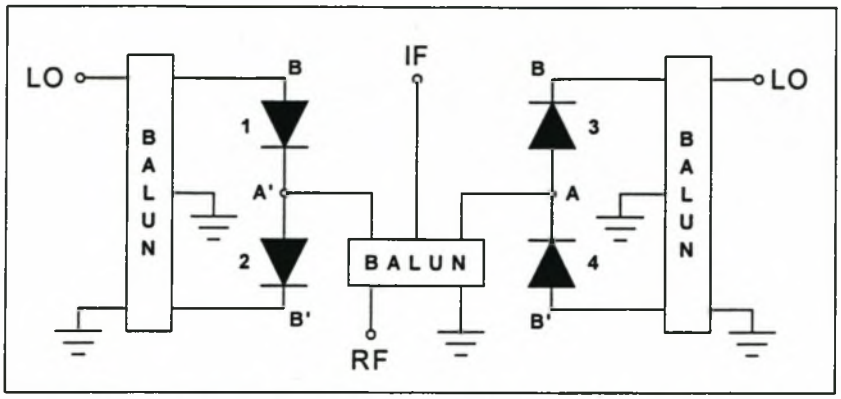

Figure 1.5 : Double Balanced Mixer using three baluns

Once again the analysis of the double-balanced-topology presented here will be intuitive, as a detailed description will be given in later sections. Since the two diodes connected to the secondary of each of the LO baluns are identical, points A and A' are virtual grounds for the LO. In the same way points B and B' are virtual grounds for the RF. During the positive half of the LO cycle, A' is ideally connected to virtual ground, while A is ideally open. The part of the RF balun's secondary between A' and the IF port is therefore connected. During the negative half of the LO cycle the part of the RF balun's secondary between A and the IF port is connected. As a result of this "switching" action the RF applied to the IF port is switched at the LO frequency. The conductance waveform due to the LO has half-wave symmetry (a result of the "switching" action), and therefore contains no even harmonic components.

For the LO : It can be shown that all the diodes contain all the harmonics of the LO. However, the lines from the 1-2 and 3-4 *pairs* of diodes (see Figure 1.5) to the secondary of the RF balun contain no frequencies at the harmonics of the LO. Consequently, for both the 1-2 and 3-4 loops, the harmonic currents must be equal but opposite in phase, cancelling at both ports of the RF secondary. Ideally the IF is completely isolated from the LO, since the RF balun is free of any LO frequency content.

For the RF : In a situation similar to that of the single balanced mixer, the 1-2 and 3-4 *pairs* of diodes permit only current components at the odd harmonics of the RF to flow between the diodes and the secondary of the RF balun. Since it can be shown that all diodes contain all harmonics of the RF, the diode currents at the even harmonics of the RF must therefore be equal but opposite in phase. The remaining odd harmonics from the 1-2 and 3-4 pairs of diodes add in the secondary of the RF balun, and since they are of equal magnitude but opposite phase, they too cancel in the ideal case, and the IF is completely isolated from the RF.

Figure 1.6 shows a typical output spectrum for a double balanced mixer (with mixing products to the 3rd order).

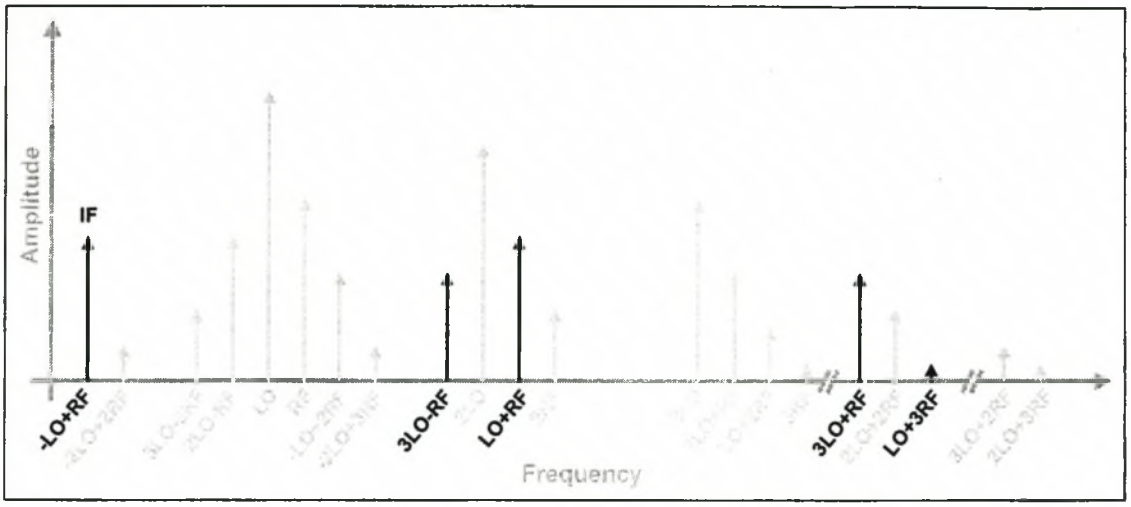

Figure 1.6 : Typical IF Frequency Spectrum of Double Balanced Mixer

Because the frequency content in the secondary of the RF balun is even more limited than the diode loop of the previously discussed single balanced mixer, the IF spectrum contains even less mixing products. Only products of odd LO and RF harmonics are present.

Double balanced mixers are seldom realized as depicted in Figure 1.5. Slight variations of the topology permit a double balanced mixer with improved performance. The *Ring Mixer* is created by connecting both points labelled B in Figure 1.5, as well as both points labelled B'. The *Star Mixer* is created by essentially extracting the IF signal from a common point connecting all four diodes. Further discussion on their operation will be omitted from this overview.

To conclude, double balanced mixers have the following general characteristics :

Characteristic	Performance
Isolation	Good isolation between LO and IF Good isolation between RF and IF
Spurious-response rejection	Only ($m\omega_s + n\omega_p$) mixing products with m **and** n odd are permitted (e.g. –3LO + RF)
AM Noise-rejection	Rejection of LO amplitude noise (similar to single balanced mixer)
Frequency Range	Low GHz-range

Table 1.3 : Summary of Characteristics for Double Balanced Mixer

1.2.2.3 Higher-Level Balanced Mixers

As evident from the previous discussions, an increase in circuit complexity generally leads to improved mixer performance. Apart from attractive isolation, good spurious response rejection and low conversion loss, higher-level balanced mixers have the additional advantage of improved power handling.

Several structures are employed to realize these high-level mixers. The *triple balanced mixer* is in analogy an extension of the double balanced mixer, just as the double balanced mixer is of the single balanced mixer. It uses two rings of four diodes each, with IF power from the two diode rings effectively combining at the IF balun or hybrid. The major disadvantages of the triple balanced mixer are an additional 3dB of LO power, and greater circuit complexity.

Another structure employs two 90° hybrids to split the RF and LO separately into quadrature signals. These are mixed separately into quadrature IF signals, which are finally combined in a 180° hybrid. The major advantage of such a scheme is excellent VSWR's due to the hybrids at the LO, RF and IF ports. The main disadvantages are increased LO power, and possible signal loss in the hybrids.

1.2.2.4 Subharmonic Mixers

The principle of operation of the balanced mixer is similar to that of the harmonic mixer. Arguments exist that the harmonic mixer performs frequency conversion without the use of "balancing structures" (e.g. hybrids), and can therefore not be considered a balanced mixer. However, authoritative texts [9] suggest that the applied signals are essentially "balanced" between the two diodes, and therefore the harmonic mixer is introduced in this text as a part of the family of balanced mixers. This section should serve as an introduction, while the finer details of the harmonic mixer will be explored at length in the following chapters.

At this point a definition [10] will be in order to avoid any confusion that might arise from the usage of the terms "harmonic mixer" and "subharmonic mixer" :

Subharmonic Mixer : The family of mixers designed to utilize an input LO at a fraction, most commonly a half, of the desired LO.

Harmonic Mixers : Another term used to describe subharmonic mixers, but most often refers to mixers employing higher multiples (greater than the 2^{nd}) of the injected LO.

Although the definition is clearly not rigid and the terms are occasionally used outside their defined context, it rarely creates a problem. In the current text the term "subharmonic mixer" and "harmonic mixer" will be used interchangeably, and the order of the "effective" LO harmonic will be used as a reference, e.g. a 4^{th} order harmonic mixer requires an LO signal on the LO port at a quarter of the effective LO.

A harmonic mixer converts the RF signal with frequency ϖ_s to an IF signal of frequency ϖ_{IF} using the *n*-th harmonic of the input LO of frequency ϖ_p. The essence of harmonic mixing is described by

$$\omega_{IF} = \omega_S - n\omega_P \qquad \text{.....(1.7)}$$

Harmonic mixing is most effectively accomplished using an *antiparallel* diode structure. A single diode mixer can also be used to perform harmonic frequency conversion, although it is then strictly not a balanced mixer.

Single Diode Operation : Subharmonic mixing can be achieved in what can be described as a "crude" method, simply by driving the diode "hard" at the LO frequency, forcing the amplitude of the higher order LO harmonics to increase. However, the fundamental $\{\varpi_s \pm \varpi_p\}$ mixing response is usually greater than the desired $\{\varpi_s - n\varpi_p\}$ mixing response, making it difficult to implement filters. These mixers are *harmonic mixers* in the strictest sense, since the RF mixes with *all* the harmonics of the LO. Single diode harmonic mixers are used where responses to a wide range of LO harmonics is necessary, typically in the input circuits of spectrum analyzers.

The single diode harmonic mixer has effective yet restricted use, and the remainder of the current text will be concerned with harmonic mixers utilizing the antiparallel diode pair.

Antiparallel Diode Pair : The most effective method of mixing an RF signal with a harmonic of the LO, is achieved by using an antiparallel diode pair. Instead of mixing the RF with all the harmonics of the LO, the antiparallel diode pair only allows mixing with selected LO harmonics. It also exhibits impressive rejection of certain spurious responses. Figure 1.7 shows the basic topology for the antiparallel harmonic mixer.

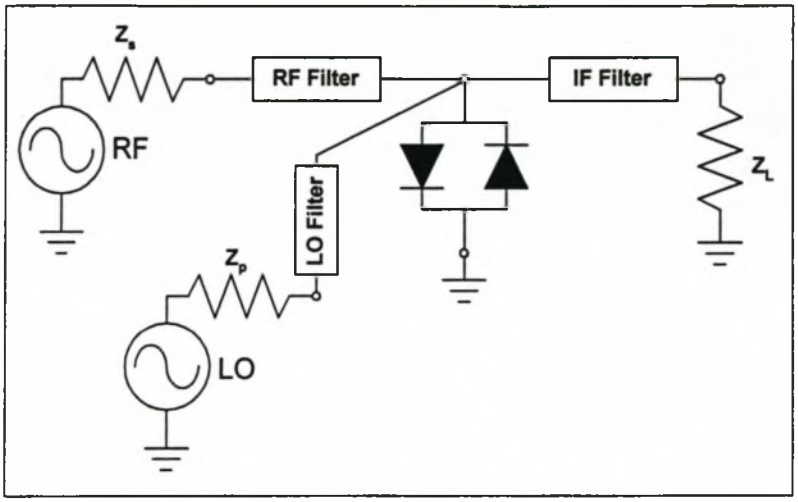

Figure 1.7 : Basic topology for Antiparallel Diode Pair Subharmonic Mixer

In a way similar to conventional mixers (i.e. mixers utilizing the fundamental LO harmonic), the antiparallel diode pair is "pumped" by the LO, while the RF signal is applied to the pair. The IF can usually be extracted relatively easily through a low pass filter. Slight variations of the above topology have been implemented, but the basic principle of operation remains the same.

The main concern during the design of the subharmonic mixer is twofold :

1) Provide the antiparallel diode pair with a frequency spectrum containing the required frequency content, and
2) Provide the antiparallel diode pair with optimum impedance terminations at the frequencies of interest.

The implementation of the above requirements, together with the overall performance of subharmonic mixers employing antiparallel diode pairs, will be the explored in the remainder of the current text.

1.3) Mixer Characteristics

The nonlinear nature of frequency generation during frequency conversion often makes the process of extracting a useful IF signal quite challenging. Mixing products close to the required IF signal in the output spectrum can cause difficulty when implementing output filters. Often input filters are required, adding to the overall complexity of the structure. Apart from simply posing a problem in the output spectrum through their individual existence, certain frequency products can themselves cause a new process of mixing, leading to a new family of frequency components in the output spectrum.

The above problem has lead to the definition of certain mixing characteristics required for "effective" mixing – these are often referred to as *figures of merit*. The primary goal is usually to minimize *conversion loss*, while the minimization of *noise figure* and *intermodulation distortion* might occasionally be of greater importance. Other parameters for designing (or for optimization after the initial design) include *reflection* at the ports (VSWR), and *compression*.

The definitions in the following section relate to mixers in general – in Chapter 2 they will specifically be applied to subharmonic mixers.

1.3.1 Conversion Loss

Conversion loss is defined as the ratio of output signal power to input signal power [8], or

$$L_c[dB] = P_{RF}[dB] - P_{IF}[dB] \qquad \text{.....(1.8)}$$

where P_{IF} is the IF output power and P_{RF} is the available RF power. The conversion loss is usually specified for a specific frequency (the IF), and for a specific bias current or LO power level. Three factors generally contribute to greater conversion loss :

1) RF and IF mismatch,
2) Loss in the diode series resistance R_S,
3) Loss in the diode junction due to the generation of intermodulation products.

Although for a single diode mixer a theoretical value of 3dB for L_c is given, a typical practical value is 4dB to 7dB.

By sensibly choosing the type of diode to use in a specific application, factor (2) and factor (3) can be minimized. Factor (1), and in a lesser degree factor (3) can be kept to a minimum by skillful design of the embedding circuit for the diode(s).

Additional techniques to reduce conversion loss have been explored [11]. By ensuring a correct reactive impedance seen by the diode at the image frequency, improvements of 3dB have been recorded (*image enhancement*) [12,13].

1.3.2 Noise

Mixers suffer from two types of noise distortion :

- *Inherent Noise* is the term used to describe the noise generated by electron movement within the semiconductors and structures. Inherent Noise determines the sensitivity of the mixer.
- *Signal Noise* refers to the perturbations that might be present within an applied signal. Signal noise manifests itself as unwanted mixing products in the frequency spectrum of the mixer.

1.3.2.1 Inherent Noise

Noise in electronic components is due to the random motion of electrons in materials. In Schottky diode mixers noise is predominantly generated by two instances of electron motion :

1) *Thermal (Johnson) noise :* Thermal noise is generated by random current fluctuations in any resistor without any external voltage applied.
2) *Shot noise :* Shot noise is generated by the stream of electrons flowing across the diode barrier at random velocities.

Apart from thermal and shot noise, Flicker noise (or "*1/f – noise*") is an additional source of noise. However, it is a low-frequency phenomenon, and for the majority of microwave mixers employing Schottky-barrier diodes the effect of flicker noise can be neglected.

In the analysis of noise, the primary units for expressing noise quantities are [14] :

- Noise Voltage, v_n
- Noise Power, N
- Equivalent Noise Temperature, T_e

These quantities are related by the following equations :

$$N = \frac{v_n^2}{R_L} = KT_e \qquad \text{..... (1.9)}$$

where K is Boltzmann's constant = 6.456 3 10^{-23}, and R_L is the load resistance into which the noise power N is delivered. In order to relate the above mentioned quantities numerically, the following relation holds for $R_L = 50\Omega$:

$$290K\big|_{R_L=50\Omega} \triangleq 4\times10^{-21}W\big|_{R_L=50\Omega} \triangleq 447pV\big|_{R_L=50\Omega}$$

Note that it is also common to include a bandwidth-component in the definition of noise power [8].

Noise Factor F relates the noise power from the input frequencies of a mixer to the noise power in the output band. Noise from the RF sideband(s) will be converted to noise in the IF band. Per definition the Noise Factor is given by

$$F = \frac{S_I/N_I}{S_O/N_O} = \frac{N_O}{L_c N_I} \qquad \text{.....(1.10)}$$

where S_I is the input signal power, S_O is the output signal power, N_I is the input noise power, N_O is the output noise power, and L_c is the conversion loss. The *Noise Figure NF* is only the Noise Factor expressed in decibels, or

$$NF = 10 \log F \qquad \text{.....(1.11)}$$

The ultimate goal of noise analysis is to characterize a mixer as a two-port device (RF signal at the input, IF signal at the output) contributing a certain amount of noise to its input noise power. The amount of noise contributed by the mixer is expressed in terms of the noise factor F (or NF), or the equivalent noise temperature T_e.

1.3.2.2 Signal Noise

Apart from the above mechanisms of internal noise generation, noise appears at the output of a mixer due to the effect of the applied external sources. Amplitude and phase noise on the LO are the major contributors of external noise.

A LO signal containing noise can mathematically be described by

$$\omega_p\big|_{noise} = \omega_p \pm \Delta_p$$

where Δ_p represents a small frequency deviation of the LO due to phase noise. Equation (1.6) can be now adapted slightly for the case when $m = 1$ and $n = -1$:

$$\omega_{if} \pm \Delta_{if} = \omega_s - \omega_p\Big|_{noise} \qquad \text{.....(1.12)}$$

where Δ_{if} represents the resulting small deviation at the IF frequency due to the noisy LO signal. In the time-domain the IF signal is superimposed upon a low-frequency oscillation.

1.3.3 Conversion Compression

Conversion Compression dictates the upper limit of a mixer's dynamic range, i.e. the RF input level above which the RF versus IF curve exhibits a certain deviation from linearity. It is necessary to specify conversion compression for a specific LO power level, since higher values of LO power allow for higher conversion compressions. This immediately suggests a trade-off during design : minimal conversion loss generally requires higher LO levels, while lower LO levels are favourable for lower cost, lower noise and additional filtering considerations. In most instances the conversion loss is the primary consideration, and the conversion compression is usually quite satisfactory at the LO power level resulting in the optimal conversion loss.

Since balanced mixers have an optimum LO for minimum conversion loss or noise, the conversion compression is conveniently specified at this LO value. Figure 1.10 shows the typical characteristic for a mixer's conversion compression. Note the *1-dB compression point* - operating the mixer past this point on the curve of conversion compression results in increased conversion loss.

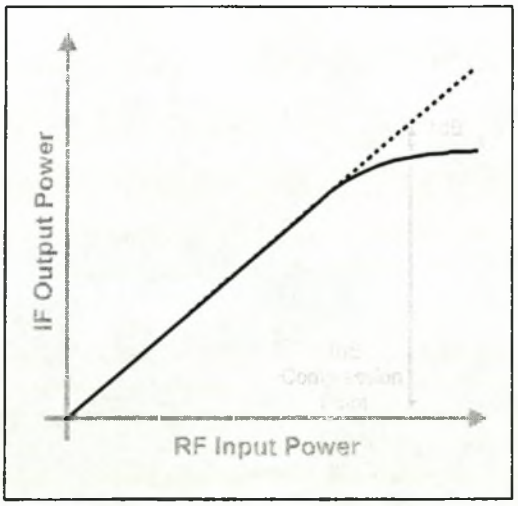

Figure 1.8 : Typical Characteristic for Conversion Compression

Although excessive RF levels are rarely a problem in receiver front-ends, conversion compression is a noteworthy factor for instruments such as spectrum analyzers.

1.3.4 Intermodulation Distortion

The undesired mixing products generated during the mixing process are called *intermodulation products*, or *spurious responses*. The effect of these products on the output of the mixer is referred to as *intermodulation distortion [40]*. It is important to identify the spurious responses, especially those potentially within the IF band, *prior* to mixer design. An amount of flexibility regarding the choice of LO and IF (the choice of RF is usually less arbitrary) can enable the designer to make an optimum decision, avoiding spurious responses which will be difficult to isolate from the IF.

This is typically done graphically with a spurious product chart as shown in Figure 1.11. The chart shown is a downconversion chart, but a similar upconversion chart can be constructed [7].

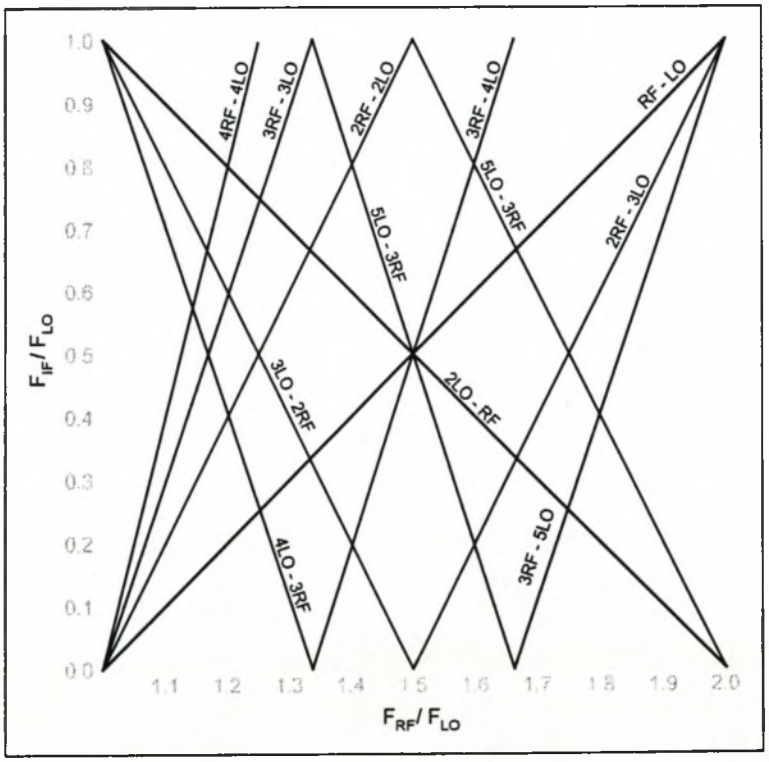

Figure 1.9 : Typical downconversion spurious response chart (limited to 5th order IM products)

The horizontal axis of the chart represents the RF input normalized to the LO frequency, while the vertical axis represents the IF output normalized to the LO frequency. The various spurs are indicated as lines on the graph. With the LO and RF as variables, a vertical line can be constructed for the chosen F_{RF} / F_{LO}. The resulting intermodulation products can be read off from the vertical axis (after denormalization). Also note that the higher the order of the

intermodulation products that are considered on the chart, the more "crowded" by lines the chart becomes.

As an example, let f_{LO} = 5 GHz, and f_{RF} between 8 and 8.5 GHz. This results in f_{IF} between 3 GHz and 3.5 GHz. Thus F_{RF} / F_{LO} lies between 1.6 and 1.7, on the horizontal axis. Likewise F_{IF} / F_{LO} lies between 0.6 and 0.7 on the vertical axis. The resulting IF passband can be visually represented by the gray square indicated on Figure 1.11. For F_{IF} = 3GHz only one spur, {RF – LO}, intercepts the gray square. This spur can be seen on Figure 1.12 as the solid line at 3GHz. Figure 1.12 shows the typical frequency spectrum of the output of a single diode mixer for the two values of the RF : f_{RF} = 8 GHz (solid lines), and f_{RF} = 8.25 GHz (dashed lines).

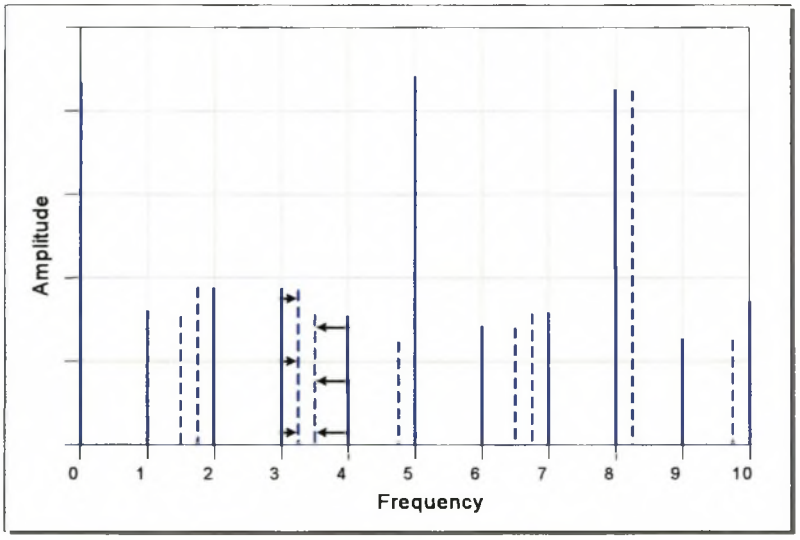

Figure 1.10 : Output Spectrum for f_{RF} = 8 GHz (solid) and f_{RF} = 8.25 GHz (dashed)

For F_{RF} = 8.25 GHz two spurs, {RF – LO} and {5LO – 3RF}, intercept the gray square. These spurs both fall in the IF passband, and their "movement" into the IF passband as the RF frequency increases can be seen on Figure 1.12.

It has been demonstrated that mixer topologies such as balanced mixers can reject certain spurious responses. However, care must be taken during the design stage to ensure that the IF, represented by a rectangular area on the spurious response chart, is relatively "free of spurs".

1.3.5 Reflection (VSWR)

The *Voltage Standing Wave Ratio*, or VSWR, of a port (e.g. the LO port) is a measure of the mismatch offered by the port to the system driving the port. The VSWR is defined as

$$VSWR = \frac{1+|\rho|}{1-|\rho|}$$

where

$$\rho = \frac{Z_L - Z_0}{Z_L + Z_0}$$

with Z_L the input impedance of the port, and Z_0 the characteristic impedance of the system (50Ω for all the circuits presented in the current text). If Z_0 = 50Ω and Z_L = 65Ω, then ρ = 0.13 and VSWR = 1.29.

A VSWR greater than unity implies that power is reflected from the port (the port is unmatched to the system). This is of course unwanted, since a non-optimally matched RF port, for example, can reflect a portion of the RF signal back into the RF source (possibly an antenna or low-noise amplifier). Similarly a non-optimally matched IF port can prevent the IF signal from optimally "exiting" the mixer. This "unavailable power" is termed the *return loss* of a port, and is given in decibels by

$$RL = -20\log|\rho|$$

With the above values for Z_L and Z_0 the return loss is found to be RL = 17dB. The port is generally well matched to the source.

In general, the input impedance of the mixer is dictated by the impedance of the diode(s). (When narrowband filters are used on the ports, their response adds significantly to the input impedance.) Considering the diode's I-V curve, it becomes clear that the input impedance of the diode is a function of bias-point. The LO level has a significant effect on the bias-point of a mixer, and consequently the input impedance of the diode(s). Therefore the LO level must be referenced when specifying VSWR. The RF signal does not have a significant effect on the bias-point, and consequently does not change the VSWR. Effectively the LO level determines the LO, RF and IF input impedance (and of course VSWR on these ports).

Apart from LO drive power, the input impedance of a diode, and therefore of the mixer, is also a function of frequency. On the Smith chart the input impedance (seen by the LO) of a typical

diode varies from high impedance to low impedance, and then back to high impedance as the frequency increases. Figure 1.13 shows the typical circles made on the Smith chart by the input impedance of the diode junction. Each circle represents a specific LO power level, while the LO frequency is sweeped. Typically a larger LO power results in larger values for junction capacitance and conductance for a specific frequency. It is evident that the diode junction presents a wide variety of input impedances by varying the LO power and frequency. This is a characteristic that is exploited during mixer design.

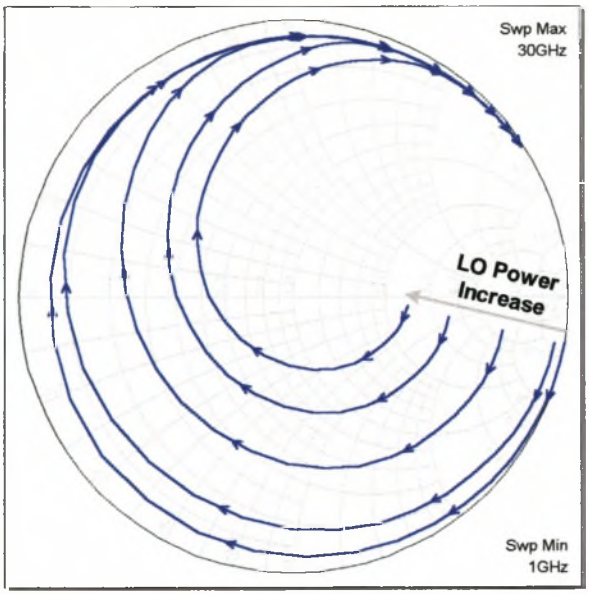

Figure 1.11 : Typical Diode Input Impedance for different LO power levels

The design of a mixer requires that the various ports are matched, resulting in optimal signal conversion.

Now that the fundamentals of frequency conversion and frequency mixers have been investigated, the stage is set for an investigation into a specific device, the harmonic mixer. The fundamental properties of the harmonic mixer will be investigated, and the above mixer characteristics will be related to them. Many of the fundamentals encountered in Chapter 1 are simply extended for use with the harmonic mixer.

Chapter 2 : *Diode Harmonic Mixers*

As the upper frequency barrier of communication systems is continuously pushed upwards by faster components such as diodes and oscillators, producing adequate power at these frequencies remains a problem. The inability to manufacture stable, powerful and yet cost effective local oscillators at high frequencies has been one of the main reasons for downconverters operating at these frequencies not having become commonplace already. However, if the need for such local oscillators can be eliminated, while still operating at high frequencies, the situation might look much better.

Harmonic mixers offer a solution to this problem. While the frequencies at which these mixers operate are typically limited mainly by the type of diode used, the harmonic mixer does not require a high frequency, high power driving source. Although the harmonic mixer can never match the conventional diode mixers as the leader in terms of conversion loss, modern harmonic mixers offer very competitive performance. While conversion loss might sometimes only lag by two or three dB's, the option of using a local oscillator at half the original frequency is often a very favorable option.

This chapter investigates the operation of the diode harmonic mixer. It starts off by describing the Schottky-Barrier diode as the fundamental component of harmonic mixers. Another fundamental structure, the antiparallel diode pair, is then described. The chapter provides a description of the methods used to analyze harmonic mixers, whereafter it elaborates on the mixer characteristics defined in Chapter 1, with respect to harmonic mixers. The chapter closes with a discussion on the analysis of the antiparallel diode pair.

2.1) The Schottky-Barrier Diode

The Schottky-Barrier Diode (or Schottky diode) is the most commonly used diode in modern mixer circuits below the mm-wave region. High switching speeds (due to the low *Reverse Recovery Time* of the barrier), low forward resistance, as well as ease of fabrication makes the Schottky diode preferable to other diodes, such as the *pn*-diodes or point-contact diodes (The point contact diode is essentially a variation on the Schottky-Barrier diode where the surface of the junction is concentrated into a point.) This section will present a brief overview of the properties of the Schottky-Barrier diode.

2.1.1 Junction Characteristics

The Schottky-Barrier diode is created by connecting a metal contact (the anode) to a semiconductor (the cathode). Conduction in a Schottky diode is by means of the emission of majority carriers over the junction boundary. The Schottky diode is therefore a *majority carrier device*, and its switching speeds are not limited by the minority effects found in minority carrier devices, such as the *pn*-diode. Platinum and titanium are the most common metals used for the anode, while a *n*-type semiconductor (e.g. GaAs) is used for the cathode due to its greater electron mobility over the p-type semiconductors [9].

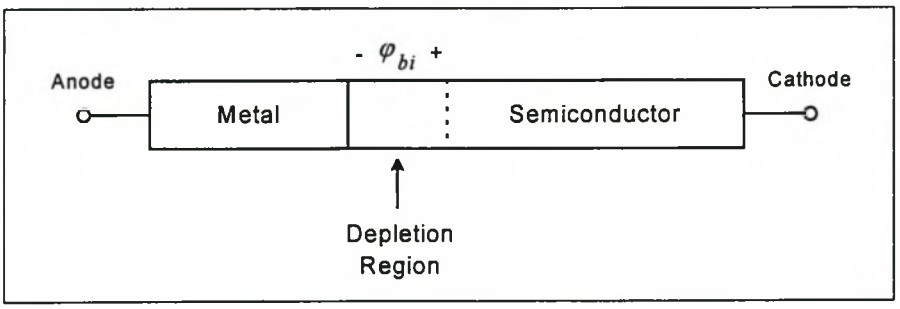

Figure 2.1 : The Schottky diode junction

While the extensive description of the Schottky junction in terms of unequal Fermi levels [9, 15] falls outside the scope of the current text, a qualitative description (with the aid of Figure 2.1) will suffice. When the metal and the semiconductor surfaces are joined, electrons from the semiconductor spontaneously move to the metal surface. This is due to the unequal Fermi levels of the metal and the semiconductor, indicating less energy, on average, for the electrons in the metal. The positively charged region that is created in the semiconductor is called the *depletion region*. This results in a *built-in potential* φ_{bi} of the junction, a crucial parameter when characterizing the Schottky diode. After several manipulations with Gauss' law and the electric field, the depletion region can be characterized in terms of its depletion charge Q_j :

$$Q_j = W\sqrt{2q\varepsilon_s\varphi_{bi}N_d} \qquad \text{.....(2.1)}$$

where W is the junction area, q is the electron charge, ε_s is the dielectric permittivity for the semiconductor, and N_d is the doping density.

When a forward bias voltage V is applied to the Schottky diode, the voltage across the junction becomes (φ_{bi}-V). Equation (2.1) therefore becomes

$$Q_j = W\sqrt{2q\varepsilon_s(\varphi_{bi} - V)N_d} \qquad \text{..... (2.2)}$$

From equation (2.2) the capacitance of the nonlinear junction (due to the effects of charge-storage) can be found by taking the derivative of the charge with respect to the junction voltage :

$$C(V) = \frac{dQ_j}{dV} = \frac{C_{j0}}{\left(1 - \frac{V}{\varphi_{bi}}\right)^{1/2}} \qquad \text{..... (2.3)}$$

where C_{j0} is the junction capacitance at zero bias. The denominator's exponent of ½ indicates the assumption of uniform doping density N_d. The current flowing though the barrier is due primarily to thermionic emission across the barrier. By relating the electron density at the junction under no bias conditions (φ_{bi}) to the electron density with a bias applied (φ_{bi}-V), the current through the junction is given by

$$I(V) = I_S\left(e^{\frac{qV}{KT}} - 1\right) \qquad \text{..... (2.4)}$$

where q is the electron charge, V is the applied bias voltage, K is Boltzmann's constant, and T is absolute temperature. I_s is the saturation current, and represents the effect of the size of the junction area and the different Fermi levels. Equation (2.4) is the *ideal diode equation.*

The operation of the real Schottky diode junction differs slightly from that described in the previous section. Imperfections on the surface of the junction, and quantum mechanical tunneling of electrons through the barrier both add to the nonlinear behaviour of the junction. However, the most significant deviation from ideality comes from the fact that the barrier height does not remain constant with increased bias voltage, but rather decreases as the voltage increases. This *barrier lowering* is due to conduction electrons in the junction experiencing a force from their image charges in the metal. Effectively a larger voltage V needs to be applied to the diode junction in order to have the same current flow as in the ideal case. The *ideality factor* η is approximated as a constant over the voltage range, and is given by

$$\eta = \frac{1}{1 - \frac{d\varphi_{bi}}{dV}} \qquad \text{.....(2.5)}$$

η is close to 1.0, usually between 1.05 and 1.25. It is an indication of the diode's nonlinearity – a larger value of η implies a decrease in the diode's nonlinearity, and a consequent increase in noise, conversion loss etc. To include the ideality factor equation (2.4) is altered as follows

$$I(V) = I_S\left(e^{\frac{qV}{\eta KT}} - 1\right) \qquad \text{.....(2.6)}$$

Equation (2.6), together with (2.3) are used to characterize the junction of the Schottky diode completely.

Apart from barrier lowering, the *series resistance* R_s presented by the diode junction also has an effect on the operation of the Schottky diode. This series resistance at lower frequencies is inversely proportional to the doping density N_d, while at the higher GHz-frequencies the dimensions of the diode start to play a significant role, and the skin-effect needs to be considered when calculating R_s. For the greater part the series resistance R_s can be modeled by a discrete resistance with a value in the order of ohms. As will be shown below, the inclusion of R_s necessitates the distinction between *junction voltage* and *terminal voltage*.

2.1.2 Intrinsic Model

To analyze and design diode frequency mixers, it is necessary to have a diode model that is valid for both *small-signal* and *large-signal* excitations. It is valid to assume that the large-signal model for Schottky diodes is *quasistatic*, since the Schottky diode is a majority carrier device. This implies that the junction capacitance and current as described by equations (2.3) and (2.6) are functions of the junction voltage alone, and change instantaneously with that voltage. The quasistatic assumption is valid for frequencies up to several hundreds of GHz.

2.1.2.1 Large-Signal Model

Figure 2.2 shows an *intrinsic large-signal* model of the Schottky diode. The model is intrinsic in the sense that the junction capacitance and conductance are taken into account, while parasitic package impedances are ignored.

The intrinsic large-signal model consists of three elements :

- A nonlinear, voltage-dependent *conductance g(V),* described by the I-V relationship of equation (2.6),
- A nonlinear, voltage-dependent *capacitance*, *C(V)* given by equation (2.3),
- A series *resistance* R_s.

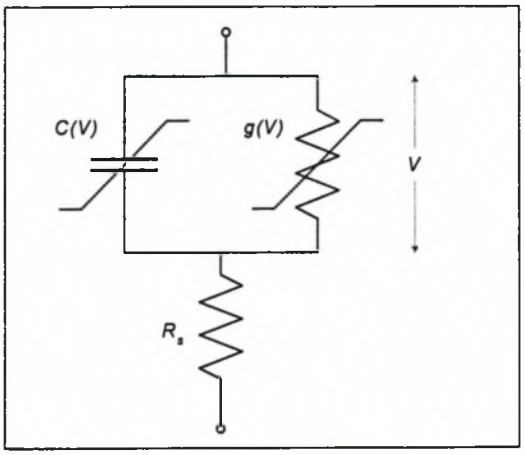

Figure 2.2 : Intrinsic Schottky-Barrier Diode Model

The model is large-signal in the sense that both the conductance *g(V)* and the capacitance *C(V)* are functions of the junction voltage *V*, as implied by the above mentioned quasistatic assumption.

2.1.2.2 Small-Signal Model

Although the model that is used for the small-signal analysis is essentially similar to the one depicted in Figure 2.2, it is implemented slightly differently from the large-signal model. The nonlinear elements are *linearized* around the instantaneous values obtained from the large-signal model, and treated as linear, time-varying elements [9, 16, 39].

The small-signal impedance consists of the *linear* small-signal junction conductance *g(V)* and the *linear* small-signal capacitance C_V. *g(V)* is the derivative of junction current (equation (2.6)) with respect to voltage, with the derivative taken around a fixed point on the I/V curve, or

$$g(V) = \frac{dI(V)}{dV} = \frac{q}{\eta KT}\left(I(V) + I_S\right) \approx \frac{q}{\eta KT} I(V) \qquad \text{..... (2.7)}$$

where I_s is sufficiently small when compared to $I(V)$, and can therefore be ignored. Figure 2.3 summarizes the relationship between large-signal and small-signal conductance.

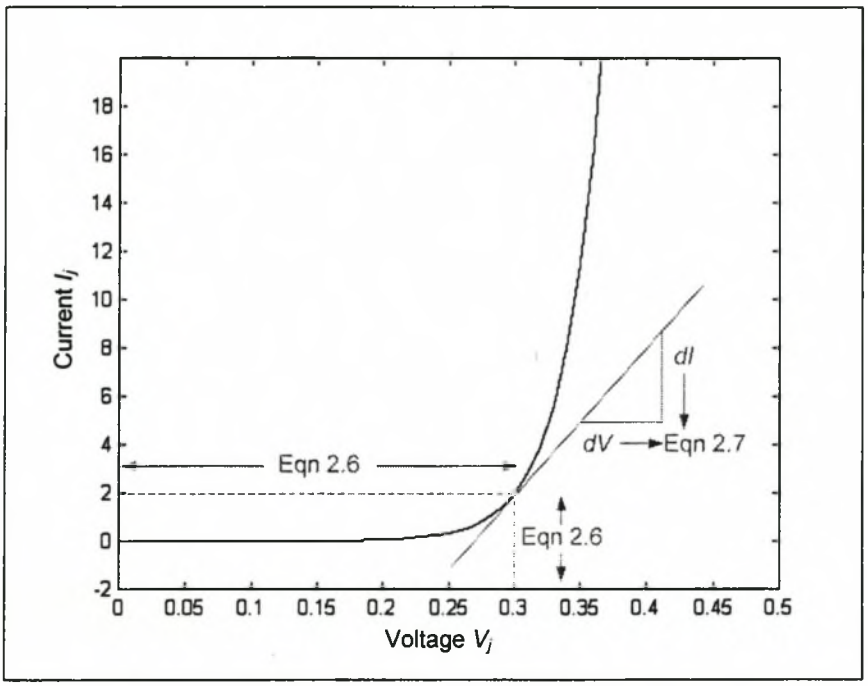

Figure 2.3 : Small- and Large-signal calculation of *g(V)*

The small-signal impedance presented by the capacitance *C(V)* also needs to be known before the diode junction can be completely characterized for small signals. Unlike the small-signal conductance *g(V)*, the small-signal capacitance is not merely the product of a constant and the current. In the time-domain, the capacitor's charge waveform is given by

$$q(t) = c(t)v(t) \qquad \text{..... (2.8)}$$

where $c(t)$ is the capacitance (modulated by the junction voltage V) given by equation (2.3), and $v(t)$ is the applied small-signal voltage. The small-signal capacitor current $i_c(t)$ is found by taking the time derivative of the charge, or

$$i(t) = \frac{dq(t)}{dt} = c(t)\frac{dv(t)}{dt} + v(t)\frac{dc(t)}{dt} \qquad \text{..... (2.9)}$$

Equations 2.7 and 2.9 are used to characterize the small-signal reactance due to the junction capacitance being driven by the LO.

2.1.3 The Complete Diode Model

The previous section described the intrinsic model of the Schottky diode. It represents the most basic model for the diode, not taking into account the parasitic impedances due to the diode packaging. While whisker–contact diodes (used in waveguides at higher GHz frequencies) have minimal parasitic inductance introduced by packaging, the surface mount Schottky diodes used up to the Ku-band contains both parasitic inductance and capacitance. Optimally designed diodes have small parasitic elements which can be compensated for by correct matching.

The main parasitic elements that need to be included in the complete diode model are *bond-wire inductance*, *lead inductance* and *package capacitance*. Figure 2.4 shows the complete diode model used extensively for analysis [15, 17]. The symbols have the following meaning :

- $C_j(V_j)$: Junction Capacitance (function of junction voltage V_j)
- $g_j(V_j)$: Junction Conductance (function of V_j)
- R_S : Diode series resistance
- L_S : Diode series inductance
- L_P : Parasitic package inductance
- C_P : Parasitic package capacitance
- V_d : Voltage applied over the entire diode

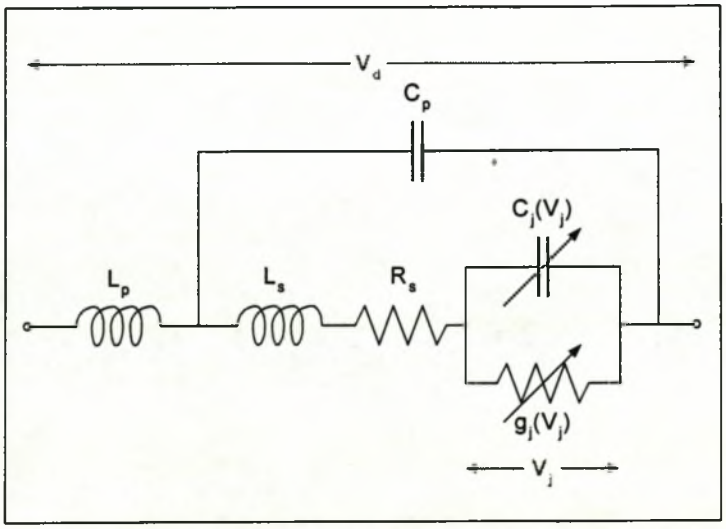

Figure 2.4 : Complete Schottky-Barrier Diode Model

The addition of more components to the diode model necessitates a new notation for the applied voltage. The voltage applied across the complete diode will be called V_d, while the part of the voltage appearing over the junction will be V_j, as shown in Figure 2.4.

The diode used for designs within the current text is the HSMS-820x series surface mount microwave mixer Schottky diode [17]. The diode is optimized for X-band and lower Ku-band operation, and has low series resistance R_s. The following values are supplied :

Saturation Current	I_s = 46 nA
Non-ideality Factor	η = 1.09
Series Resistance	R_s = 6Ω
Series Inductance	L_s = 1.3 nH
Package Inductance (per pin)	L_p = 1.0 nH
Package Capacitance (total)	C_p = 0.08 pF

Table 2.1 : Selected Diode Parameters for HSMS-820x-series

2.2) The Antiparallel Diode Pair

In the single diode mixer in the previous section, one diode was used to generate a spectrum containing the full range of harmonics. When more than one diode is used (as in the variations of the balanced mixers), it is possible to generate spectra containing less frequency content, resulting in a lower conversion loss. However, in all of these mixers the frequency conversion takes place between the RF and the *fundamental* of the LO, resulting in an IF of the form $\{\omega_{IF} = \omega_s - \omega_p\}$.

Although it is possible to obtain frequency conversion of the form $\{\omega_{IF} = \omega_s - n\omega_p\}$ with a single diode, it was shown in the previous chapter that this method is not efficient, since the majority of power is still lost to fundamental mixing. It is necessary to utilize a diode-structure that will minimize mixing with the fundamental of the LO, while maximizing frequency conversion between the RF and a *harmonic* of the LO. It will be shown that the antiparallel diode-configuration is such a structure. The ability of the antiparallel diode pair to generate only certain frequencies of its driving signal has also led to its wide application in the field of frequency multipliers [15].

2.2.1 Single Diode Fundamentals

To understand the fundamental operation of the antiparallel diode pair, it is necessary to briefly consider the operation of a single diode. Figure 2.5 shows the junction conductance *g(t)* for a single diode driven by an LO signal.

The junction conductance reaches a maximum *once* during every LO cycle, and by taking the Fourier transform of the conductance waveform *g(t)*, it is evident that the diode's junction conductance changes periodically at the frequency of the LO. It is this mechanism that controls the mixing action of the single diode and balanced mixers.

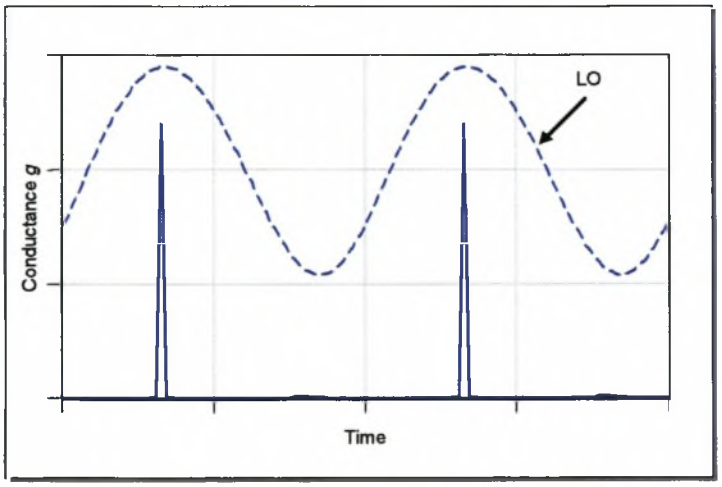

Figure 2.5 : Conductance waveform *g(t)* for a single diode

2.2.2 The Antiparallel Configuration

When two diodes are joined in parallel as shown in Figure 2.6, an *antiparallel* diode structure is created [2]. It will be shown that g_p, the conductance of the diode pair, provides the mechanism for "higher order mixing", i.e. frequency conversion with harmonics of the LO [2].

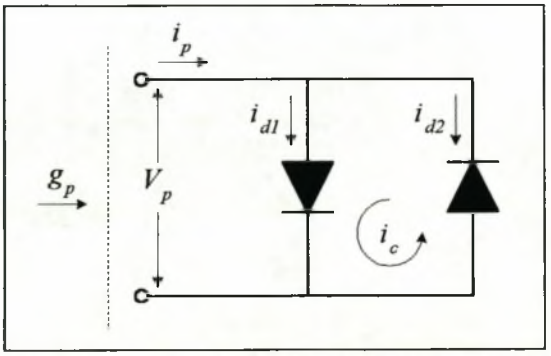

Figure 2.6 : Antiparallel diode configuration

Using the notation of Figure 2.6, and using intrinsic diode models for the purpose of the discussion, the differential conductance of the diode pair is given by taking the derivative of the instantaneous current i_p with respect to the voltage V_p, or

$$g_p = \frac{di_p}{dV_p} \qquad \text{.....(2.10)}$$

The individual diode currents i_{d1} and i_{d2} combine as follows to form the i_p, the diode current for the pair of diodes (Figure 2.6):

$$i_p = i_{d1} + i_{d2} \qquad \text{.....(2.11)}$$

The loop current i_c flows inside the loop, and will be considered in the following sections. Expressions for the diode pair conductance, g_p, will now be developed. Once the input impedance of the diode pair can be expressed in terms of i_p and V_p, the techniques of mixer analysis and design can be implemented in the usual fashion.

Equation (2.11) can be expanded as follows using equation 2.6 (note that the series resistance R_s has been omitted for the purpose of this investigation; its effect will be considered in later sections) :

$$i_p = i_{d1} + i_{d2} = I_S\left[e^{\frac{qV_p}{\eta KT}} - 1\right] + I_S\left[e^{\frac{-qV_p}{\eta KT}} - 1\right] \qquad \text{.....(2.12)}$$

It is assumed that the two diodes of the antiparallel pair are identical. Although the diode pair is usually fabricated on the same wafer (and therefore the diodes have very similar I_s, η and R_s), this assumption is only valid to a certain extent. The effect of *diode unbalance* will be considered separately. Equation (2.12) can be reduced to [2]

$$i_p = I_s\left(e^{\alpha V_p} - e^{-\alpha V_p}\right) \qquad \text{.....(2.13)}$$

where α is known as the *diode slope parameter*, and represents the effect of the non-ideality factor η and temperature T. For the HSMS-series diodes used for designs within the current text, the diode slope parameter is $\alpha = 34V^{-1}$.

Since the voltage V_p is known, and the current i_p can be expressed in terms of V_p, it is possible to find the conductance g_p of the antiparallel pair using equation (2.10) :

$$g_p = g_1 + g_2 = \frac{di_{d1}}{dV_p} + \frac{di_{d2}}{dV_p} \qquad \text{.....(2.14)}$$

Note that the parallel conductances simply sum to the total conductance. Using equation (2.13) it is possible to reduce equation (2.14) to

$$g_p = \alpha I_s \left(e^{\alpha V_p} + e^{-\alpha V_p} \right) = 2\alpha I_s \cosh\left(\alpha V_p\right) \qquad \text{.....(2.15)}$$

Inspection of equation (2.15) reveals that the conductance g_p has *even* symmetry around V_p (due to the *cosh*-function), and as a result reaches *two* positive peaks for every one positive peak of the LO. Figure 2.7 shows the junction conductance *g(t)* for the antiparallel diode pair.

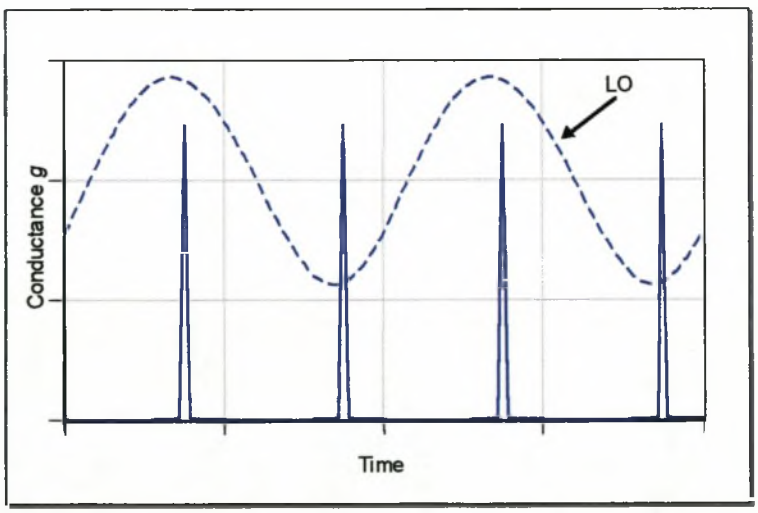

Figure 2.7 : Junction Conductance *g* for Antiparallel Diode Pair

2.2.3 Two-Tone Analysis

During normal mixer operation, the driving voltage $V_p(t)$ of the antiparallel pair consists of the sum of the large signal LO and the small signal RF. Mathematically this signal can be expressed as

$$V_p(t) = V_{LO}\cos(\omega_{LO}t) + V_S\cos(\omega_S t) \quad \text{.....(2.16)}$$

The junction conductance $g(t)$ is modulated by only the LO voltage, and therefore equation (2.16) can be reduced to

$$V_p(t) \approx V_{LO}\cos(\omega_{LO}t) \quad \text{.....(2.17)}$$

Substituting equation (2.17) into equation (2.15) produces

$$g_p = 2\alpha I_S \cosh(\alpha V_{LO}\cos(\omega_{LO}t)) \quad \text{.....(2.18)}$$

which can be expanded into [2]

$$g_p = 2\alpha I_S \begin{bmatrix} I_0(\alpha V_{LO}) \\ +2I_2(\alpha V_{LO})\cos(2\omega_{LO}t) \\ +2I_4(\alpha V_{LO})\cos(4\omega_{LO}t)+\ldots \end{bmatrix} \quad \text{.....(2.19)}$$

where $I_n(\alpha V_{LO})$ are modified Bessel Functions of the second kind [5]. At this stage the junction conductance waveform $g(t)$ of the antiparallel diode pair can be described completely in terms of the modulating voltage V_p. It is noteworthy that $g(t)$ consists of a dc value described by the first term in equation (2.19), as well as harmonics at the even frequencies of the LO. To find the *total* current (large- and small-signal) flowing in the antiparallel diode pair, it is necessary to "superimpose" the complete driving voltage V_p onto the conductance waveform $g_p(t)$. Using Ohm's law, and from equation (2.16)

$$i_p = g_p(t)\times(V_{LO}\cos(\omega_{LO}t) + V_S\cos(\omega_S t)) \quad \text{.....(2.20)}$$

and by substituting equation (2.19) into equation (2.20), the total current for the diode pair is

$$\begin{aligned} i_p = \; & A\cos(\omega_{LO}t) + B\cos(\omega_S t) + C\cos(3\omega_{LO}t) + D\cos(5\omega_{LO}t) \\ & + E\cos(2\omega_{LO} + \omega_S)t + F\cos(2\omega_{LO} - \omega_S)t \\ & + G\cos(4\omega_{LO} + \omega_S)t + H\cos(4\omega_{LO} - \omega_S)t \\ & + \ldots \end{aligned} \qquad \ldots\ldots\ldots\ldots (2.21)$$

where *A, B, C,...*are at this stage arbitrary coefficients. From equation (2.21) a number of noteworthy observations are made. From inspection it becomes clear that the composite current i_p flowing through the antiparallel diode pair contains only components with frequency $\{m\omega_S 6 n\omega_{LO}\}$ where $(m+n) = 1,3,5,\ldots$ i.e. an **odd** integer. Equation (2.21) mathematically displays the mechanism by which the antiparallel diode pair converts an RF signal to an IF signal using a multiple of the LO, e.g. $\omega_{IF} = \omega_S - 2\omega_{LO}$ or $\omega_{IF} = 4\omega_{LO} - \omega_S$. Since the amplitude of the RF signal is usually both fixed and small, harmonics of the RF signal other than the first are impractical to use.

Figure 2.6 also indicates that a loop current i_c circulates within the loop formed by the antiparallel diode pair. Because of the assumption of identical diodes i_c can be expressed as

$$i_c = \frac{i_{d1} - i_{d2}}{2} \qquad \ldots\ldots\ldots\ldots (2.22)$$

Using the usual trigonometric identities and equation (2.6), equation (2.22) can be expanded into

$$i_c = I_S\left(\cosh(\alpha V_p) - 1\right) \qquad \ldots\ldots\ldots\ldots (2.23)$$

which can in turn be expanded using equation (2.16) :

$$i_c = \frac{I_S}{2}\left[\begin{aligned} & \frac{V_{LO}^2 + V_S^2}{2} + \frac{V_{LO}^2}{2}\cos(2\omega_{LO}t) + \frac{V_S^2}{2}\cos(2\omega_S t) \\ & + V_{LO}V_S\{\cos(\omega_{LO} - \omega_S)t + \cos(\omega_{LO} + \omega_S)t \\ & + \cos(3\omega_{LO} - \omega_S)t + \cos(3\omega_{LO} + \omega_S)t + \ldots\} \end{aligned}\right] \qquad \ldots\ldots\ldots\ldots (2.24)$$

Important observations are made from inspection of equation (2.24). The loop current i_c flowing within the loop formed by the antiparallel diode pair contains only components with frequency $\{m\omega_S 6 n\omega_{LO}\}$ where $(m+n) = 0,2,4,...$, *i.e.* an **even** integer. Equation (2.24) contains the mechanism by which the antiparallel diode pair suppresses the even harmonic mixing products, e.g. $\omega_{IF} = \omega_S - \omega_{LO}$ or $\omega_{IF} = 3\omega_{LO} - \omega_S$, as well as the even harmonics of the LO, e.g. $2\omega_{LO}$, $4\omega_{LO}$, etc.

2.2.4 IF Frequency Spectrum

Figure 2.8 shows the typical output spectrum of the antiparallel diode pair driven by LO and RF signals. It is significant to note that the first harmonic of the LO is located relatively far from the IF, i.e. there is no significant frequency content between the IF and the LO. It is therefore easy to realize a low-pass filter to extract the IF from the mixer. This is a very desirable characteristic of harmonic mixers.

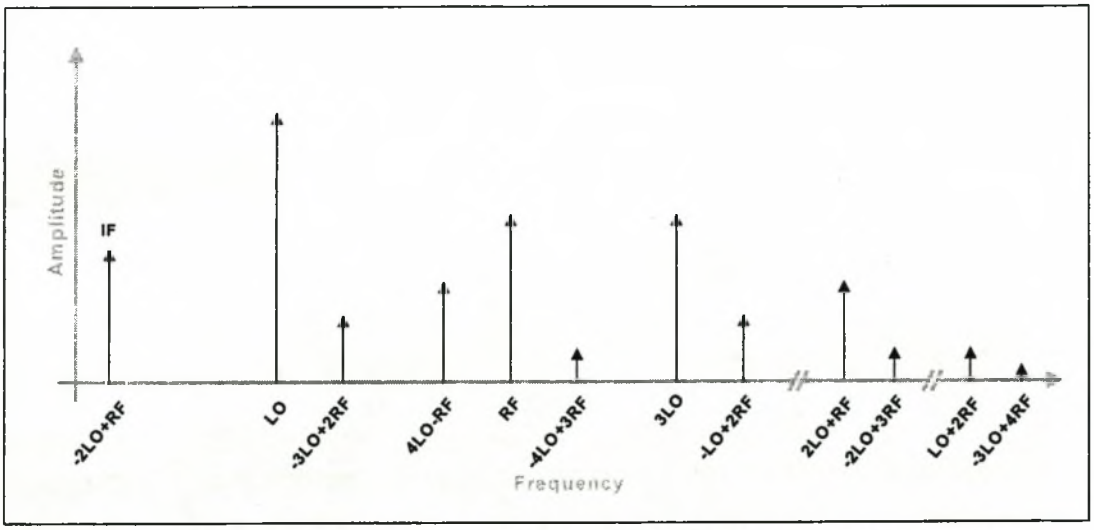

Figure 2.8 : Output Spectrum of Antiparallel Diode Pair (up to 4th harmonic)

When compared to the output spectrum of typical double balanced diode mixers (Figure 1.6), it is clear that the frequency content in the output spectrum is significantly reduced due to the suppression of certain frequencies. It is important to note that this suppression is reduced by *diode unbalance*; a factor that may become significant when the mixer is realized. Diode unbalance will be discussed in section 2.6.

This concludes the fundamental description and characterization of the antiparallel diode pair. It is clear that the antiparallel diode pair is an ideal "building block" for a harmonic mixer : it permits current containing only odd harmonics of the LO (and mixing products with $m+n$ odd) to

flow through, while confining current with even LO harmonics (and mixing products with $m+n$ even) to the loop formed by the diodes. In the following section the analysis of the antiparallel diode pair will be considered.

2.3) Analysis

As it was gathered from the previous sections, the antiparallel diode pair excited by a LO signal and a RF signal contains a range of spectral components. Consequently currents and voltages exist at all of these frequencies. The goal of mixer analysis is to quantitatively describe these voltages and currents at the various frequencies. Once the currents and voltages are known, it becomes possible to find expressions for the mixer's small-signal parameters : conversion loss, port impedances, noise figure, etc.

Mixer analysis is divided into two parts : a *large-signal analysis*, which solves the junction voltages and currents due to an LO excitation, and a *small-signal analysis*, which determines the diode impedance at the frequencies $\omega_n = \omega_0 + n\omega_p$ for n = ...-2, -1, 0, 1, 2... For consistency with existing texts, the IF will henceforth be denoted by ω_0. The RF for a 2nd order harmonic mixer will therefore be given by $\omega_2 = \omega_0 + 2\omega_p$ or $\omega_{-2} = \omega_0 - 2\omega_p$. The analysis of any diode circuit under LO and RF excitation can be represented graphically as in Figure 2.10.

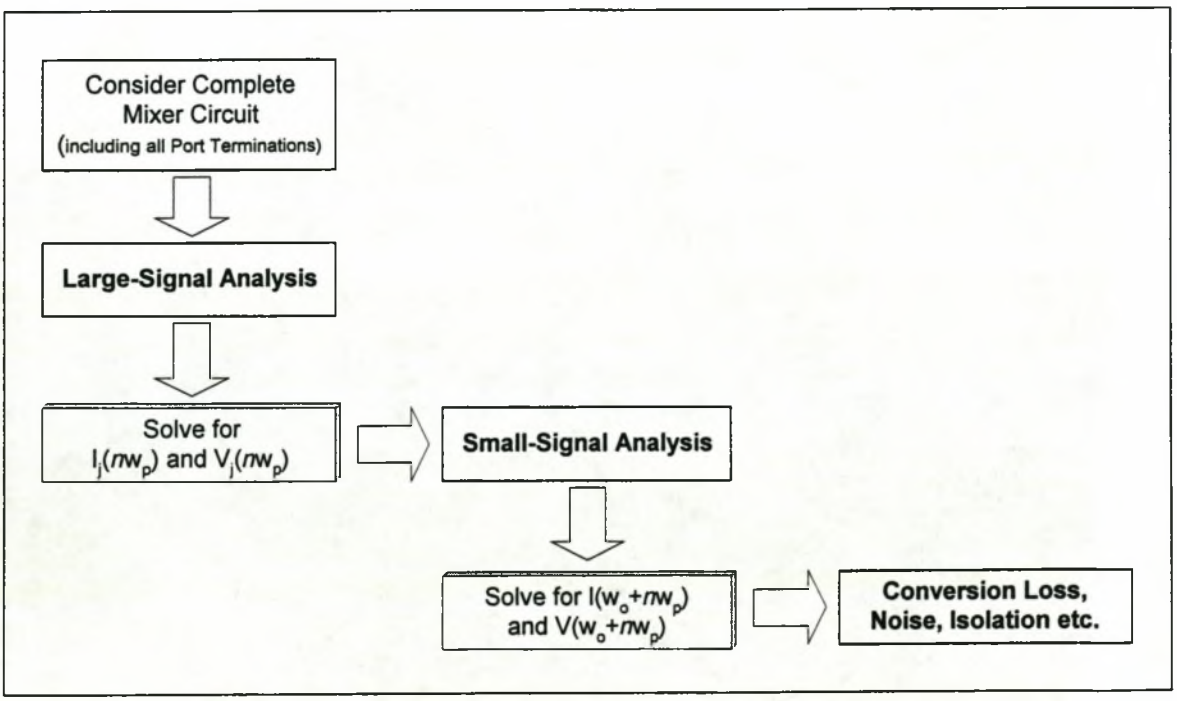

Figure 2.9 : Diagram of Generalized Mixer Analysis

The following discussion of mixer analysis will follow the topology presented in Figure 2.10. Once the large-signal and small-signal analysis have been done, the mixer performance will be related to the "figure of merit" mixer properties introduced in Chapter 1.

2.3.1 Large-Signal Analysis

The first step in the analysis of the diode circuit is a large-signal analysis. The junction of the diode(s) contains both a conductance and a capacitance that are strong nonlinear functions of the diode junction voltage $V_j(t)$. It is required to solve the currents through these elements at the various frequencies of the applied junction voltage. Once the currents and voltages are solved, the Fourier components of the junction conductance can be calculated, and simultaneously the junction conductance waveform $g(t)$ can be computed, i.e. a time-domain waveform of the pumped diode conductance can be obtained. Although it is the Fourier components rather than the time-domain waveform that are used in the following small-signal analysis, the shape of $g(t)$ can nevertheless provide useful information regarding the order of the change in conductance as the junction is pumped by the LO.

Various techniques to obtain the voltages and currents at the LO have been presented. [18, 19, 13]. The *harmonic balance technique* has evolved to a very robust solution algorithm, and is the most popular technique used in modern software packages. This technique will be presented in the following section. Although not as popular as the HB (harmonic balance) technique, the *reflection algorithm* [20] remains a useful tool in large-signal analysis, and is included in Appendix A for completeness.

2.3.2 Harmonic Balance for Single Diode [18, 19]

The harmonic balance technique determines the junction current and voltage at each LO harmonic by "balancing" the currents of the linear and the nonlinear parts of the diode circuit. A brief overview of the HB technique for a single diode will be given, whereupon the technique will be modified for the antiparallel diode pair.

The aim of the technique is to find the time-domain junction voltage $V_j(t)$, or alternatively $V_j(n\omega_p)$ for $n = ..., -2, -1, 0, 1, 2, ...$ in the frequency domain, where ω_p represents the LO. Once the junction voltage is known, the junction current $I_d(t)$ or $I_d(n\omega_p)$ is also known.

The large-signal junction characteristics are completely described in terms of the large-signal junction voltage V_j by the following equations :

$$I_d(V_j) = I_0\left(e^{\frac{qV_j}{\eta KT}} - 1\right) \qquad \text{.....(2.25)}$$

$$I_c(V_j) = C_{j0}\frac{dV_j}{dt} \qquad \text{.....(2.26)}$$

where

$$C(V_j) = \frac{dQ_j}{dV_j} = \frac{C_{j0}}{\left(1 - \frac{V_j}{\varphi_{bi}}\right)^{1/2}} \qquad \text{.....(2.27)}$$

The circuit that will be analyzed usually contains a diode junction *embedded* within a linear network. This linear network includes the diode series resistance, package parasitic impedances, the matching networks, and any source and load impedances (usually the RF source and IF terminating impedance). Figure 2.11 shows the typical setup with LO source, IF and RF terminations (large signal excitation, therefore no RF signal is applied), and the complete diode.

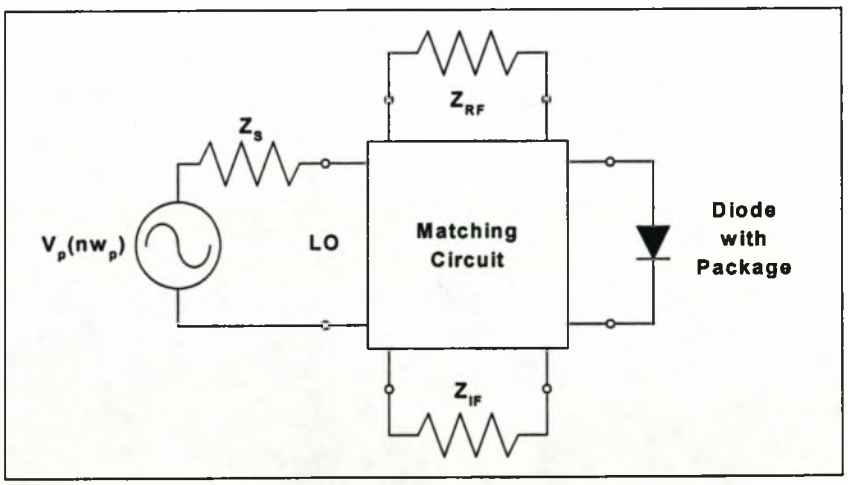

Figure 2.10 : Equivalent Circuit of Mixer with Single Diode

By manipulating the elements shown in Figure 2.11, it is possible to divide the entire circuit into a linear part and a nonlinear part. The linear part will include the LO source, all terminating impedances (Z_S, Z_{RF} and Z_{IF}), the entire matching circuit, the linear time-invariant components of

the diode package, and the diode series resistance R_s. The nonlinear part will consist of the junction conductance (modeled as a voltage dependent current source $I_g(V_j)$) in parallel with the nonlinear capacitor $C_j(V_j)$. The entire linear circuit (with the exception of the LO source) can be expressed as a row matrix $Y_E(n\omega_p)$ with its elements equal to the equivalent complex admittance at the harmonics of the LO. Figure 2.12 shows how the circuit from Figure 2.11 can be manipulated into a linear and a nonlinear part.

Once the circuit has been divided into a linear and nonlinear part, it becomes easy to understand the fundamentals of the harmonic balance method. While the linear part of the circuit contains time-invariant frequency dependent elements that is best described in the frequency domain, the nonlinear part of the circuit contains a time-variant capacitance and conductance that is best described in the time domain. An estimate of V_j is initially made at all the harmonics of the LO, whereupon the linear and nonlinear harmonic currents, I_l and I_{nl}, are calculated. An error function is created by the difference between I_l and I_{nl}, and V_j is chosen repeatedly (usually by means of a numerical method) until the error function is sufficiently small. Finally $V_j(n\omega_p)$ is known for all the harmonics, and the large signal time-domain LO waveform $V_j(t)$ can be constructed.

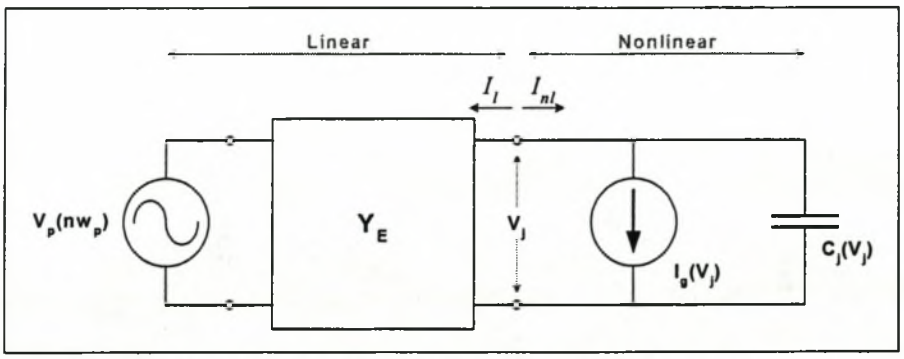

Figure 2.11 : Division of diode circuit in Linear and Nonlinear parts

From Figure 2.12 it is clear that the following condition (Kirchoff) must hold between the linear circuit and the nonlinear junction :

$$I_l(n\omega_p) = -I_{nl}(n\omega_p) \qquad \text{.....(2.28)}$$

for $n = 0,1,2,\ldots N$, or in vector form :

$$\begin{bmatrix} I_l(0) \\ I_l(\omega_p) \\ I_l(2\omega_p) \\ \vdots \\ I_l(N\omega_p) \end{bmatrix} = - \begin{bmatrix} I_{nl}(0) \\ I_{nl}(\omega_p) \\ I_{nl}(2\omega_p) \\ \vdots \\ I_{nl}(N\omega_p) \end{bmatrix} \quad \text{..... (2.29)}$$

The initial estimate of V_j will produce values of I_l and I_{nl} that can be used to create the *current-error vector* of the form

$$F(V_j) = I_l + I_{nl} \quad \text{..... (2.30)}$$

A numerical method is used to find $V_j(n\omega_p)$ so that equation (2.30) eventually becomes

$$F(V_j) = 0 \quad \text{..... (2.31)}$$

The computation of the current-error vector involves operations in both the time domain and the frequency domain. The matrix of the time-invariant currents in the linear circuit is computed as follows (from Figure 2.12) :

$$I_l = Y_E 3\ (V_j - V_n) \quad \text{..... (2.32)}$$

The currents in the nonlinear junction arise from equations in the time domain. The nonlinear current I_{nl} is made up of the resistive current I_g and the reactive current I_c, or

$$I_{nl} = I_g + I_c \quad \text{..... (2.33)}$$

where I_g is defined by equation (2.6), and I_c is found using equation (2.3) :

$$i_c = \frac{d}{dt} Q_d = \frac{d}{dt}\left(C_{j0}\varphi_{bi}\sqrt{1-\frac{V_j}{\varphi_{bi}}} \right) \quad \text{..... (2.34)}$$

Instead of finding the time-derivative using numerical techniques (which may be cumbersome), the capacitor current is easily found in the frequency domain :

$$i_c = \Im^{-1}\{j\Omega Q_d\} \qquad \text{..... (2.35)}$$

where Ω is a diagonal matrix with $(n\omega_p)$ for $n = 1,2,3,...N$ on its diagonal axis. The current-error vector $F(V_j)$ can now be computed in the time domain :

$$F(V_j) = \Im^{-1}\{I_l\} + i_{nl} \qquad \text{..... (2.36)}$$

The numerical technique for finding V_j to satisfy equation (2.36) can be one of a variety of optimization techniques [9]. The Newton-Raphson iteration is used most commonly. After p iterations V_j is described by Newton's method as follows (in the time domain) :

$$V_j^{p+1} = V_j^p - J^{-1}3F(V_j) \qquad \text{..... (2.37)}$$

where J is the Jacobian matrix, defined as

$$J = \frac{\partial}{\partial V_j} F(V_j) = Y_E + \frac{\partial I_g}{\partial V_j} + j\Omega \frac{\partial Q_d}{\partial V_j} \qquad \text{..... (2.38)}$$

V_j is found using various matrix manipulations of its comprising terms. Since only an overview of the method is presented here, these manipulations are omitted.

Once the voltage V_j is solved for all the harmonics of the LO the junction can be completely characterized in terms of its voltage $V_j(n\omega_p)$ and current $I_j(n\omega_p)$. Since V_j is known, it is possible to find the junction conductance waveform $g_j(t)$ via equation (2.25), as well as the junction capacitance waveform $C_j(t)$ via equation (2.27). As mentioned at the beginning of the section, the Fourier components of the total junction conductance $G(j\omega_p)$ at the harmonics of the LO can now be found from Ohm's law :

$$G(j\omega_p) = \frac{I_j(j\omega_p)}{V_j(j\omega_p)} \qquad \text{..... (2.39)}$$

and the time-domain junction waveform $g(t)$ can be found through taking the inverse Fourier-transform of equation (2.39).

Using the HB method to solve the junction currents and voltages of the antiparallel diode pair involves only slight alterations of the technique for a single diode described above, as will be shown in the next section.

2.3.3 Harmonic Balance for Antiparallel Diode Pair

When analyzing the antiparallel diode pair, one essentially has to analyze a circuit containing two diodes, and therefore two nonlinearities. Although the basic analysis remains the same (such as described in the previous section), there are two possible methods, depending on the complexity of the problem :

- The circuit can be reduced to a single nonlinearity, and analyzed in a way similar to a single diode;
- The circuit can be treated as a multiport network, and analyzed accordingly.

While the first method often only caters for trivial solutions, the second method accommodates for a non-trivial circuit. The second method will be presented first.

2.3.3.1 Multiport Network [13]

The expansion of a mixer with an antiparallel diode pair into a multiport network is similar to the representation in Figure 2.12. The entire embedding circuit is connected to the two diodes A and B via a series of ports. These are not physical ports, but rather ports representing the various harmonics of the LO. Figure 2.13 contains such a representation.

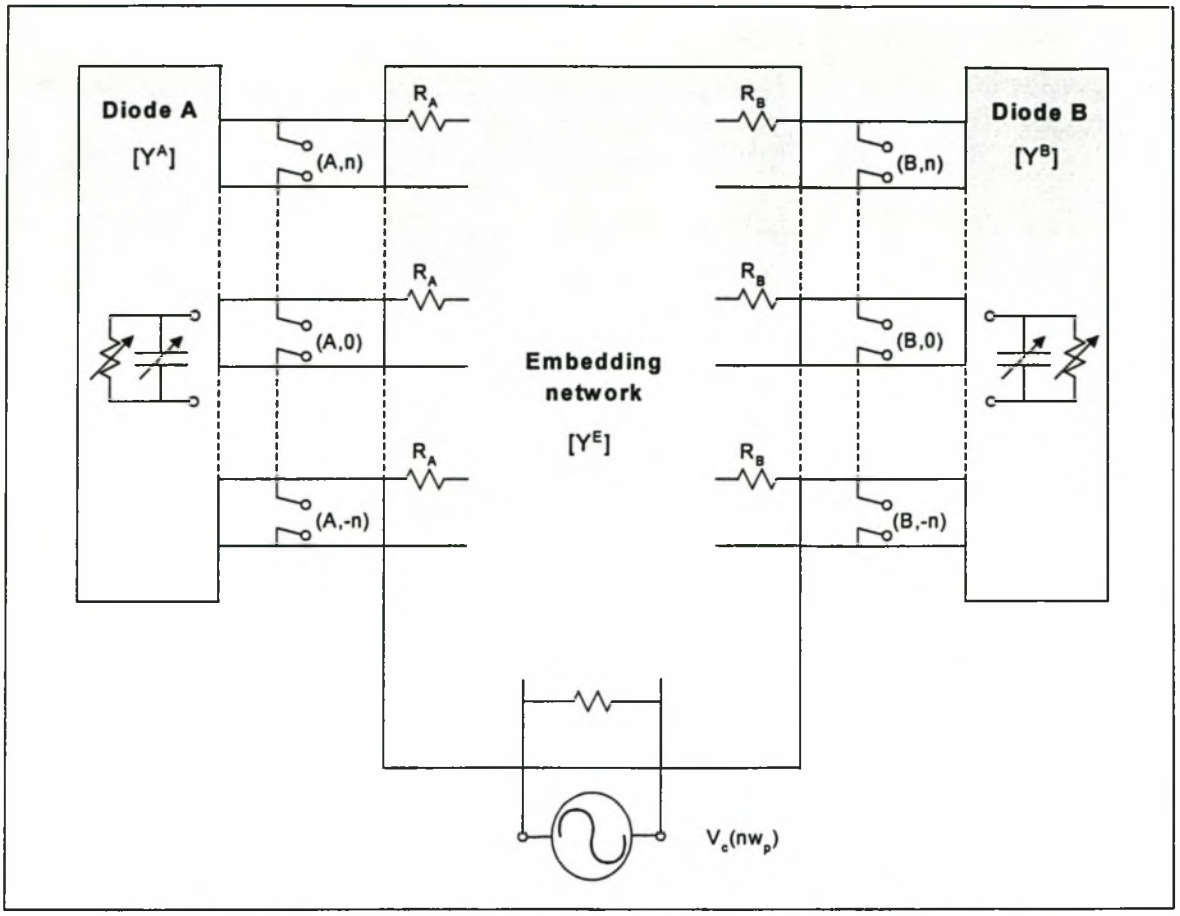

Figure 2.12 : Large-Signal circuit of a mixer with an antiparallel diode pair

Diode A is connected to the linear network through a series of ports at the frequencies $n\omega_p$ (for n = ...*-1, 0, 1,* ...), representing the harmonics of the LO. Diode B is connected in a similar fashion. The LO is applied at port C, similar to the single diode mixer.

The analysis of the multiport is similar to the previous analysis, except that vectors are now replaced by vectors of vectors. The linear current vector of equation (2.29) now become vectors of current vectors, or

$$\boldsymbol{I}_l = \begin{bmatrix} \boldsymbol{I}_{l,A} \\ \boldsymbol{I}_{l,B} \\ \boldsymbol{I}_{l,C} \end{bmatrix} \qquad \text{..... (2.40)}$$

where, for instance, $\boldsymbol{I}_{l,A}$ is the matrix

$$\boldsymbol{I}_{l,A} = \begin{bmatrix} I_l(0) \\ I_l(\omega_p) \\ I_l(2\omega_p) \\ \vdots \\ I_l(N\omega_p) \end{bmatrix} \qquad \text{..... (2.41)}$$

Similarly the nonlinear current vector of equation (2.29) becomes

$$\boldsymbol{I}_{nl} = \begin{bmatrix} \boldsymbol{I}_{nl,A} \\ \boldsymbol{I}_{nl,B} \end{bmatrix} \qquad \text{..... (2.42)}$$

Note that no nonlinear current component flows in port C. The estimated voltage (V_j in the previous section) is also put in vector format :

$$\boldsymbol{V} = \begin{bmatrix} V_A \\ V_B \\ V_C \end{bmatrix} \qquad \text{..... (2.43)}$$

In a way similar to equation (2.32), the linear current components $\boldsymbol{I}_l$ are found as follows :

$$\boldsymbol{I}_l = \boldsymbol{Y}\boldsymbol{V} \qquad \text{..... (2.44)}$$

where $\boldsymbol{Y}$ is a 3-by-3 matrix with sub-matrixes similar to Y_E. The nonlinear current components are found by solving equation (2.42) (effectively solving for each diode separately). Once the linear and nonlinear current components are known (for a specific value of $\boldsymbol{V}$), the error function $\boldsymbol{F}$ can be minimized, eventually solving for V_A and V_B.

It is clear that the obtaining the large-signal solution for the antiparallel diode pair via the multiport method is merely a "matrix-extension" of the harmonic balance method for the single diode. The alternative to the multiport method, i.e. the equivalent diode method, will now be considered briefly.

2.3.3.2 Equivalent Diode

The equivalent diode method evaluates the entire mixer circuit at every harmonic of the LO, and produces an equivalent (and usually rather simple) circuit containing only one diode. The analysis for a single diode described in section 2.3.2 can then be applied almost exactly. A drawback of this analysis is that it is often limited to a specific mixer, and is therefore not generic like the multiport method. The equivalent diode method can justifiably be viewed as a specific case of the multiport analysis.

Since the equivalent diode method is often specific to a certain mixer configuration, its implementation will be demonstrated using a specific mixer. Figure 2.14 shows a typical topology for a harmonic mixer. The antiparallel diode pair (consisting of identical diodes A and B, with their series resistance R_s and series inductance L_s) is driven by an LO source with impedance Z_{LO}. In general, the impedance Z_{LO} can represent the termination for a number of source and load impedances.

The key to the successful implementation of the equivalent diode method for this circuit lies in the symmetry of the configuration. The circuit as seen by the LO is symmetrical, except for the polarity of the diodes. This causes the even order LO harmonics to be out of phase over the diodes, producing zero voltage over the parallel LO branch. The odd LO harmonics are in phase over the diodes, producing a voltage over the parallel LO branch [21]. The equivalent circuits seen by each diode at the various LO harmonics are summarized by Figure 2.15.

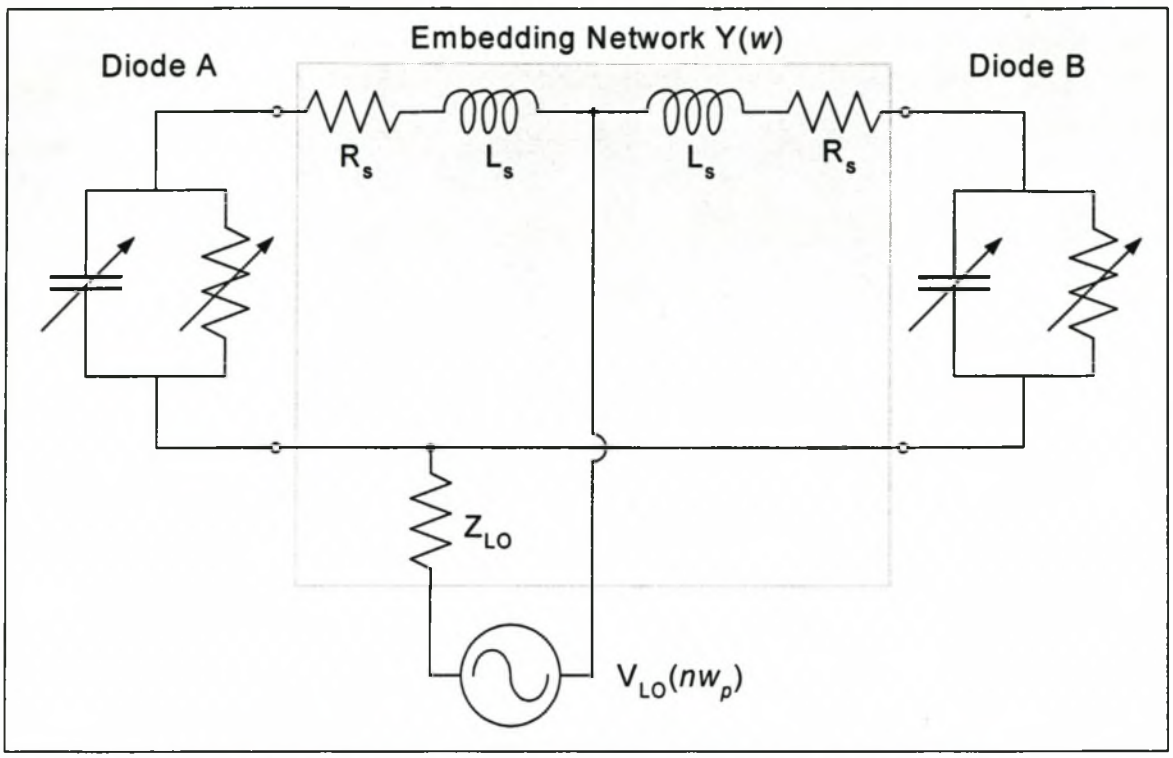

Figure 2.13 : Equivalent circuit of Antiparallel diode pair driven by LO

The matrix $I_l(n\omega_p)$ of equation (2.29) representing the linear current components can now be constructed using the circuits of Figure 2.15. The remainder of the analysis, i.e. the nonlinear current components, minimization of the error function, and solution for $V(n\omega_p)$, is conducted exactly according to the process described in section 2.3.2.

On completion of the large-signal analysis, the set of harmonic voltages $V_j = V_j(n\omega_p)$ and harmonic currents $I_d = I_d(n\omega_p)$ for n = 0,1,2,... are known. In the next section it will be shown how the small-signal parameters for the antiparallel diode pair is obtained once the large signal analysis has been done.

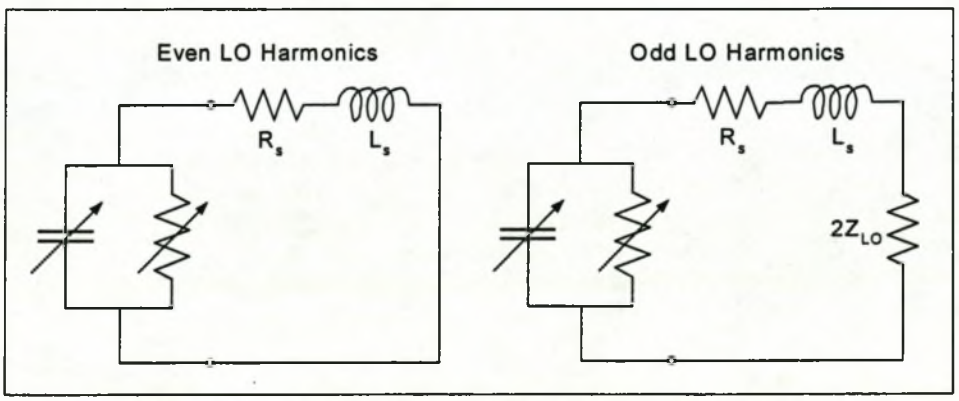

Figure 2.14 : Equivalent Mixer Circuits at harmonics of the LO

2.4) Small-Signal Diode Parameters

Once the LO is solved in the way described in the preceding section, all large-signal quantities are known, and the small-signal analysis is done. Defining the small-signal impedances of the mixer involves not only the LO frequency ω_p (as was the case with the large-signal analysis), but also the IF frequency ω_0. The small-signal analysis will give the input impedance to the mixer at all the frequencies ω_n, where

$$\omega_n = \omega_0 + n\omega_p \qquad \text{..... (2.45)}$$

and n is the n-th LO harmonic. The list of input impedances can be calculated most effectively through matrices, which gave rise to the term *"conversion matrix"*. Conversion matrices are first generated separately for the junction conductance and junction capacitance of the separate diodes (thus a total of four matrices, of which two pairs are identical in the ideal scenario of balanced diodes). Thereafter the admittance matrix $\boldsymbol{Y}_e$ for the embedding network (Figure 2.13) of the entire mixer is constructed (the admittance matrix is used instead of the impedance matrix, allowing admittance components to be simply added together). Finally the conversion matrix $\boldsymbol{Y}_M$ for the entire mixer (including the antiparallel diode pair) is constructed.

2.4.1 Conversion Matrix for Junction Conductance

The voltage across the junction can be represented by a set of time-domain phasors $v(t)$ given by [9]

$$v(t) = \sum_{n=-\infty}^{\infty} V_n \angle\left(\left(\omega_0 + n\omega_P\right)t\right) = \sum_{n=-\infty}^{\infty} V_n e^{j\left(\omega_0 + n\omega_P\right)t} \qquad \text{..... (2.46)}$$

where V_n is the voltage component at frequency ω_n (obtained by the HB method)and ω_0 is the IF frequency. Note that the waveform $v(t)$ is a sum of phasor quantities – effectively a summation of sinusoids of magnitudes and angles contained in V_n, and with frequency given by $(\omega_0 + n\omega_p)$. $v(t)$ is expressed here as a complex function in the time-domain. In a similar way the current through the nonlinear conductance is defined as

$$i(t) = \sum_{n=-\infty}^{\infty} I_n e^{j\left(\omega_0 + n\omega_P\right)t} \qquad \text{..... (2.47)}$$

From the definition, the Fourier series of a time-varying resistance $r(t)$ is

$$r(t) = \sum_{n=-\infty}^{\infty} R_n e^{jn\omega_P t} \qquad \text{..... (2.48)}$$

The R_n-elements are the small-signal values for the junction resistance. They are found using equation (2.7) (section 2.1.2.2). $r(t)$ therefore represents the time-domain waveform of the resistive part of the diode junction, as the diode is pumped by the LO.

Using Ohm's law, the relationship between equations (2.46) – (2.48) is given by equation (2.49). Note that the number of harmonics n has been limited to a finite number so that n = $-N$, ..., N. This corresponds to the number of harmonics used in the large-signal solution. In matrix notation:

$$\begin{bmatrix} I_{-N} \\ \vdots \\ I_N \end{bmatrix} = \begin{bmatrix} G_0 & \cdots & G_{-2N} \\ \vdots & \ddots & \vdots \\ G_{2N} & \cdots & G_0 \end{bmatrix} \begin{bmatrix} V_{-N} \\ \vdots \\ V_N \end{bmatrix} \qquad \text{..... (2.49)}$$

or

$$\boldsymbol{I} = \boldsymbol{G_j V} \qquad \text{..... (2.50)}$$

The elements of the junction conductance conversion matrix $\boldsymbol{G_j}$ are a function of both the LO frequency ω_p and the applied IF signal, and provides the solution to the small signal impedance of the junction conductance for the frequencies $\omega_n = \omega_0 + n\omega_p$ for the first N harmonics.

2.4.2 Conversion Matrix for Junction Capacitance

The small-signal voltage over and current through the junction capacitance are again given by equations (2.46) and (2.47). The small-signal junction capacitance is given by equation (2.9) :

$$i_c(t) = \frac{dq(t)}{dt} = c(t)\frac{dv(t)}{dt} + v(t)\frac{dc(t)}{dt}$$

Similar to equation (2.50), the small-signal voltages and currents for the junction capacitance are related by the following equation :

$$\boldsymbol{I} = j\Omega \boldsymbol{C}_j \boldsymbol{V} \qquad \text{.....(2.51)}$$

where $\boldsymbol{C}_j$ is the junction capacitance conversion matrix (similar to the conductance conversion matrix of equation 2.49). Ω is a diagonal matrix with elements $jn\omega_p$, accounting for the frequency dependence of the impedance presented by the junction capacitance. The elements of matrix $\boldsymbol{C}_j$ are the Fourier components of the time-varying capacitance. Therefore $j\Omega\boldsymbol{C}_j$ provides the small-signal impedance of the junction capacitance for the frequencies $\omega_n = \omega_0 + n\omega_p$ over the first N harmonics.

2.4.3 Mixer Conversion Matrix

Instead of treating the antiparallel diode pair separately from the rest of the mixer, it is preferred to find a conversion matrix representing the entire mixer. This is done to assist subsequent small-signal analysis [22].

The process of generating the small-signal conversion matrix for the entire mixer can be better understood when the mixer is once again treated as a multiport network (section 2.3.3.1). Figure 2.13 is altered slightly to make provision for the additional frequencies. Figure 2.16 shows the new model for the mixer.

Figure 2.16 shows the entire mixer circuit including the antiparallel diode pair (diodes A and B with their series resistances R_A and R_B respectively). The diodes are evaluated at frequencies $\omega_o+n\omega_p$. This evaluation consists of the large-signal and small-signal analysis described in the above sections, and is represented by the various "ports" between the diode and the remainder of the mixer circuit. This remainder, or embedding network $\boldsymbol{Y}_E$, contains the diodes' series resistances, all matching networks, etc., and is evaluated at frequencies $\omega_o+n\omega_p$ using linear circuit analysis. It is significant that port C (representing the source and load impedances) contains more ports than the single port it contained for the large-signal analysis. This facilitates the small-signal analysis of the mixer at frequencies $\omega_o+n\omega_p$.

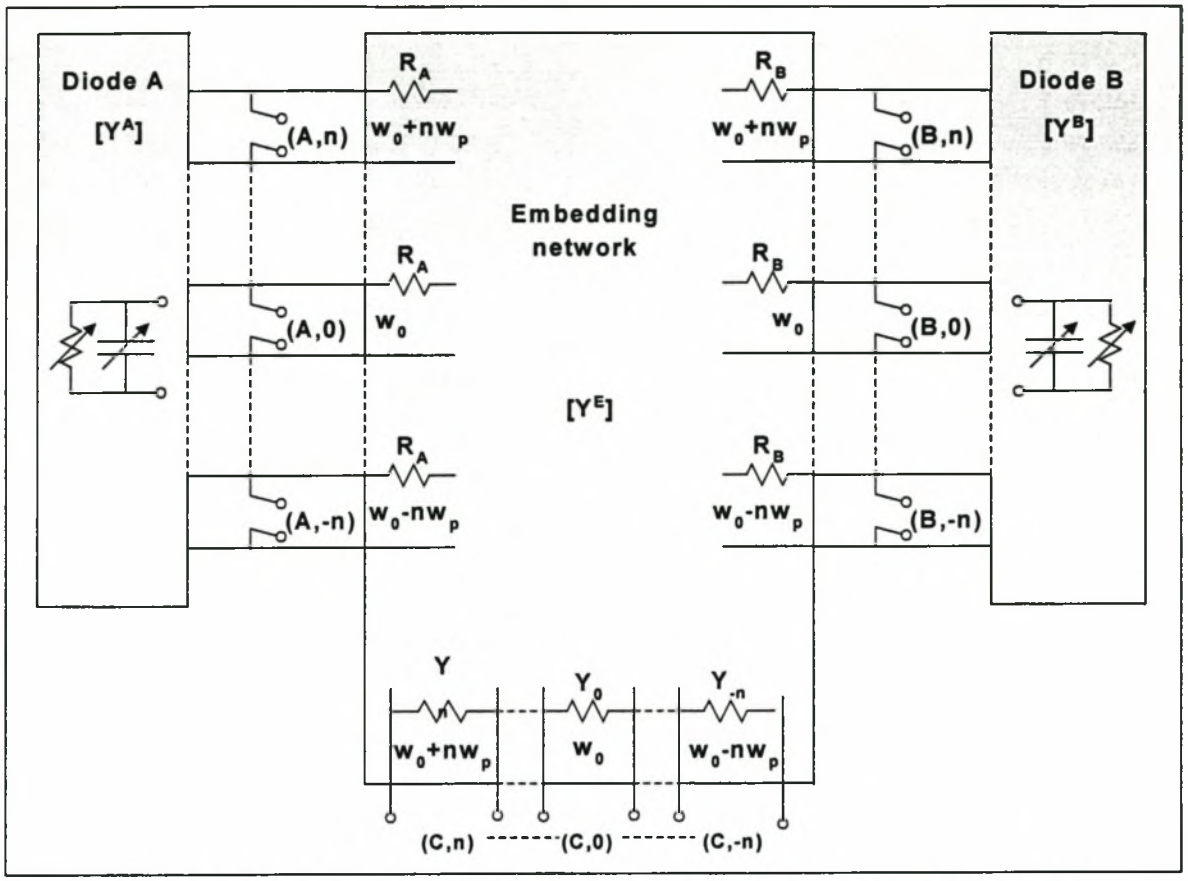

Figure 2.15 : Small-Signal equivalent model for mixer with antiparallel diode pair

For a typical harmonic mixer the following holds for port *C*:

- ω_0 represents the IF and Y_0 is the IF-port admittance with $Y_0 = 1/50\ \Omega$;
- $\{\omega_o+2\omega_p\}$ is the RF frequency, with $Y_2 = 1/50\ \Omega$;
- The remainder of the ports represents the various mixing frequencies, and are either not considered if they are significantly small, or are reactively terminated, short- or open-circuited, depending on the design.

The first step to finding the complete mixer conversion matrix is to determine the conversion matrices separately for the two diodes, A and B. The junction conversion matrices are found from equations (2.50) and (2.51), and the conversion matrices for the entire diode (excluding package parasitics) are then found by summing the corresponding elements of equations (2.50) and (2.51), or

$$Y_A = G_{j_A} + j\omega C_{j_A}$$
$$Y_B = G_{j_B} + j\omega C_{j_B} \qquad \text{..... (2.52)}$$

In order to illustrate the method, a harmonic mixer circuit is analyzed using only two harmonics. The conversion matrix for diode A, Y_A, is constructed as follows :

$$Y_A = \begin{bmatrix} (G_{j_0} + j\omega_0 C_{j_0}) & (G_{j_{-1}} + j\omega_0 C_{j_{-1}}) & (G_{j_{-2}} + j\omega_0 C_{j_{-2}}) & (G_{j_{-3}} + j\omega_0 C_{j_{-3}}) & (G_{j_{-4}} + j\omega_0 C_{j_{-4}}) \\ (G_{j_1} + j\omega_1 C_{j_1}) & (G_{j_0} + j\omega_1 C_{j_0}) & (G_{j_{-1}} + j\omega_1 C_{j_{-1}}) & (G_{j_{-2}} + j\omega_1 C_{j_{-2}}) & (G_{j_{-3}} + j\omega_1 C_{j_{-3}}) \\ (G_{j_2} + j\omega_2 C_{j_2}) & (G_{j_1} + j\omega_2 C_{j_1}) & (G_{j_0} + j\omega_2 C_{j_0}) & (G_{j_{-1}} + j\omega_2 C_{j_{-1}}) & (G_{j_{-2}} + j\omega_2 C_{j_{-2}}) \\ (G_{j_3} + j\omega_3 C_{j_3}) & (G_{j_2} + j\omega_3 C_{j_2}) & (G_{j_1} + j\omega_3 C_{j_1}) & (G_{j_0} + j\omega_3 C_{j_0}) & (G_{j_{-1}} + j\omega_3 C_{j_{-1}}) \\ (G_{j_4} + j\omega_4 C_{j_4}) & (G_{j_3} + j\omega_4 C_{j_3}) & (G_{j_2} + j\omega_4 C_{j_2}) & (G_{j_1} + j\omega_4 C_{j_1}) & (G_{j_0} + j\omega_4 C_{j_0}) \end{bmatrix}$$

where for example G_{j-2} is the junction conductance evaluated at $\omega_{n=-2} = \omega_0 - 2\omega_p$, and ω_3 represents the frequency $\omega_{n=3} = \omega_0 + 3\omega_p$. The conversion matrix for diode B is constructed in a similar way, and when the diodes are identical, $Y_A = Y_B$.

The conversion matrix for the embedding matrix, Y_E, is found relatively easily from linear circuit analysis. However, since there are three ports to be considered (A, B and C), special care has to be taken when defining Y_E. The most popular notation constructs Y_E as a 3-by-3 matrix containing nine individual sub-matrices. Y_E is defined as follows :

$$Y_E = \left[\begin{array}{c|c|c} Y_E^{AA} & Y_E^{AB} & Y_E^{AC} \\ \hline Y_E^{BA} & Y_E^{BB} & Y_E^{BC} \\ \hline Y_E^{CA} & Y_E^{CB} & Y_E^{CC} \end{array}\right] \qquad \text{.....(2.53)}$$

The sub-matrices represent the relation of the different ports to each other, and have the general form $Y_E^{(port)(port)}(\omega_n)$. Y_E^{AA}, for example, represents the input admittance of the embedding network at port A for the frequencies $\omega_n = \omega_0 + n\omega_p$, while Y_E^{AC} represents the admittance of the embedding network from port A to port C. The sub-matrices of Y_E are diagonal matrices, since the linear network implies no coupling between the various frequencies inside the embedding network [22]. The sub-matrices are the same size as the diode conversion matrices, i.e. with dimension 2N+1 when N harmonics are considered.

The final step in setting up the mixer conversion matrix is to add the conversion matrices of the individual diodes to the conversion matrix of the linear network. By coupling the diodes in parallel with the embedding network (the typical topology, denoted by Figure 2.16), the diode

conversion matrices can be added to the conversion matrices representing the embedding network's input impedance presented to the diodes, i.e. Y_E^{AA} and Y_E^{BB}. Equation (2.53) therefore becomes

$$Y_M = \left[\begin{array}{c|c|c} Y_E^{AA} + Y_A & Y_E^{AB} & Y_E^{AC} \\ \hline Y_E^{BA} & Y_E^{BB} + Y_B & Y_E^{BC} \\ \hline Y_E^{CA} & Y_E^{CB} & Y_E^{CC} \end{array}\right] \quad \text{.....(2.54)}$$

where Y_M is the compound conversion matrix of the entire mixer. Note that the addition of the diodes to the embedding network does not alter the coupling between the various ports, and therefore the remainder of the sub-matrices of Y_E is unaffected by the addition.

The mixer conversion matrix can be inverted to find the mixer impedance matrix, or [22]

$$Z_M = [Y_M]^{-1} \quad \text{.....(2.55)}$$

That concludes the small-signal solution of the mixer. In the following section Z_M will be used to find typical mixer parameters such as conversion loss, input impedance and VSWR.

2.4.4 Input Impedance

In Chapter 1 it was established that the diode's input impedance is a function of both the LO and RF signals (hence the terms small-signal and large-signal impedance). It is therefore only natural to expect that the diode conversion matrix (which is the result of both a small-signal and large-signal analysis) provides a convenient way of calculating the input impedance.

It will be necessary to distinguish between two different input impedances :

- The *mixer input impedance* : The mixer input impedance is the impedance seen when looking into a port of the mixer (typically the IF port). This impedance includes the effects of both the antiparallel diode pair, and the embedding network.
- The *diode input impedance* : The diode input impedance is the impedance of the antiparallel diode pair alone, excluding the embedding circuit.

The input impedance looking into any port *(C,k)* where $\omega_k = \omega_0 + k\omega_p$ is defined as [22]

$$Z_{port_k} = Z_M^{(C,k)(C,k)} \triangleq Z_M^{CC}(k,k) \qquad \text{..... (2.56)}$$

However, equation (2.56) includes the port admittance Y_k, as shown in Figure 2.16. To obtain the mixer input impedance, it is therefore necessary to remove the effect of Y_k, or

$$Z_{in_k} = \left[Z_M^{(C,k)(C,k)} - \frac{1}{Y_k} \right] \qquad \text{..... (2.57)}$$

The input impedance of the antiparallel diode pair will prove to be a quantity of interest during the design of the harmonic mixer. In an oversimplified way it can be seen that the LO signal dictates the impedance seen by an input port at the small-signal frequencies (ω_s and ω_n). Mixer design then requires the correct embedding structure to ensure maximum power transfer at the IF and LO. This topic will be handled in detail later.

2.4.5 Conversion Loss

In Chapter 1 conversion loss was defined as the ratio of output signal level to input signal level, or

$$L_c[dB] = P_{RF}[dB] - P_{IF}[dB]$$

where P_{IF} is the IF output power ad P_{RF} is the available RF power. Although conversion loss is defined by this expression, a general expression for the conversion loss of a harmonic mixer containing an antiparallel diode pair within an embedding network needs to be found.

Such an expression is found using the small-signal mixer analysis described in the previous section [9], since the mixer impedance matrix Z_M is already in a convenient form to carry out the analysis. The specific method determines the conversion loss L_c *from* a specific sideband $\omega_k = \omega_0 + k\omega_p$ *to* the IF ω_0. Usually the sideband in question will be the RF signal, and $k = 2$ for the typical harmonic mixer.

A small current is applied to the RF port ($k = 2$), resulting in a response at the IF port [22]. This small current is represented by

$$\delta I^{(C,k)}$$

and the resulting response at the IF port is given by

$$\delta V^{(C,0)} = Z_M^{(C,0)(C,k)} \delta I^{(C,k)} \quad \text{..... (2.58)}$$

where $Z_M^{(C,0)(C,k)}$ is the impedance between the RF port and the IF port. The power available from the RF source is given by

$$P_{RF} = \frac{\left|\delta I^{(C,k)}\right|^2}{4\,Re\{Y_k\}} \quad \text{..... (2.59)}$$

where Y_k is the input admittance of the RF source (from Figure 2.16) [9]. The IF output power is given by

$$P_{IF} = \left|\delta V^{(C,0)}\right|^2 Re\{Y_0\} \quad \text{..... (2.60)}$$

where Y_0 is the termination admittance at the IF. Eliminating the small current $\delta I^{(C,k)}$ and small voltage $\delta V^{(C,0)}$ from equations (2.58) – (2.60), the conversion loss from the RF to the IF is found to be

$$L_{0,k} = \frac{1}{4\left|Z_M^{(C,0)(C,k)}\right|^2 Re\{Y_k\} Re\{Y_0\}} \quad \text{..... (2.61)}$$

where k refers to the RF (but could refer to any frequency in general). Further quantitative analysis of equation (2.61) will not be carried out in the current text, but further insight into the calculation of the conversion loss can be gained by considering a method proposed by [9]. The mixer is again divided into a linear and nonlinear part, as shown by Figure 2.17 :

The arrows indicate power flow through the circuit. The amplitude of the RF excitation signal V_s can be expressed as

$$V_s = \sqrt{8P_T Re\{Z_e(j\omega_s)\}} \quad \text{.....(2.62)}$$

where P_T is the available power (unknown) that can be delivered to the pumped diode pair, represented by $\boldsymbol{Z_p}$. The current flowing in the loop is found using the diode conversion matrix $\boldsymbol{Z_p}$:

$$\boldsymbol{I} = (\boldsymbol{Z_p} + \boldsymbol{Z_e})^{-1} \boldsymbol{V_s} \quad \text{.....(2.63)}$$

where $\boldsymbol{Z_e}$ is the conversion matrix of the linear part of the circuit. The output power into the embedding circuit represented by $\boldsymbol{Z_e}$ at frequency ω_n is

$$P_n = \tfrac{1}{2}|\boldsymbol{I}(\omega_n)|^2 Re\{Z_e(j\omega_n)\} \quad \text{.....(2.64)}$$

The conversion loss is now found using equations (2.62) and (2.64) :

$$L_c = \frac{P_n}{P_T} \quad \text{.....(2.65)}$$

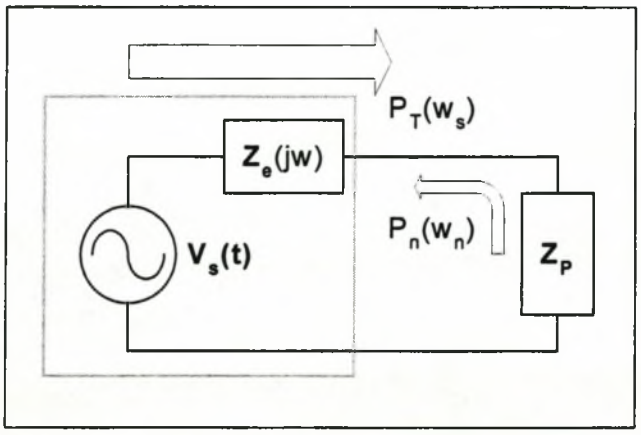

Figure 2.16 : Alternative Small-signal representation of Diode Mixer (with Power Flow)

2.5) Noise

The fundamentals for mixer noise analysis have been established remarkably early. Although a reliable model was only obtained in the 1970's, the properties of noise correlation in mixers have

been understood before that time. Since the topic of noise is an extensive field in its own right [11, 14], the current text will only present the fundamentals.

In Chapter 1, mixer noise was categorized as either *inherent* noise, or *signal* noise. In Schottky diode mixers the dominant inherent noise sources are :

1) Thermal Noise – Generated in the series resistance,
2) Shot Noise – Generated in the junction.

The dominant signal noise source for the Schottky diode is noise sidebands on the LO. In a frequency mixer the noise-processes are rather simple to understand. The challenge arises when the correlation properties of the noise is investigated. As it will become evident, the time-varying junction creates the phenomenon by which the noise properties at all the mixing frequencies is linked to one another – from there the idea of correlation.

2.5.1 Thermal Noise

As mentioned briefly in the preceding section, thermal noise has its origin in the series resistance R_s. Thermal noise arises from the random agitation of electrons, and it is present in every medium capable of dissipating power. Apart from being temperature dependent, thermal noise is also frequency dependent, although it is the bandwidth B and not the absolute frequency that is of importance.

The noise added to the diode circuit by a resistance R can be modeled by an equivalent voltage source having the mean-square voltage given by

$$\overline{v^2} = 4KTBR \qquad \text{..... (2.66)}$$

where K is Boltzmann's constant and T is the absolute temperature [9]. The mean-square arises from the fact that the noise is a random process, but can be characterized in terms of its average. Note that equation (2.66) is only valid for non-cryogenic temperatures and frequencies below the sub-millimeter range. Equation (2.66) is a generalization of Planck's black body radiation law [8] at the mentioned temperatures and frequencies. Figure 2.18 shows the Schottky diode model adapted to include the effect of thermal noise.

2.5.2 Shot Noise

The electrons crossing the junction of the Schottky diode cause the current waveform to be approximated as a series of pulses, leading to the term "shot" noise. The instantaneous current varies with time due to the random nature of the flow of electrons, but the average current remains constant, and is a function of the dc current flowing through the junction.

The shot noise in a Schottky diode can be adequately modeled by an equivalent current source (rather that a voltage source, as was the case with thermal noise). The mean-square equivalent current source for the shot noise due to a current I_j flowing trough the junction is given by

$$\overline{i^2} = 2qBI_j \qquad \text{..... (2.67)}$$

where q is the charge of an electron. It must be noted that I_j is the current flowing through the resistive part of the junction [9]. Once again frequencies in the sub-millimeter range are implied. Higher frequencies reach the order of the inverse of the electron transit time across the junction. Figure 2.18 also shows the Schottky diode model adapted to include the effect of shot noise.

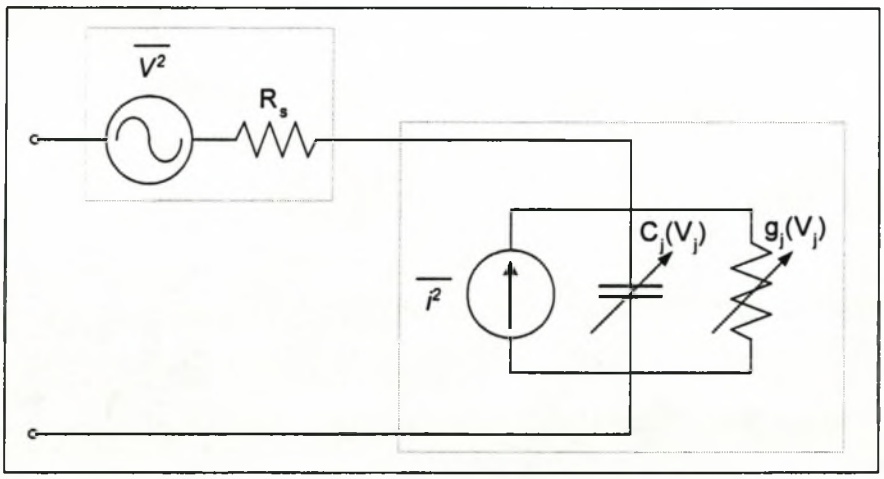

Figure 2.17 : Adaptation of the Schottky Diode model to include the effects of shot noise and thermal noise

2.5.3 Noise Correlation

Thermal and shot noise are treated as white Gaussian noise, therefore having a continuous and uniform spectrum within the frequency band B. To demonstrate how frequency components of the *unpumped* diode are not correlated, [9] dc-biased a Schottky diode, and created two noise waveforms at different frequencies by applying band-pass filters to the diode's noise. Since the

original two noise waveforms are only a function of the dc bias, it follows that the resulting mixing products are themselves functions of only the dc bias, and are therefore uncorrelated.

However, the situation changes once the diode is pumped by an LO signal. Although the thermal noise remains constant under LO excitation (since the series resistance R_s remains constant), the shot noise becomes a strong function of the applied LO signal. The shot noise "originates" at all the harmonics of the LO, and is then converted to all the mixing frequencies by the process of frequency mixing. Eventually the noise components at any mixing frequency include noise components from all the other mixing frequencies, and the noise components are therefore correlated.

The aim of an analysis will be to find the IF noise voltage due to the noise components from all the mixing frequencies. This is done considering the thermal noise and the shot noise separately.

2.5.3.1 Shot Noise

Following the large-signal analysis and the solution of the junction current $I_j(j\omega_p)$, it is possible to construct a matrix of noise currents at the mixing frequencies using equation (2.67). Using analysis similar to the small-signal analysis carried out in the previous sections, the impedance conversion matrix of the diode is related to the matrix of noise currents, resulting in the shot noise voltage across the junction at any frequency ω_m. Finally the shot noise correlation matrix C_s is created, giving the correlation between shot noise at the various mixing frequencies [22, 23].

2.5.3.2 Thermal Noise

The thermal noise does not vary with the applied LO, and is therefore uncorrelated at the various frequencies. Following the same procedure as above, the thermal noise correlation matrix C_t reduces to a simplified form of C_s. In effect C_t becomes a diagonal matrix.

The total noise voltage for a single diode at any frequency is a sum of the thermal and shot noise components, and employing C_t and C_s the total noise power dissipated in the load Z_e (Figure 2.17) at any frequency ω_m is given by

$$P_m = \frac{\overline{v_m^2} Re\{Z_e(j\omega_m)\}}{|Z_e(j\omega_m) + R_s|^2} \quad \text{..... (2.68)}$$

where v_m^2 is found using C_t and C_s. The single sideband noise temperature, or T_{SSB}, relates the total noise power to a single input source, and is a convenient way of expressing noise performance for one input frequency :

$$T_{SSB} = \frac{P_m}{KBG_{mn}} \quad \text{..... (2.69)}$$

where G_{mn} is the transducer gain between the input frequency ω_n and the output frequency ω_m [9]. For the antiparallel diode pair, [22] defines the single sideband noise temperature as

$$T_{M_2} = \frac{Z_M^{(C,0)} C \left[Z_M^{(C,0)} \right]^{*T}}{4K\, Re[Y_2] \times \left| Z_M^{(C,0)(C,2)} \right|^2 B} \quad \text{..... (2.70)}$$

where $Z_M^{(C,0)}$ is the input impedance to the mixer at the IF port and frequency, Y_2 is the source admittance of the RF signal, $Z_M^{(C,0)(C,2)}$ relates the coupling impedance between the IF and RF frequencies, C is the sum of the correlation matrices C_t and C_s, B is the bandwidth, and the $^*T$-superscript indicates the conjugate transpose of the vector.

2.5.4 Signal Noise [24]

The presence of noise sidebands on the LO is often a very real problem in receivers. The sideband noise-components mix with the LO, producing low frequency mixing components which are often situated very uncomfortably in the IF band (Chapter 1, Figures 1.8 and 1.9). However, in Section 2.2.5 (Figure 2.9) the antiparallel diode pair's ability to reject these mixing products from the IF band was described. The noise sideband mixes with 2LO, producing mixing products well outside of the IF band. This property is a function of the similarity of the diodes.

Simulation of the X-band mixer with identical diodes described in Chapter 4 shows typical rejection values in excess of 105dB. Although a realistic figure will be less, the ideal figure will be used for comparison in the following section.

2.6) Diode Unbalance

As with any balanced mixer, harmonic mixers suffer from the effects of diode unbalance. This effect is caused by a slight variation in the characteristics of the diodes, mainly due to manufacturing. This variation leads to unsymmetrical diodes, and the currents (and frequencies) that were confined to the diode loop in the ideal case, begin to "leak" into the embedding mixer circuit. The effects of diode unbalance have been investigated by [2, 25]. The most significant result of diode unbalance is definitely a decrease in isolation.

Most of the diode parameters are subject to a certain degree of variation. [2] has investigated the effect of variation in I_S and η, while [25] investigated a variation in R_S. The HSMS-8202 used for the designs in Chapter 4 specifies variations for C_{j0} and R_S [17]. In the current text the variation of these parameters will be investigated for the diodes used in the X-band 2nd-harmonic mixer designed in Chapter 4. The parameter variations will be considered individually with reference to the mixer's performance.

2.6.1 Theory

The variation of the diode saturation current I_S will now be expressed mathematically. Similar derivations can be made for the other parameters, but they will be omitted here due to space limitation.

[2] evaluates the effect of a variation in I_S by comparing the resulting different conductances g. If the difference in I_S is denoted by ΔI_S, the effective saturation currents for the two diodes become

$$I_{S1} = I_S + \Delta I_S \quad \text{and} \quad I_{S2} = I_S - \Delta I_S$$

respectively. From equation (2.15) the conductance for the pumped diode pair can now be given by [2]

$$g_p = 2\alpha I_s \left[\cosh(\alpha V_p) + \frac{\Delta I_S}{I_S} \sinh(\alpha V_p) \right] \qquad \text{.....(2.71)}$$

The ΔI_S-term introduces a *sinh*-dependence to the conductance. The asymmetrical *sinh*-function (as opposed to the symmetrical *cosh*-function) provides the mathematical mechanism for the unbalance effects.

2.6.2 Analysis

The effects of diode unbalance will now be investigated. The nominal values for the ideal HSMS-8202 diodes will be used, and are given below. The typical deviations from ideality, according to [17], are also indicated :

- $C_{j0} = 0.18 \pm 0.04\ pF$
- $R_S = 6 \pm 2\ \Omega$
- $\eta = 1.09 \pm 0.02$
- $I_S = 4.6e^{-8} \pm 0.5e^{-8} A$

The mixer containing the HSMS-8202 is pumped at an optimal LO level. The simulated conversion loss and isolation of selected frequency products are shown in the table below. The $\{\omega_{RF} - \omega_{LO}\}$ mixing product is an even order mixing product that should ideally be well isolated from the IF.

Diode Parameter Deviation	Conversion Loss [dB]	LO-to-IF Isolation [dB]	$\{\omega_{RF} - \omega_{LO}\}$ Isolation [dB]	LO Noise Isolation [dB]
Identical Diodes	7.2	30	140	110
$\Delta C_{j0} = 0.04\ pF$	7.7	30	70	49
$\Delta R_S = 2\Omega$	7.5	30	88	45
$\Delta\eta = 0.02$	7.3	30	100	74
$\Delta I_S = 0.5e^{-8} A$	7.2	30	110	90

Table 2.2 : Comparison of Mixer Performance for Diode Unbalance caused by variation of Diode Parameters. Only one parameter is varied at a time.

The results show that the mixer exhibits various levels of sensitivity to the diodes with unequal parameters. As it was expected, the level of isolation is significantly influenced by unbalance, while the conversion loss shows only slight deterioration. The unequal junction capacitance C_{j0} has the most profound effect on the level of unbalance, while the permitted variation in the saturation current I_S has an almost negligible effect on the isolation.

2.7) The Antiparallel Diode Pair – A Quantitative Analysis

Before the design of harmonic mixers is discussed in Chapter 4, a quantitative analysis of the antiparallel diode pair is done. The aim of this analysis is to investigate the antiparallel diode pair as a building block of harmonic mixers, and to become familiar with its performance. The waveforms of the antiparallel diode pair under LO drive will be investigated, whereafter the input impedance will be investigated. Finally a model for the antiparallel diode pair (which will be used for the designs in Chapter 4) is extracted.

2.7.1 LO Excitation

Figures 2.19 and 2.20 show a typical large-signal solution for the voltage waveform V_j appearing over the junctions of an antiparallel diode pair of HSMS-8202 Schottky diodes. For the purpose of the investigation the diodes are assumed to have no parasitic inductance or capacitance, and are driven at +3dBm at a frequency of 5 GHz.

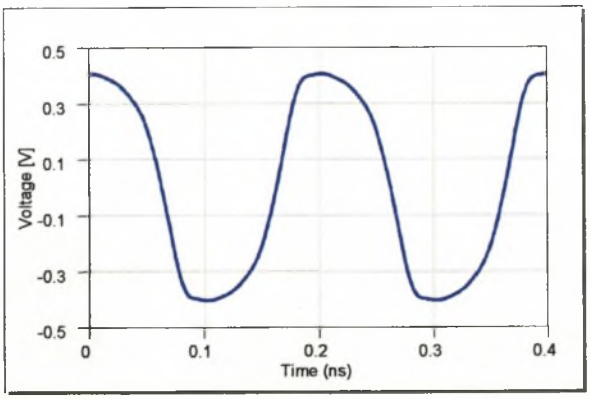

Figure 2.18 : Antiparallel diode pair LO time-Waveform

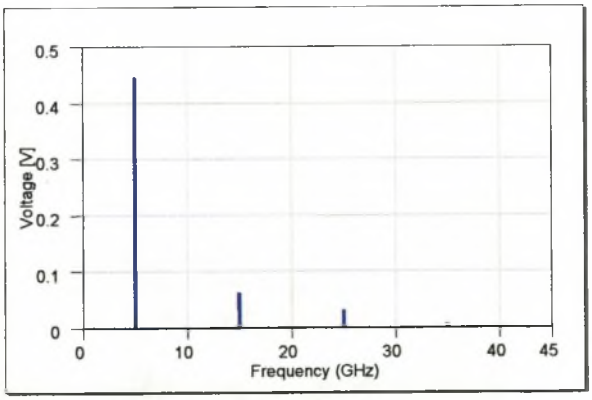

Figure 2.19 : Spectrum of Antiparallel Diode Pair LO Waveform

From the above figures it is noted that the LO is made up of mainly the 1st and 3rd harmonics at 5GHz and 15 GHz respectively. Unlike that of a single diode, the LO waveform for the antiparallel diode pair contains no dc component, and is symmetrical around the zero voltage axis.

The conductance $g_p(t)$ and capacitance $C_p(t)$ waveforms occurring as a result of the applied LO signal are shown in the figures below.

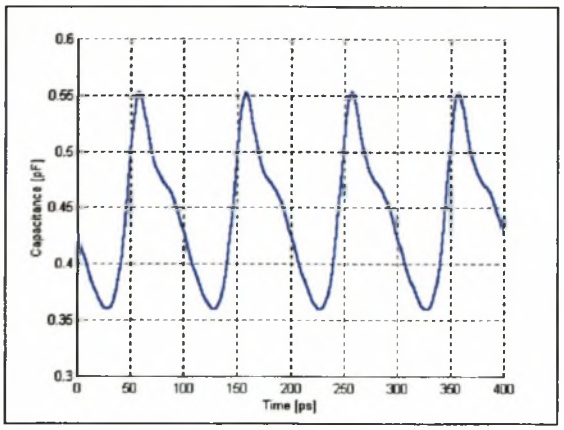

Figure 2.20 : Antiparallel Diode Pair Capacitance modulated by LO

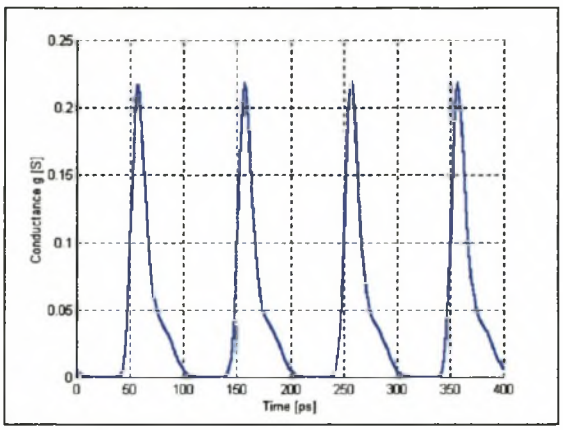

Figure 2.21 : Antiparallel Diode Pair Conductance modulated by LO

From Figures 2.21 and 2.22 it is clear that the conductance $g_p(t)$ plays the dominant role in the mixer's small-signal properties. The exponential characteristic causes the junction resistance to vary from several ohms to tens of kilo-ohms, while the inverse square-root characteristic of the junction capacitance only varies in the order of tens of picofarads. The conductance waveform has a fundamental frequency of twice the LO frequency – it is this mechanism that forms the heart of the antiparallel diode pair.

2.7.2 Large-Signal Input Impedance

By driving the antiparallel diode pair at various levels of power, a range of input impedances can be achieved. By keeping the LO power fixed and varying the frequency, a clockwise rotation is achieved on the smith chart (the effect of the junction capacitance). Figure 2.23 shows the traces obtained for the pair of HSMS-8202 Schottky diodes in an antiparallel configuration driven at power levels ranging from –10dBm to +10dBm over a frequency range of 40 GHz. Figure 2.24 shows the comparative traces for a single Schottky diode (HSMS-8101) under the same conditions.

From Figure 2.23 it can be seen that the antiparallel pair input impedance is governed by the real conductance $g_P(t)$ for lower frequencies, but becomes a stronger function of the junction capacitance $C_P(t)$ as the frequency increases. At frequencies beyond 40 GHz the input impedance becomes a function of almost exclusively the junction capacitance. Another phenomenon that is confirmed by the comparison of Figures 2.23 and 2.24, is the greater input impedance for a given

LO power of the antiparallel diode pair when compared to the single diode pair. Due to its parallel topology, the antiparallel diode pair has a greater junction conductance $g_p(t)$, while the junction capacitance $C_p(t)$ almost doubles. This is confirmed by Figure 2.25 below. The figure shows a plot of the calculated capacitance for both a single diode, and an antiparallel diode pair.

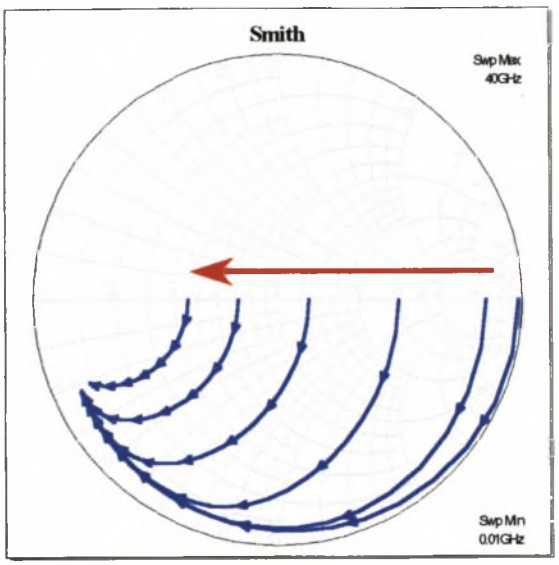

Figure 2.22 : Input Impedance of Antiparallel Diode Pair as function of LO Power. The arrow indicates increased LO Power.

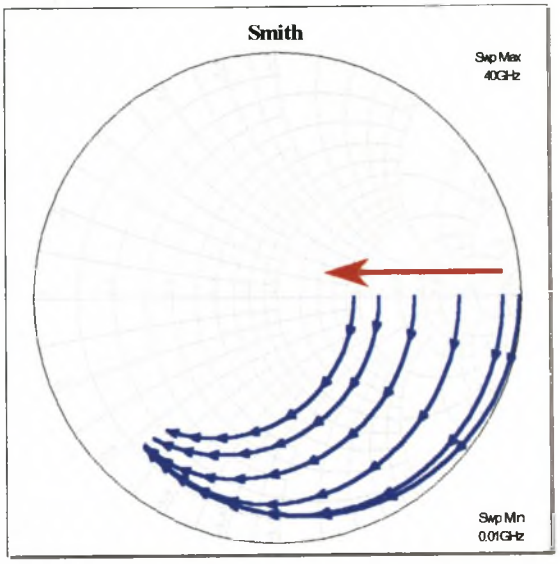

Figure 2.23 : Input Impedance of Single Diode as function of LO Power. The arrow indicates increased LO Power.

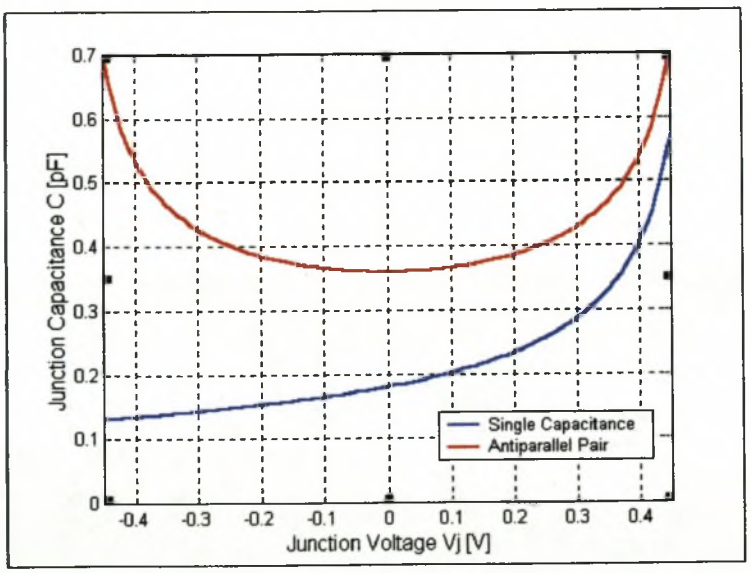

Figure 2.24 : Junction Capacitance as a function of Junction Voltage V_j for single diode and the Antiparallel diode

When the frequency is kept constant (5 GHz) and the LO is swept from –10 dBm to +10 dBm, the plot of Figure 2.26 is obtained for the antiparallel diode pair. It clearly shows how the input impedance is a function of LO power.

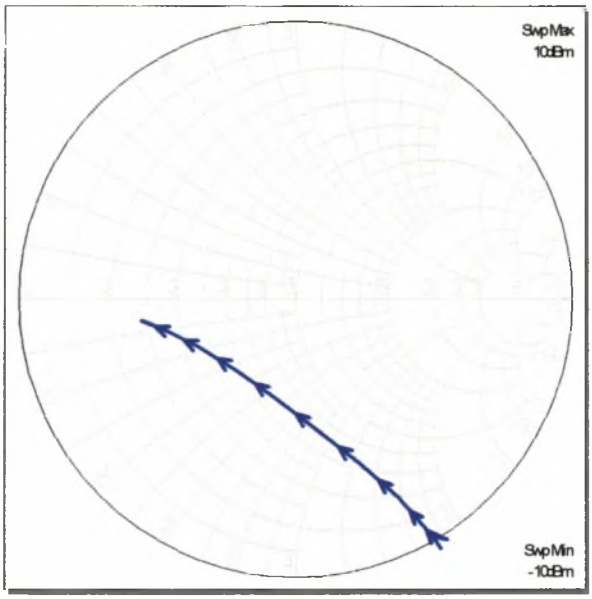

Figure 2.25 : Input Impedance of the Antiparallel Diode Pair for swept LO Power at 5 GHz

When the input impedance curve of Figure 2.26 is divided into real and imaginary parts, the plots of Figures 2.27 and 2.28 are obtained :

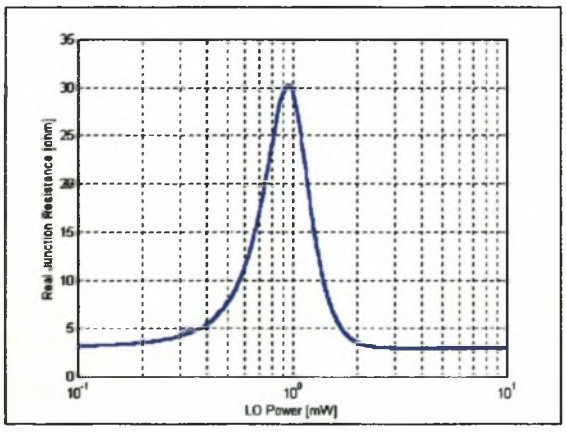

Figure 2.26 : Real part of the Antiparallel Diode Pair Junction Impedance

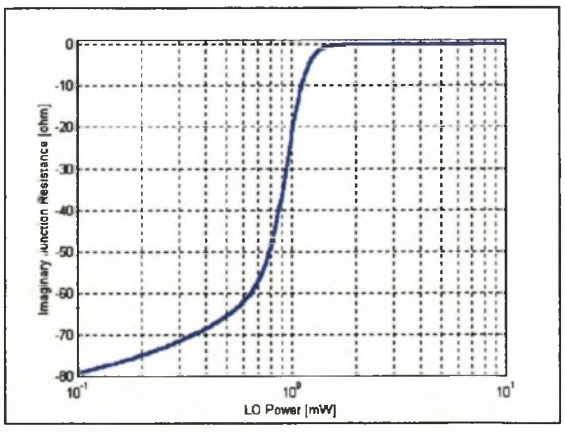

Figure 2.27 : Imaginary part of the Antiparallel Diode Pair Junction Impedance

From Figure 2.27 it is clear that there is an optimum real impedance presented by the antiparallel diode pair. Matching of this point to the source impedance will ensure minimum conversion loss.

2.7.3 Model

In order to carry out a successful mixer design, it is necessary to have an adequate model for the antiparallel diode pair. Although the topology for the HSMS-8202 has been established earlier in the chapter (Figure 2.4), it is necessary to verify the model with a measurement, and to modify the model if necessary.

The parameter values for the model of the HSMS-8202 Schottky diode as given in Table 2.1 were verified by measuring the diode pair over 12 GHz, for LO power levels of –10 dBm, 0dBm and +10 dBm. The diode was mounted in a jig comprising a SMA-connector on either side, and the sets of measurements were taken. A sufficient model [26] was used for the SMA-connector, and the measured diode model could be extracted from the measurements. The diode parameters were optimized within their range of possible values [17], and finally a model for the HSMS-8202 diodes was extracted. The traces for the different power levels are shown in Figure 2.29.

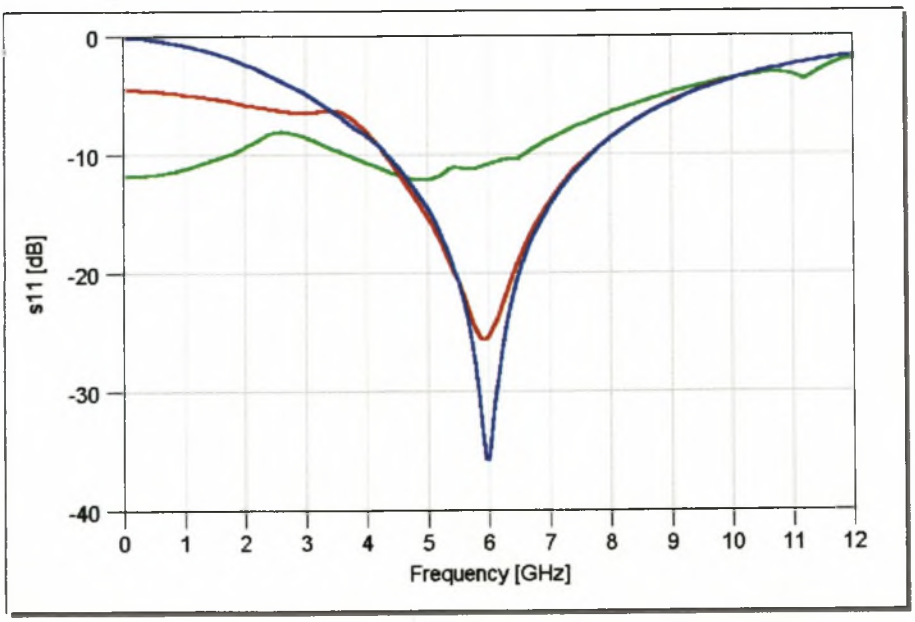

Figure 2.28 : Simulated Reflection Coefficient for the HSMS-8202 diode pair driven by LO levels of –10 dBm (blue), 0 dBm (red) and +10 dBm (green)

The final model for the diode pair is shown in Figure 2.30. The unpumped diodes have a resonance in the vicinity of 6 GHz, but this disappears as the diode is driven harder by the LO. This model is used for the mixer designs in Chapter 4. Although more extensive topologies have been suggested for the SOT-23 package [27], the model implemented in the current text proved to be adequate.

The optimization did not alter the values of the intrinsic diode parameters significantly, although values for the package parasitics were altered slightly. The model is considered valid for frequencies up to X-band.

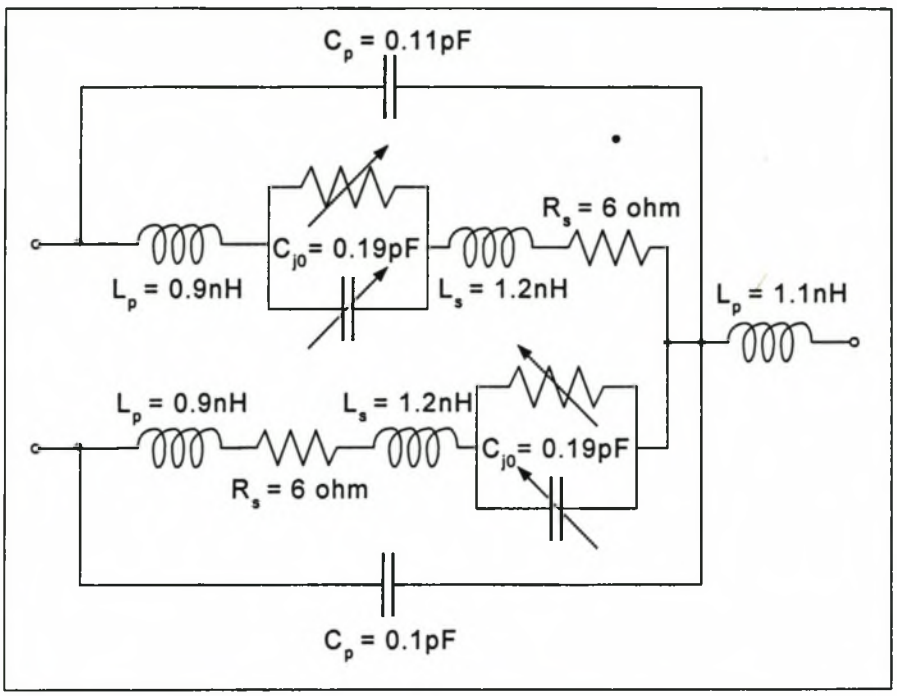

Figure 2.29 : Final Model for HSMS-8202 Antiparallel Diode Pair

The operation of the harmonic mixer is now sufficiently characterized, and the antiparallel diode pair is available as a well-defined building block of the mixer. The next chapter will move away from the analysis of the harmonic mixer, and will investigate its synthesis. Chapter 4 will focus on a practical implementation.

Chapter 3 : *Design Considerations*

The fundamental requirement of a frequency mixer is frequency conversion. However obvious this statement may seem, it is still the main task of a mixer to produce an output signal of lower (or higher) frequency using the available two input signals. The quality of this produced output signal will vary in accordance with the intended application.

Usually the primary requirement for the IF signal (in the case of a downconverter; an identical argument can be presented for the RF signal in an upconverter) is adequate power of the output signal – in other words, minimized conversion loss. The power of the applied RF signals is in most instances minimal, since only a low-noise preamplifier is inserted between the receiver antenna and the downconverter in a typical front-end application. Any RF power that can be preserved by minimizing conversion loss does not have to be gained by excessive gain stages (which are prone to noise and other forms of signal degradation).

Apart from minimal conversion loss, it is also preferable for a mixer to produce a clean IF spectrum. Isolation from the LO and RF signals is usually the secondary requirement in mixer design. Isolation is strongly associated with the topology of the mixer, as certain topologies inherently produce IF signals which are "clean" of frequencies other than the IF (the balanced mixer structures, for example, described in Chapter 1). However, the LO frequency usually requires additional effort to be removed from the IF spectrum, due to its superior power (typically the LO signal is larger in magnitude in the order of 20dB and more).

The available LO power is also a consideration which might be of concern. However, the choice of a harmonic mixer usually implies an inherent LO power consideration, i.e. lower frequency and higher power. It is therefore not often a problem to produce adequate LO power once the type of harmonic mixer has been chosen, since the LO frequency usually lies in a region where adequate power can be generated without additional effort.

Other factors such as input impedance and noise are rarely primary considerations for the design of a mixer, and they are often implied in the design specifications. Even physical factors such as size can be a consideration.

Although it may seem as if the harmonic mixer design demands numerous requirements to be met simultaneously, this is rarely the case. The proposed design procedure is to a large extent modular, and design steps can be added or left out in accordance with the requirements. However, before the design procedure can be developed, it is necessary to consider the possible requirements for mixer design in depth. This is the done in the following sections.

3.1) "The Design Requirement"

A mixer is designed in accordance with a set of requirements. These will now be discussed, with emphasis on the requirement of low conversion loss and high port isolation. Due to its extensive nature, and for lack of available space, this work will not consider the noise requirement as a primary design consideration.

3.1.1 Frequency Allocation

The very first issue in the design of a harmonic mixer is the choice of frequencies. The primary choice of frequency (i.e. the frequency that will dictate the choice of the others) lies between the RF and the IF. No flawless argument can be presented as to which frequency needs to be fixed first. On the one hand, the RF should be the primary choice, since the choice of RF is usually dictated by the nature of the application (e.g. satellite communications, where frequencies need to be confined to fixed frequency bands). On the other hand, the IF signal might be chosen first due to the availability of components within the IF band (e.g. the GSM-band).

Once the RF and IF frequencies have been fixed, the LO frequency can be attended to. The choice of LO frequency is generally dictated by the LO power availability. Should ample LO power be available up to frequencies of half the RF, a 2^{nd}-harmonic mixer can be utilized. Should LO power be available to frequencies of only a quarter of the RF frequency, a 4^{th}-harmonic mixer can be employed. LO power at even lower frequencies can utilize a harmonic mixer of orders higher than the 4^{th}.

Once the IF is located at the correct frequency, the issue of minimal conversion loss can be addressed.

3.1.2 Optimum Conversion Loss

The harmonic mixer's conversion loss between two frequencies was defined by equation (2.61) in Chapter 2 as

$$L_{0,k} = \frac{1}{4\left|Z_M^{(C,0)(C,k)}\right|^2 Re\{Y_k\} Re\{Y_0\}}$$

Apart from the numerical utilization of equation (2.61), it is significant to note that the following three factors contribute towards conversion loss :

1. RF source termination (denoted by the factor $Y_M^{(C,k)}$) : RF power can be lost before even entering the mixer due to a mismatch between the RF source and the RF port. In the examples presented later in the current work, care has been taken to always ensure 50Ω at the RF port.
2. IF load termination (denoted by the factor $Y_M^{(C,0)}$) : The converted IF power can be prevented to optimally "exit" the mixer due to a mismatch between the IF port and the IF load. It is necessary to ensure that the resistive parts of the IF port impedance and IF load impedance are ideally equal.
3. Coupling between conversion frequencies (denoted by the factor $Y_M^{(C,0)(C,k)}$) : Without launching into an elaborate discussion pertaining to the mechanics of frequency conversion in the antiparallel diode pair, it will be considered sufficient to say that amongst others, the junction series resistance R_S adds to conversion loss by means of resistive losses. The series inductance L_s does not have resistive losses, but becomes a high impedance at higher frequencies, adding to the conversion loss. By the same token the parasitic package components C_p and L_p also increase conversion loss.

From the above discussion it is clear that obtaining a low conversion loss can only *partially* be achieved by optimum design. The diode characteristics play an important role in determining conversion loss, and the correct choice of diode is essential to satisfying the requirement of minimal conversion loss.

3.1.3 Port Isolation

Rejecting the LO, RF and certain mixing products from the IF port is the most important goal of port isolation. A secondary goal is often to reject the IF signal from the RF and LO ports, since

any resistive termination other than the IF port causes an increase in conversion loss. Often the RF signal is also rejected from the LO port, again for the minimization of conversion loss.

Although the isolation requirements of the previous paragraph seem to be difficult to realize simultaneously, the process is often less complicated than it seems. The subharmonic mixer provides inherent isolation from even order LO harmonics, as well as odd order mixing products. The use of open-ended and shorted stubs is often employed as a further means to isolate ports from unwanted frequencies. Finally, the use of filter structures in addition to the aforementioned methods generally provides all the isolation that is needed. The use of these methods will be demonstrated in the design examples.

3.2) Choice of Diode

The choice of diode(s) is an important part of the design process. Factors such as low conversion loss and noise temperature are influenced significantly by the properties of the diode.

Since it is impossible to escape the effects of junction resistance and capacitance of real diodes, or the effect of the parasitic package elements, it becomes necessary to minimize these through diode selection. For the beam lead diodes typically used at X-band, the junction capacitance is often the limiting factor : a minimum capacitance of 0.1pF restricts the use of theses diodes to under 30 GHz [9]. A series resistance of 5Ω is typical, while a series inductance of 1nH is often observed. Different diode structures (e.g. dot-matrix or point-contact) are used at higher frequencies to minimize C_{j0}, R_S and L_S.

A common method used to express the frequency capability of the diode is by means of the cut-off frequency f_{co}, where

$$f_{co} = \frac{1}{2\pi C_{j0} R_S} \qquad \text{.....(3.1)}$$

f_{co} often proves to be no more than a guideline, and should be treated accordingly, i.e. as a first-order diode choice [28].

The choice of diode can be simplified if the designer has a knowledge of the sensitivity of the diode to the specific parameter. The following figures compare the sensitivities of the

antiparallel diode pair to junction capacitance C_{j0}, series resistance R_S, non-ideality factor η and series inductance L_S. The comparison should serve as an example, as results will vary depending upon the mixer circuits. Figures 3.1 to 3.4 show the results from the simulation. The HSMS-8202 antiparallel diode pair is used in a standard 2nd-harmonic mixer configuration. It is pumped by a 5 GHz LO, and the IF power is measured as the RF is swept through 10 GHz to 50 GHz. For every sweep one of the diode parameters is increased by a realistic amount.

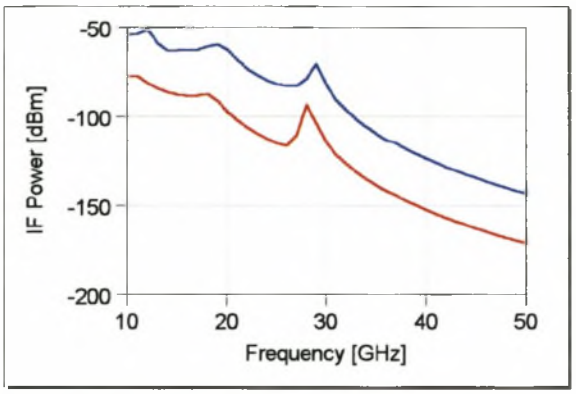

Figure 3.1 : IF Output Power for variation in Junction Capacitance : C_{j0} = 0.18pF (blue line) and C_{j0} = 0.36pF (red line)

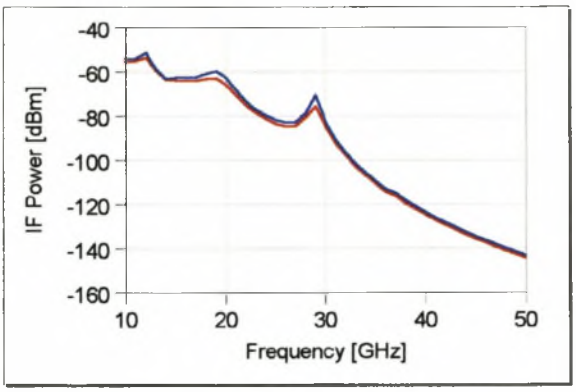

Figure 3.2 : IF Output Power for variation in Series Resistance : R_S = 6Ω (blue line) and R_S = 12Ω (red line)

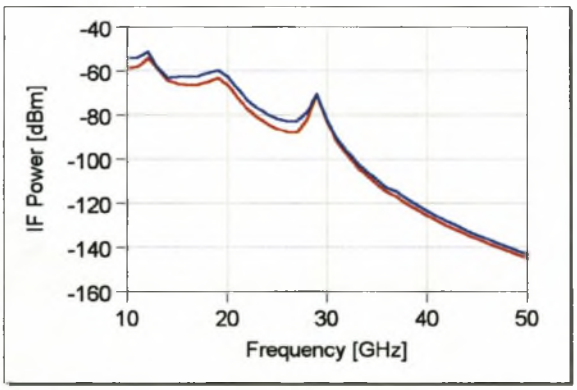

Figure 3.3 : IF Output Power for variation in Diode Non-Ideality : η = 1.09 (blue line) and η = 1.18 (red line)

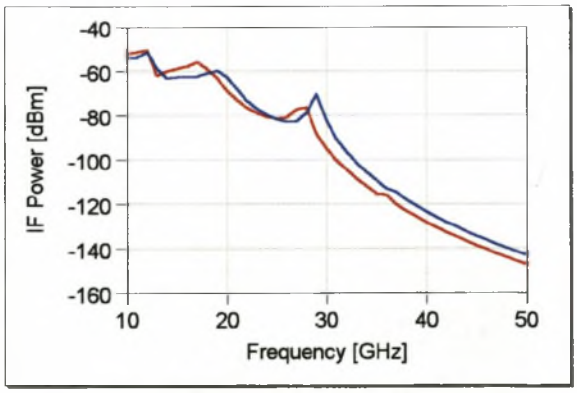

Figure 3.4 : IF Output Power for variation in Series Inductance : L_S = 1.3nH (blue line) and L_S = 1.6nH (red line)

From these graphs it can be seen that the diode pair is very sensitive to an increase in junction capacitance, and therefore the capacitance is usually a quantity that manufacturers aim to minimize. The specific configuration is moderately sensitive to an increase (doubling) of series resistance, while more ideal diodes tend to produce a better conversion loss at lower frequencies. Figure 3.4 shows that an increase in series inductance can actually increase diode performance at the lower frequencies (due to better reactive matching), while the series inductance causes an

increase in conversion loss at higher frequencies as the effect of the inductance becomes more prominent.

Such an analysis should provide the designer with the background for making an optimum choice when considering various diodes.

3.3) Design Topologies

The antiparallel diode pair can be used in more than one configuration. The mechanism of the harmonic mixing remains essentially the same, although the different topologies have inherent advantages and drawbacks.

3.3.1 Series Topologies [2]

The series topologies consist of the antiparallel diode pair with one port on the one side, and two ports on the other side. Figures 3.5 and 3.6 illustrate the two options offered by the series topology.

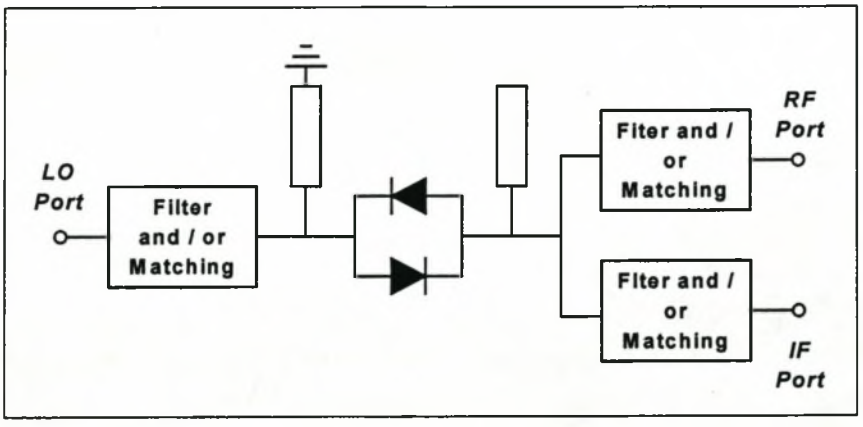

Figure 3.5 : Isolated Series Topology

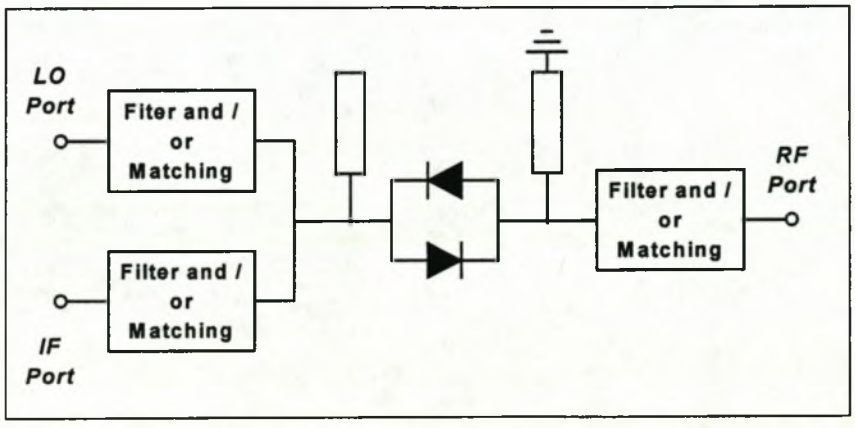

Figure 3.6 : Non-Isolated Series Topology

3.4.1 Specifications

The design starts off with a set of specifications. These can include frequencies, limits for conversion loss, port isolation, etc. The specifications enable the designer to consider and possibly make choices concerning the topology, the order of the LO harmonic used, the method of realization, etc.

3.4.2 Choice of Frequencies

The frequencies not stipulated by the initial specifications are now chosen. At this stage it is important to consider any possible spurious responses generated due to a poor choice of frequencies. Once the LO, RF and IF have been fixed, the next step is to choose the topology.

3.4.3 Topology

A topology is chosen, if it has not already been done in 3.4.1. This choice is influenced by factors such as port isolation, intended complexity of the circuit, method of realization (e.g. stripline), frequency bands, etc.

An outline for the intended design must also be constructed at this stage. Filters and matching circuits need to be considered, and preliminary choices are made for the order of the filters, etc.

3.4.4 Choice of Diodes

It has been established that it is crucial to consider the specifications of the diodes used in the design. In many cases this choice may be limited by the availability of the diodes. A low junction capacitance is crucial for high frequency designs, while low series resistance is preferred for lower frequency designs.

3.4.5 Basic Design

The goal of the basic design is to find the small-signal input impedances at the small-signal frequencies. This is done in order to design the port filters and the matching networks. For the basic design, the chosen topology is used with only two ports : a large-signal port for the LO, and a small-signal port for the RF. With the circuit driven by the LO, and with the RF applied on the small-signal port, the small-signal input impedances at the RF and LO ports are measured. The spectrum at the RF port is also considered. A value for the LO power is chosen in the

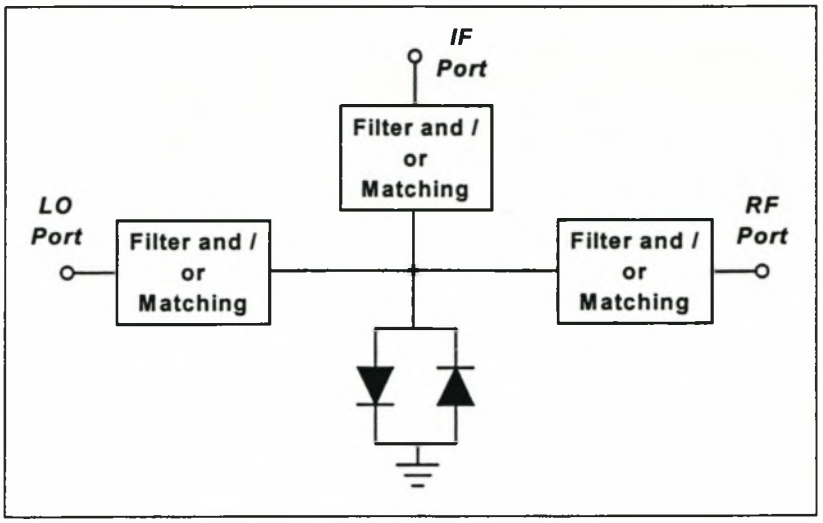

Figure 3.7 : Shunt Topology

Since the shunt topology adds and extracts all the signals through one side of the antiparallel diode pair, this sometimes necessitates the use of complex filtering structures, or diplexers. Shunt stubs (like that of the series topologies) are seldom used.

3.3.3 Additional topologies

The series and shunt topologies were used to realize the majority of harmonic mixers encountered in literature. Occasionally the antiparallel diode pair is used in a conventional double balanced mixer structure, where the conventional single diodes are then replaced by the back-to-back diodes [32]. The antiparallel diode pair has also been used in a triple balanced mixer topology, resulting in a unique three-dimensional structure [33]. Quadrature mixers utilizing antiparallel diode pairs have also been recorded [24].

3.4) Design Overview

Before the design examples are presented in Chapter 4, it is necessary to briefly consider the design procedure developed for use in the current text. The procedure developed is to a large extent a step-by-step design, starting with the design specifications and ending with the realization of the design. Only the outline of the procedure will be given, as a detailed discussion of each step is given in Chapter 4.

3.3.1.1 Isolated Series Topology [3, 29]

The isolated series topology of Figure 3.5 provides a very popular method for realizing harmonic mixers. It has the IF and RF ports on one side of the diode (the small-signal side), and the LO on the other side (the large-signal side). The separation of large and small signals provides a convenient way of isolating the IF signal, contributing to this topology's popularity.

The mixer utilizes two optional shunt stubs on either side of the antiparallel diode pair. On the small-signal side the open-ended stub is 90° long at the LO frequency, presenting a short to the LO (so that LO current flows through the diode pair), and at the same time removing the LO from the small-signal side. On the large-signal side the shorted stub is 180° long at the RF frequency, presenting a short to the RF frequency, and also providing a ground return path for the IF signal.

3.3.1.2 Non-Isolated Series Topology [30]

The non-isolated series topology is less popular due to the fact that additional measures need to be taken to remove the LO from the IF port. If the LO and IF frequencies are far apart, this becomes less of a problem. The non-isolated series topology may also utilize stubs, but the open-ended and shunt stubs are interchanged. The non-isolated series topology has been implemented in waveguide structures, where options are often reduced.

3.3.2 Shunt Topology [31]

The shunt topology of Figure 3.7 is another popular mixer structure. It has all three ports connected to one side of the antiparallel diode pair, while the other side is grounded. Sometimes the LO and IF are respectively added and extracted through the same port, reducing the number of physical ports to two.

vicinity of minimum conversion loss (the datasheets usually provide typical values for LO power).

Once the small-signal input impedances are known, the matching networks and filters can be designed. The output spectrum is considered in order to establish the order of the required filter(s).

3.4.6 Extended Design

The extended design adds another small-signal port, the IF port, to the topology. Since there are now two ports in parallel (the RF and IF, or the LO and IF), it becomes difficult to match the ports individually. This can possibly be overcome by a simultaneous solution or optimization. In the current text, an approximation was made. Since one of the harmonic mixer's characteristics is frequency components (IF, RF and LO) that are spaced far apart, it is possible (within reasonable bounds of the specific design) to consider only one of the shunt ports, while the other is approximated as an open circuit (due to the effect of its matching circuit or filter). From this principle, is it possible to design the output filters and matching networks for the IF and RF ports, ensuring that the assumption is indeed met. The process will be illustrated in Chapter 4.

3.4.7 Simulation

After the initial design has been completed (usually with lumped elements or transmission lines), it is necessary to simulate the entire circuit. If the assumption of 3.4.6 was not met by the initial design, a second design must be carried out. It is also possible to optimize the circuit, especially if it is simulated using non-ideal (e.g. microstrip or stripline) components. The effects of ground straps, enclosures or possible unintended coupling between structures also need to be verified. Another important factor to consider is the sensitivity of structures to component tolerances – if a structure is more tolerant of dimensions etc. than can be met by the design procedure, it might be necessary to consider an alternative.

After the design procedure has been carried out, the circuit can be realized. Two design examples are presented in Chapter 4, and it was found that the above design procedure yielded very good results.

Chapter 4 : *Implementation and Measurements*

Two designs were carried out to demonstrate the principles discussed in the previous chapters, one at S-band and one at X-band. A detailed exposition of the design process, with specific reference to the design procedure presented in Chapter 3, as well as the results, will be presented here for both cases.

4.1) S-Band Mixer

The first harmonic mixer design is for a S-band down-converting mixer. A number of specifications are fixed for the mixer, setting out a basic direction the design procedure should take. The design procedures for the filters implemented in the S-band mixer are given in Appendix B.

The design of the mixer is done with the aid of Microwave Office. The design package includes, amongst others, a large-signal circuit solver implementing the harmonic balance method, as well as EM models for microstrip components, allowing the mixer to be simulated as a microstrip circuit.

4.1.1 Specifications

An RF frequency of ω_{RF} = 2.45 GHz is chosen, as this frequency falls in an ISM-band, is often used for telemetry applications, and is also commonly used for applications such as WLL (*wireless local loop*). The design will be for as wide a bandwidth as possible, although a value between 100 MHz and 200 MHz would be sufficient. The IF is restricted to a value below 500 MHz, since available VHF components can then be used in the post-mixer stages. It was decided to implement a 2^{nd}-harmonic mixer.

4.1.2 Choice of Frequencies

With the RF fixed on ω_{RF} = 2.45 GHz, the LO and IF need to be chosen. The mixer will be a lower-sideband mixer in order to keep the LO frequency as low as possible. Finally the LO was fixed at value of ω_{LO} = 1.1 GHz, which resulted in an IF with frequency

$$\omega_{IF} = \omega_{RF} - 2\omega_{LO} = 250\ MHz \qquad \text{.....(4.1)}$$

The choice of LO and IF allows a bandwidth of 100 MHz to 200 MHz, while the IF lies safely within a frequency range where standard VHF components can be utilized. The choice of frequencies can be summarized as follows :

$$\omega_{RF} = 2.45\ GHz$$
$$\omega_{LO} = 1.1\ GHz$$
$$\omega_{IF} = 250\ MHz$$

4.1.3 Topology

The next step in the design process is to choose a topology for the subharmonic mixer. Since the isolated series-topology is a popular topology in the field of subharmonic mixers, this topology is chosen for the S-band mixer.

It is further decided to follow the classic approach where the large-signal LO is isolated from the small-signal RF and IF. The antiparallel diode pair will be pumped by the LO signal on one side, while the RF signal and IF signal will respectively be injected and extracted on the opposite side. A shorted stub will be used on the LO side, while an open stub will be implemented on the side of the RF and IF. Figure 4.1 shows the intended topology.

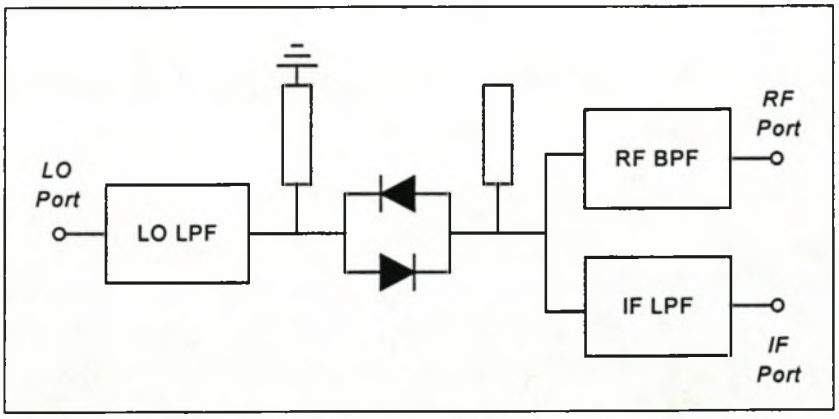

Figure 4.1 : Intended topology for S-band 2nd harmonic mixer

Filters will be used on all three of the ports. This is a preliminary decision, and the intended use of filters will be evaluated again when the spectra for all the ports are known. The IF is low enough to implement a lumped-element low-pass filter, while the RF is high enough to

implement a coupled-line band-pass filter. A low-pass filter, most likely consisting of distributed elements, is proposed for the LO.

Finally, a relatively inexpensive microstrip substrate intended for use in the lower GHz-region is chosen. It has the following characteristics :

$$\varepsilon_r = 3.86$$
$$h = 0.787$$
$$t = 0.05$$

4.1.4 Choice of Diodes

The HSMS-8202 series Schottky diodes will be used exclusively in this text. Table 2.1 and [17] provide a detailed description of the diode characteristics. The HSMS-820x series is ideally suited for use in the intended application. It has a low series resistance R_s of typically 6 ohms, and the junction capacitance C_{j0} is typically 0.18 pF, making it suitable for applications well into X-band. Other suitable diodes include [27].

Although the HSMS-820x series are available in a variety of packages, the HSMS-8202 is ideal for use in a subharmonic mixer. It comprises two antiparallel diodes, housed in a SOT-23 package. The characteristics of the entire diode (including package) are well defined in its datasheets, and in Chapter 2 an optimal model for the diode was extracted from measurements. It is this model that will be used in the design of the mixer.

4.1.5 Basic Design

The basic design of the S-band subharmonic mixer is shown in Figure 4.2 (Microwave Office schematic). It comprises a large-signal port *P1*, the antiparallel diode pair *S1*, a small-signal port *P2*, and the stubs *TL1* and *TL2* (implemented as ideal transmission lines).

Using the setup of Figure 4.2, the next step is to find the port impedances of the circuit. An initial value of +1dBm was chosen for the LO power, since this is suggested in the datasheets. A nonlinear analysis is performed, and the port impedances are as follows :

$$Z_{in}\Big|_{\omega_{LO}}^{Port1} = (73 + j0.8)\Omega$$
$$Z_{in}\Big|_{\omega_{RF}}^{Port2} = (93 + j11.65)\Omega$$
$$Z_{in}\Big|_{\omega_{IF}}^{Port2} = (43 + j4.62)\Omega$$

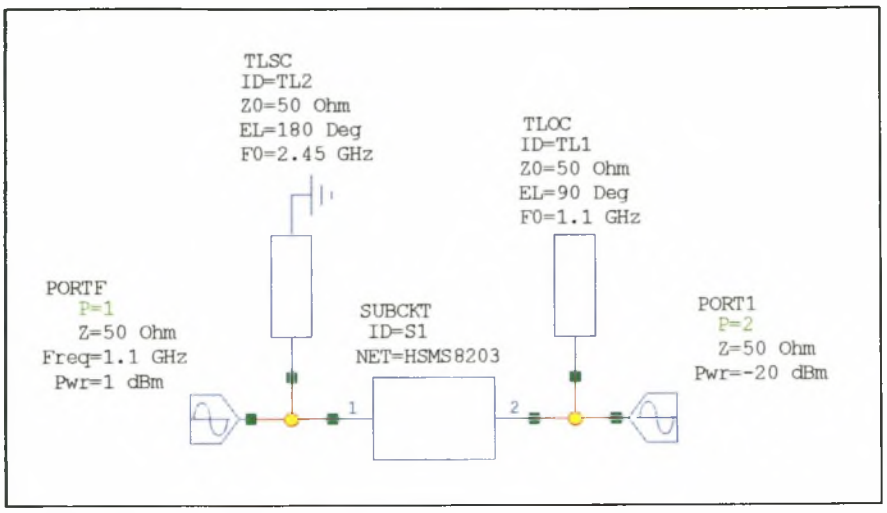

Figure 4.2 : MWO layout of the Basic Design

Figure 4.3 shows a plot of the input impedance of the small-signal port from 100 MHz to 3 GHz. The effect of the open stub can be seen, shorting the input impedance to ground at 1.1 GHz and providing the required isolation between the LO and the small-signal port.

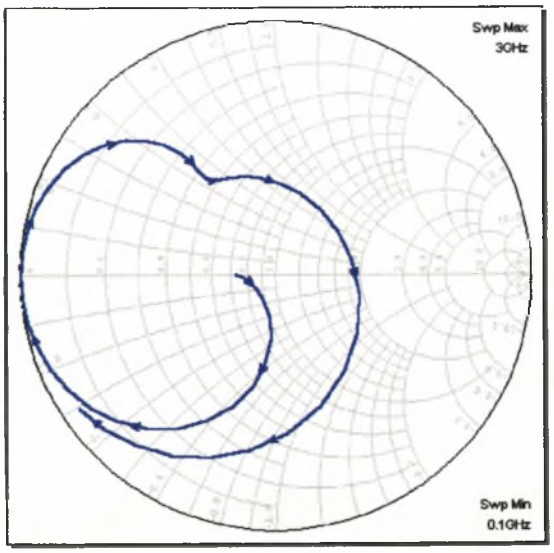

Figure 4.3 : Impedance on the Small-Signal port

Figure 4.4 shows the output spectrum for the small-signal port (Port 2 on Figure 4.2). The RF signal of –20 dBm is clearly visible as the largest signal on the plot. The IF signal $\{\omega_{RF} - 2\omega_{LO}\}$ at 250 MHz is relatively strong (-32dB) for an unmatched mixer, but since the real part of the input impedance of the IF frequency is close to 50Ω, this result is to be expected. Also visible on figure 4.4 is the image frequency at $\{\omega_{RF} + 2\omega_{LO}\} = 4.65$ GHz. The image is clearly not reactively terminated, and contains power that can possibly be relinquished to the IF, if

terminated correctly [1]. Also note that the LO is not present in the output signal (no harmonics are present either). This is of course due to the combination of the antiparallel diode pair, and the open circuit stub.

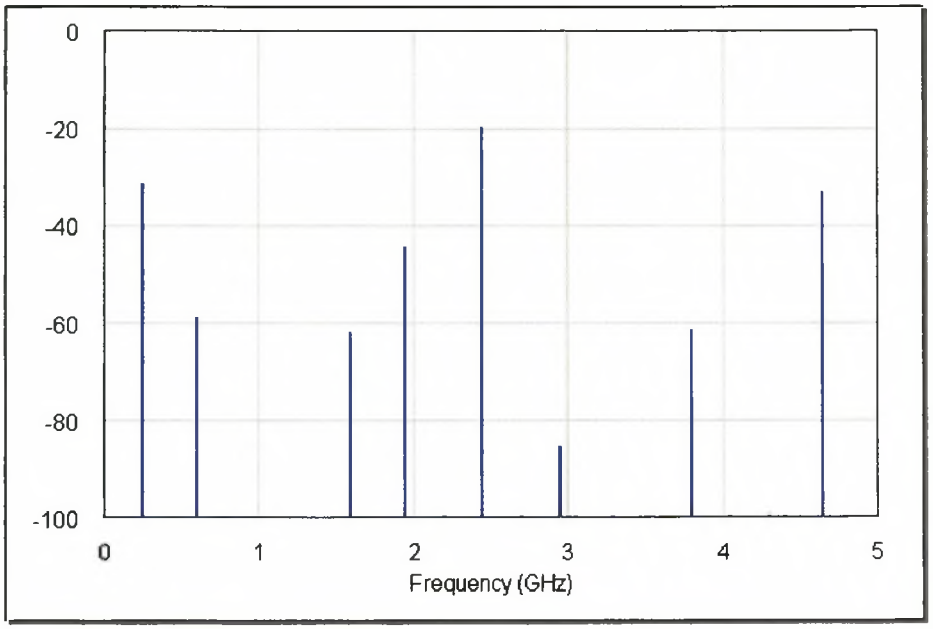

Figure 4.4 : Output Spectrum of the Small-Signal Port (Port 2 on Figure 4.2)

This concludes the basic design for the S-band subharmonic mixer. Although a third port still needs to be added to the topology, the basic work has been done to create a topology capable of producing a significant IF signal. In the remainder of the design, this IF signal will be maximized and isolated using matching, filtering and tuning.

4.1.6 Extended Design

It is necessary to introduce the third port on the small-signal side of the antiparallel diode pair, through which the IF can be extracted. The 3rd port is designed in such a way that it does not upset the input impedance seen by the existing port at 2.45 GHz. In other words, the 3rd port (or IF port) should let frequencies around 250 MHz pass, while it presents a high impedance to signals at 2.45 GHz. Filtering provides a solution to this problem.

In addition to using filters to isolate the IF port and the RF port, matching may be required to ensure optimum RF power transfer between the RF port and the antiparallel diode pair, as well as optimum IF power transfer between the IF port and the antiparallel diode pair. Since the design

is for moderate bandwidth, stubs and lines are expected to provide an adequate response. The intended topology for the design is shown below.

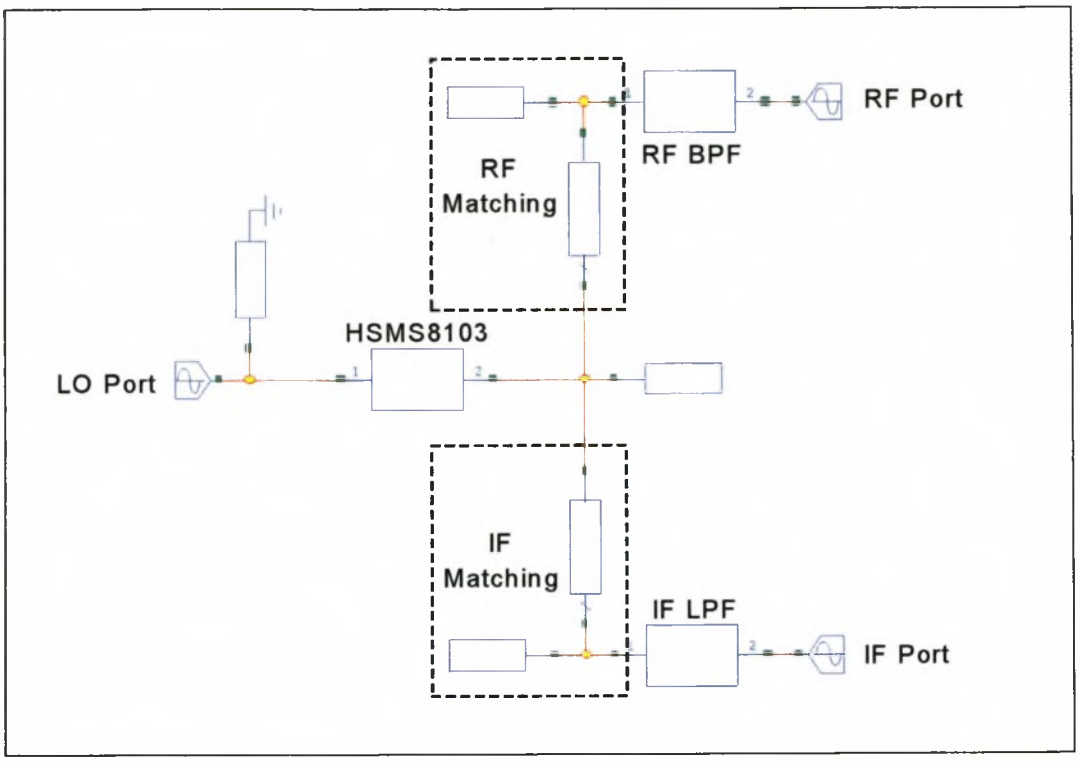

Figure 4.5 : Intended Topology showing Matching Circuits and Filters

4.1.6.1 IF Low-pass Filter

Since the IF lies within the VHF-band, lumped elements are used to realize the IF filter. A 5th-order LC-ladder topology is chosen, providing an estimated isolation of 47dB at ω_{LO} = 1.1 GHz, and 84dB at ω_{RF} = 2.45 GHz (Of course the isolation at ω_{RF} is almost impossible to realize with lumped elements, due to the parasitics of the elements. As it will become evident, the values provide a good first-order approximation of the isolation at ω_{RF}.) The simulated response is shown in Figure 4.6.

Ideally the low-pass filter provides the antiparallel diode pair with a 50Ω termination at ω_{IF}, while it becomes a short for the higher frequencies. The next step is to design the band-pass filter for the RF.

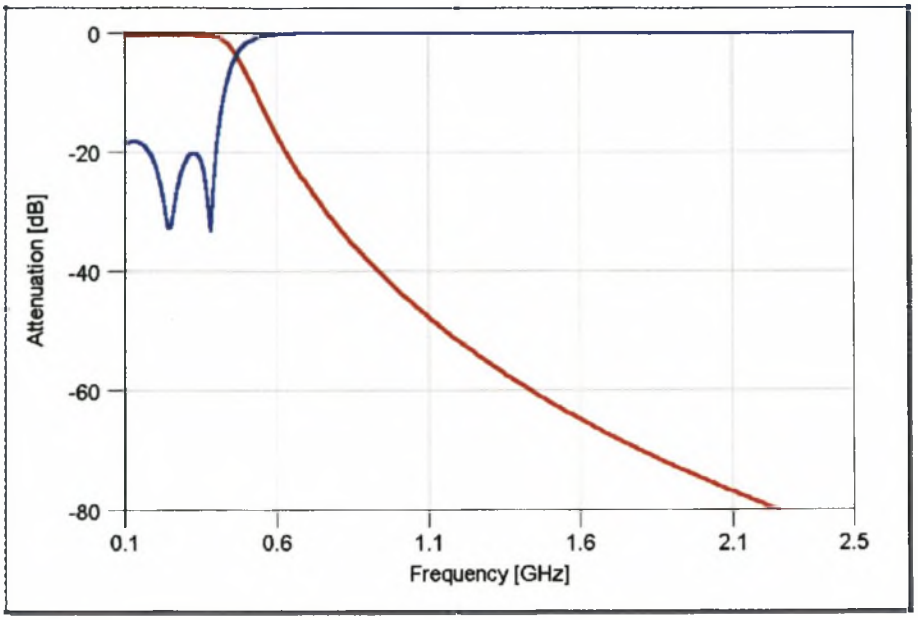

Figure 4.6 : Low-Pass Filter Frequency Response (s_{11} = blue, s_{21} = red)

4.1.6.2 RF Band-Pass Filter

The RF band-pass filter should ideally pass the band of frequencies around 2.45 GHz, while presenting an open circuit to the other frequencies. The width of the pass-band determines the bandwidth of the mixer to a great extent, a factor that needs to be considered when choosing topologies. In order to gain moderate bandwidth while still maintaining a relatively simple design, a 2nd-order band-pass filter was realized [8, 34]. The filter response is shown in Figure 4.7.

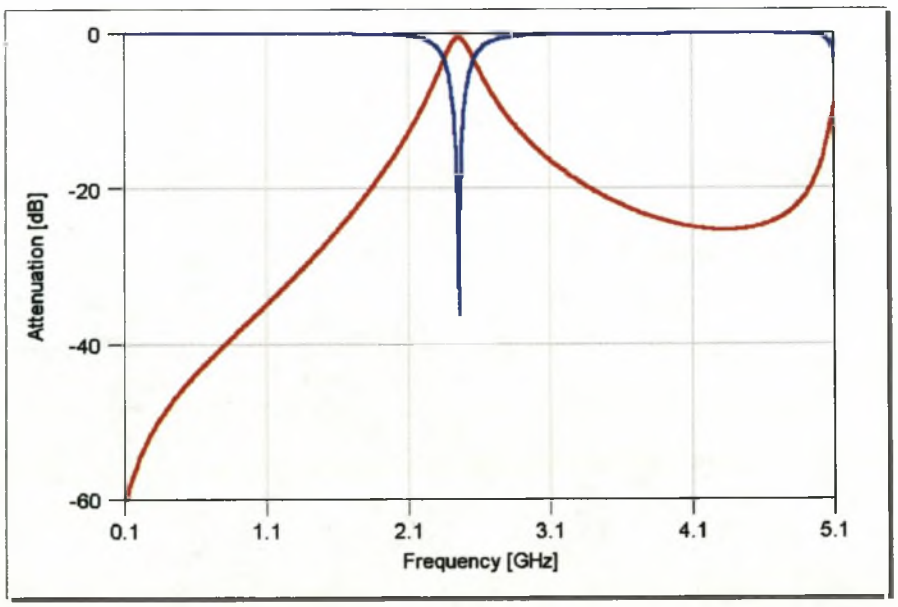

Figure 4.7 : Band-Pass Filter Frequency Response (s_{11} = blue, s_{21} = red) for realized microstrip filter

The filter has an attenuation of 0.5 dB in the center of the pass-band, while the –3 dB bandwidth of the filter is about 100 MHz. It is expected that the mixer will have an equivalent bandwidth.

Once the filters have been implemented, the antiparallel diode pair should see a 50Ω termination at 250MHz and 2.45GHz at the IF port and RF port respectively. This is indeed the case at the IF frequency (Figure 4.9), but not yet at the RF (Figure 4.8). Since the IF low-pass filter has a shunt inductor as its first element, the antiparallel diode pair is shorted to ground at frequencies above the IF cut-off frequency, and a 50Ω match at the RF frequency is not possible. This can be corrected by isolating the IF filter from the remainder of the circuit at the RF frequencies. The IF matching network, proposed in Figure 4.5 and consisting of a stub and a line, should solve this problem.

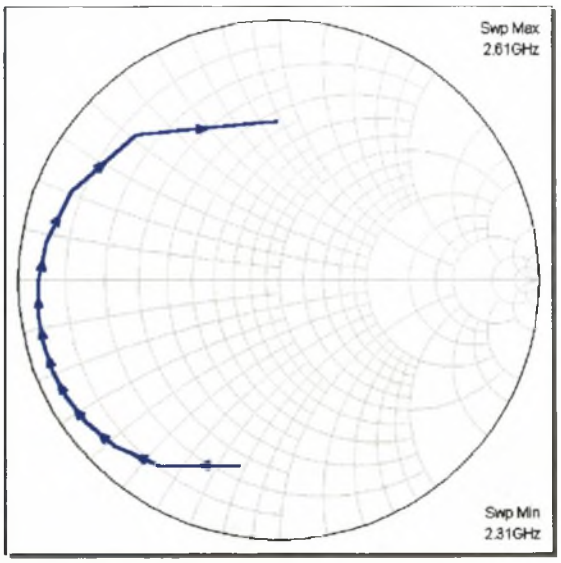

Figure 4.8 : RF port Input Impedance for 2.3 – 2.6 GHz

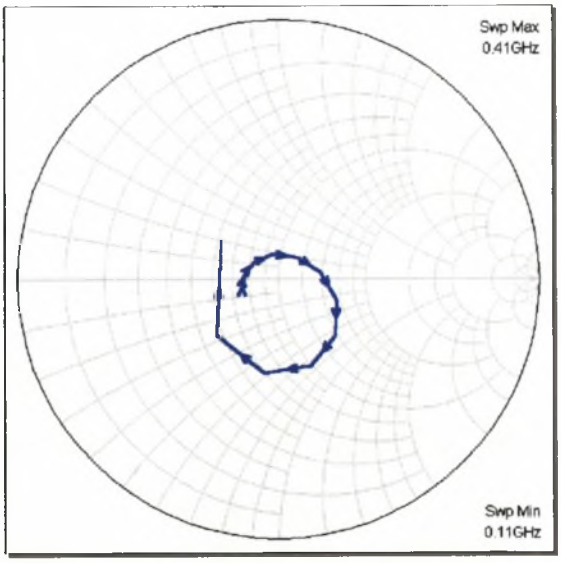

Figure 4.9 : IF port Input Impedance from 100MHz – 400MHz

4.1.6.3 IF Matching Network

The purpose of the IF matching network is twofold :

- Match the 50Ω IF port to the IF filter at 250 MHz
- Isolate the IF port from the antiparallel diode pair at 2.45 GHz.

At 250MHz, the input impedance of the antiparallel diode pair at the IF port is $\{64 + j7\}\Omega$. This is matched to the antiparallel diode pair using a single line with an impedance of 58Ω. The line is

chosen to be 90° long at 2.45 GHz, resulting in an open circuit at the RF. The single line provides an adequate match, and it is not necessary to add a shunt stub. The new RF and IF input impedances are shown in Figures 4.10 and 4.11.

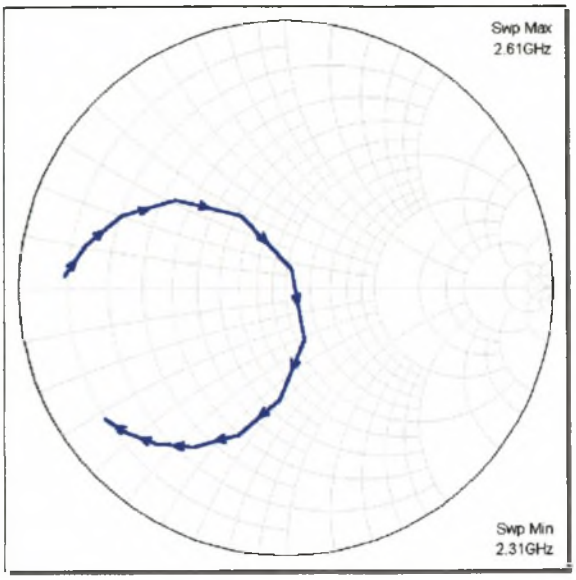

Figure 4.10 : RF port Input Impedance from 2.3 GHz to 2.6 GHz (after the addition of the IF matching network)

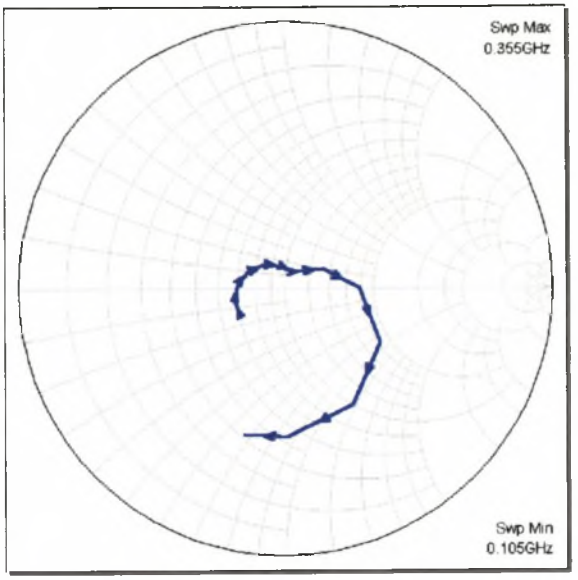

Figure 4.11 : IF port Input Impedance from 100 MHz to 400MHz (after the addition of the IF matching network)

4.1.6.4 RF Matching Network

The only purpose of the RF matching network is to match the 50Ω RF port to the antiparallel port at 2.45 GHz. The RF band-pass filter already provides isolation between the IF and RF ports at 2.45 GHz.

Although the RF port input impedance is very close to 50Ω at 2.45 GHz (after the addition of the IF matching stub), the input impedance at frequencies around 2.45 GHz still approach a short circuit (see Figure 4.10) due to the limited bandwidth of the IF matching stub, and the shorting-effect of the IF filter. The intended effect of the RF matching circuit is therefore to provide additional bandwidth to the RF match, while still providing a adequate match to the 50Ω RF port.

An ideal transmission line with an impedance of 67Ω and a length of 168° at the RF shifts the curve on the Smith chart towards the desired location. Figures 4.12 and 4.13 show the final plots for the input impedance at the RF and IF ports.

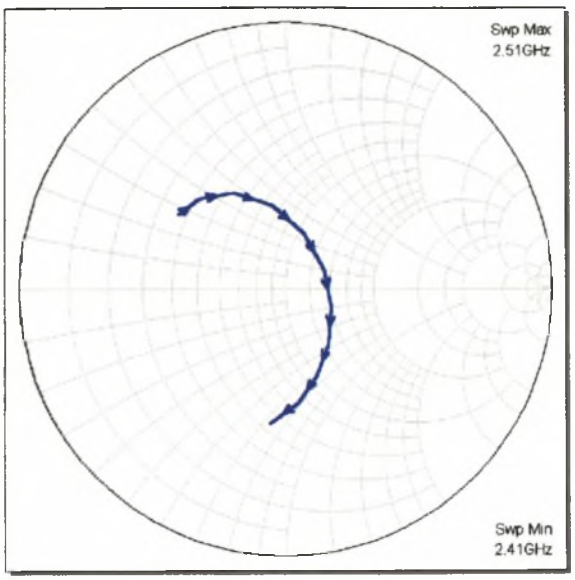

Figure 4.12 : Final RF port Input Impedance for 2.3 – 2.6 GHz (after the addition of the IF and RF matching networks)

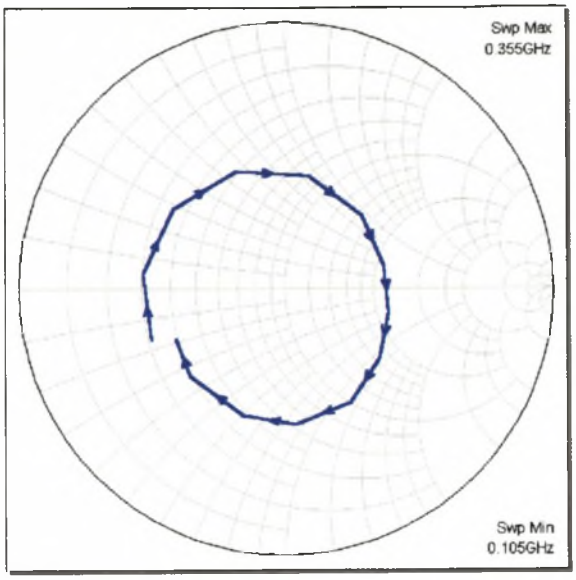

Figure 4.13 : Final IF port Input Impedance from 100MHz – 400MHz (after the addition of the IF and RF matching networks)

4.1.6.5 LO Isolation

Once the RF and IF ports have been matched and isolated, the design on the small-signal side of the mixer is complete. However, the LO port on the large-signal side presents a 50Ω termination to many frequencies other than the LO signal. These frequencies include the IF frequency, as well as mixing products between 1GHz and 3GHz. By reducing the real termination at these frequencies, the conversion loss can be slightly improved. Figure 4.14 shows the frequency spectrum at the LO port.

A low-pass filter was chosen to isolates the LO port. Ideally a band-pass filter should be used, rejecting all signals (including the IF and the image frequency) from the LO port. Since the LO and IF frequencies are spaced relatively close (~25%) and relatively low (<1.1GHz), a simple microstrip band-pass structure is difficult to realize. The low-pass filter will therefore provide additional isolation (and increased bandwidth) from the RF signal, but will not terminate the IF signal reactively. It was later found that a reactive termination would have resulted in a 2dB to 3dB improvement in conversion loss.

A quarter-wave stub filter was chosen to realize the microstrip structure [8]. The frequency response of the filter is shown in Figure 4.15.

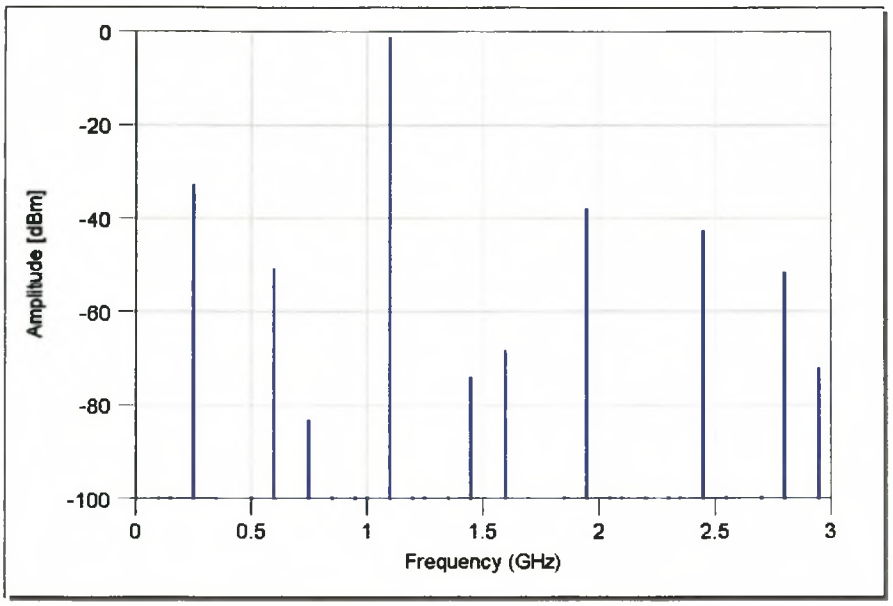

Figure 4.14 : Frequency Spectrum at LO port (before isolation)

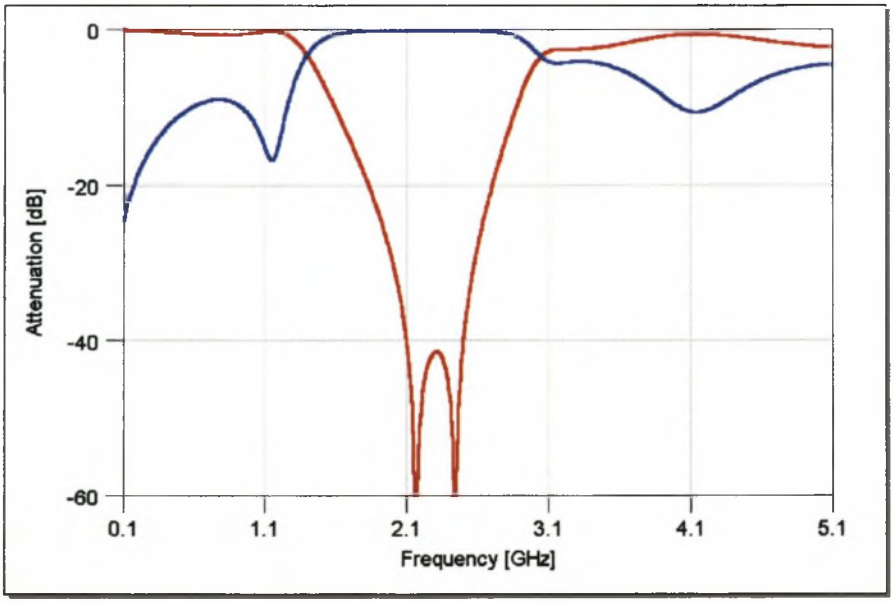

Figure 4.15 : Frequency Response of implemented LO LPF (s_{11} = blue and s_{21} = red)

4.1.7 Microstrip Simulation

The circuit is transformed to microstrip, and simulated using a low-frequency (<3 GHz) substrate with $\varepsilon_r = 3.86$ and $h = 0.787$. The initial design (containing transmission lines) is simulated in Microwave Office, using the available EM-models offered for microstrip structures.

For the simulation all ideal transmission lines from the initial design are replaced with microstrip lines of the correct length and width, and are joined by the necessary T-junctions or cross-

junctions (the simulation package utilizes adequate models for these structures). The shorted stub on the large-signal side is realized with a microstrip line connected to ground by a ground strap. The chip inductors are modeled with Q = 40, a realistic value at the frequency.

Before the simulation was done on the microstrip circuit, the circuit was optimized for minimized conversion loss. The optimization is justified by the addition of the T-junctions and cross-sections. The error-function for the optimization was created by making line lengths and widths variables, and then computing the corresponding conversion loss. Since the design process has already placed the error-function within the vicinity of the absolute minimum for the specific design, it was necessary only to search locally for a minimum value for the error-function. Two of the optimization methods included in the design package were utilized : the Local Random Optimization and Simplex Optimization. The local random optimization was implemented first due to its effectiveness when a large number of variables are used. Once the local random optimizer flattened out, a simplex optimization (or downhill search) was implemented, evaluating N points on the error surface, and finally converging accurately to the minimum value for the error function. The local random optimization flattened out within ~1000 iterations, while the simplex optimization required ~500 iterations to achieve a minimum.

Figure 4.16 shows the IF output power against swept LO input power for a RF of –20dBm. The mixer has an optimum conversion loss of 8.7dB [-20 – (-28.7)], and this is achieved at an LO power of –0.5dBm.

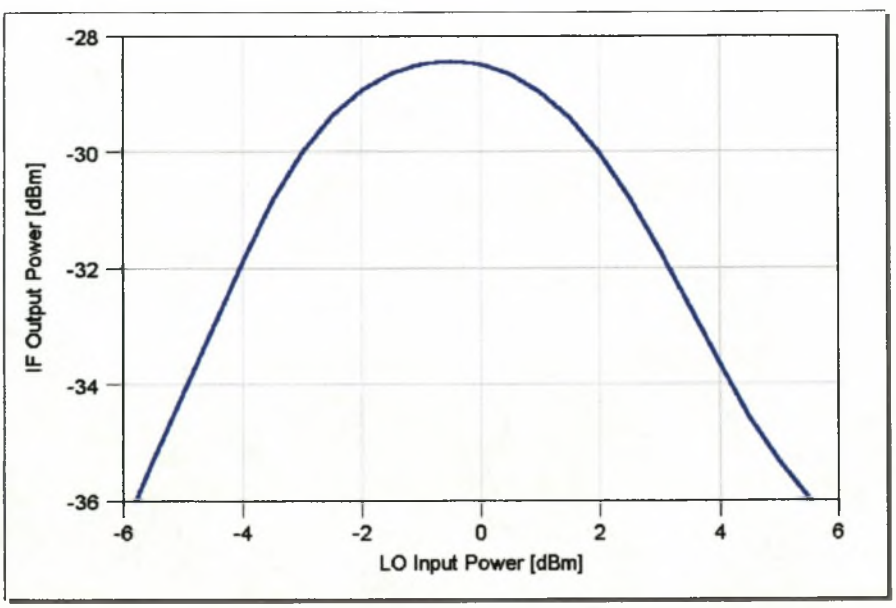

Figure 4.16 : Simulated IF power as a function of LO power for the S-band Harmonic Mixer

Figure 4.17 shows the expected output spectrum at the IF port (with an applied LO power of 0dBm). Apart from the IF signal, the LO and RF signals are visible. The predicted IF-to-LO isolation is 52dB, while the predicted IF-to-RF isolation is 80dB.

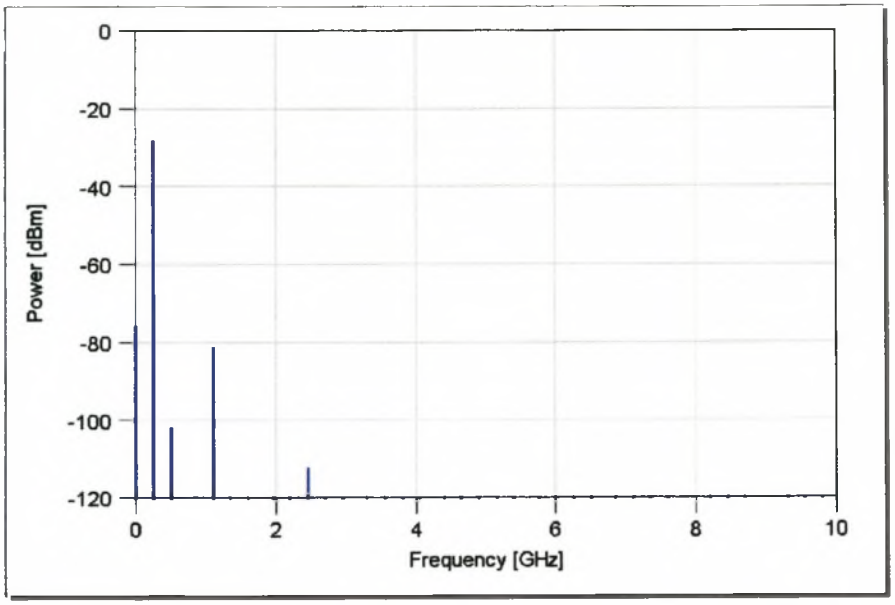

Figure 4.17 : Simulated Output Spectrum at the IF Port (with –0.5dBm LO applied)

Finally the bandwidth of the mixer is found with a simulation. Figure 4.18 shows the frequency of the applied RF signal as input, while the power of the corresponding IF response is plotted as the output. From 4.18 the mixer is expected to have a 3dB-bandwidth of ~200 MHz.

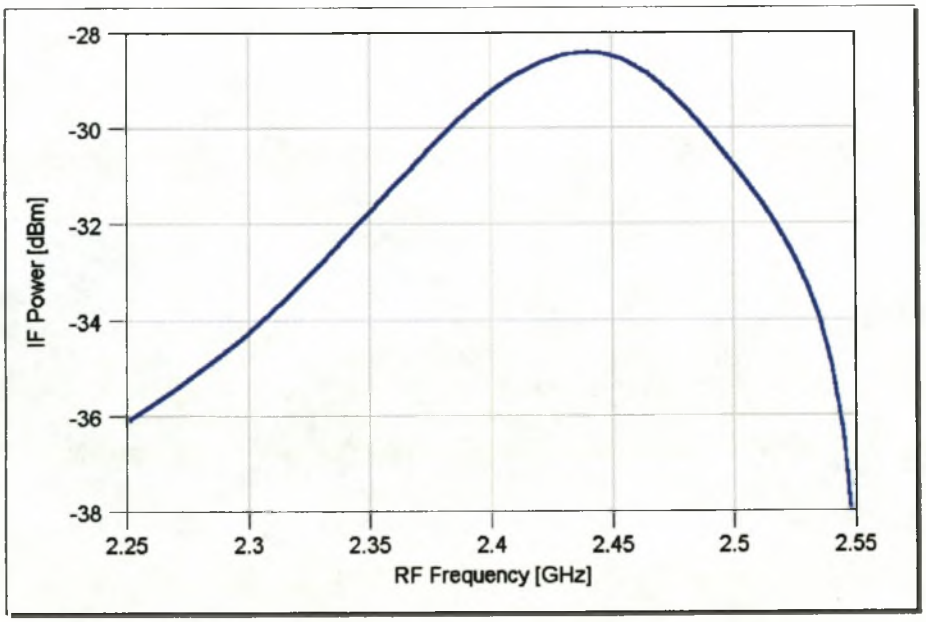

Figure 4.18 : Simulated plot of RF frequency vs IF power

4.1.8 Realization

The S-band harmonic mixer was realized in microstrip using a low-frequency substrate with ε_r = 3.86 and h = 0.787. The lumped-element IF low-pass filter was realized using 0805-type surface mount components. A layout of the final mixer is shown in Figure 4.19. The footprints for the 0805-type components, as well as the diodes' SOT-23 package are also visible. Also note that the SMA-connectors are connected to the ports via lengths of 50Ω line.

A photograph of the manufactured mixer is shown in Figure 4.20. Note that the lines from the diode to the IF and LO ports were bent through 90° to minimize surface space. Further minimization using mitered lines was possible, although this was not done.

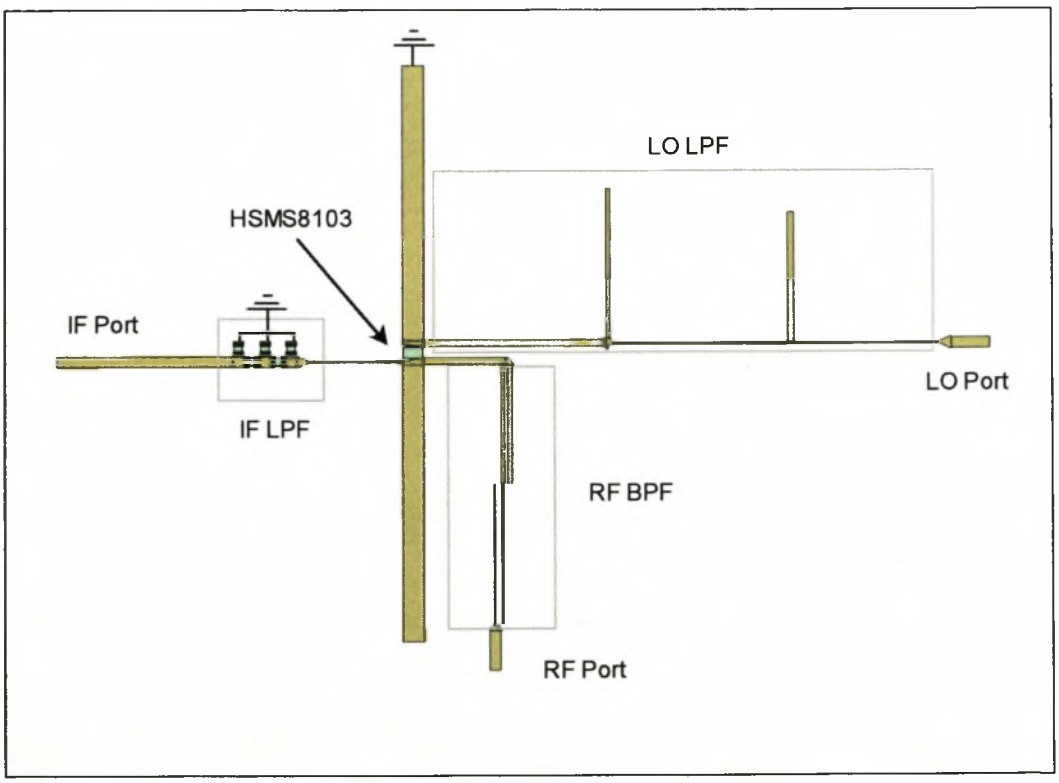

Figure 4.19 : Final S-band mixer layout (Scale 1 : 1)

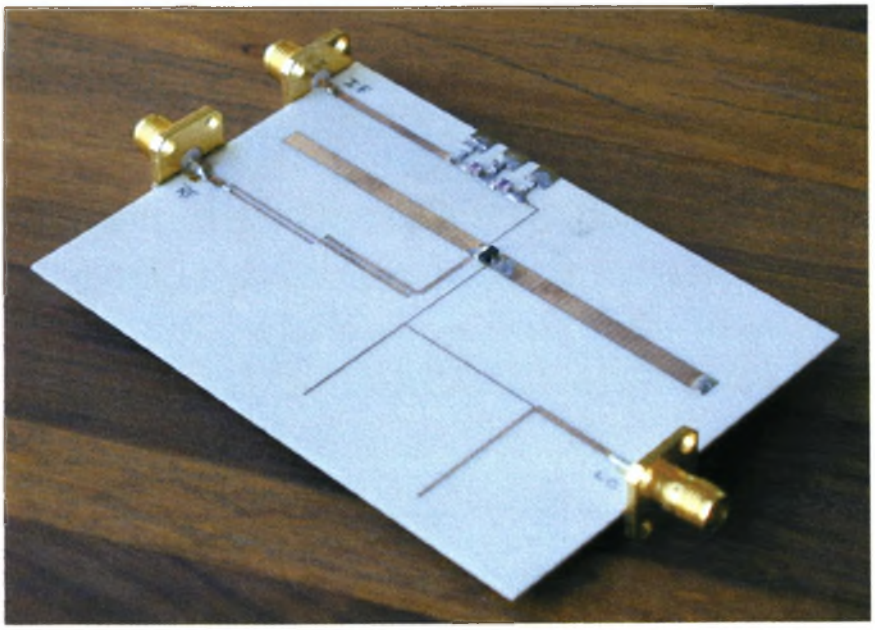

Figure 4.20 : The Manufactured S-band Harmonic Mixer

4.1.9 Measurements

The performance of the S-band harmonic mixer was measured to determine conversion loss, isolation and bandwidth. The measurements generally agreed very well with the predicted results.

Figure 4.21 shows the mixer's measured conversion loss by plotting input LO power against output IF power. The power of the applied RF signal is –20 dBm. The minimum conversion loss is 10.3dB (1.8dB worse than the predicted value of Figure 4.16). This optimum conversion loss is achieved with 0.5dBm LO power (1dBm higher than the predicted value). The shape of the measured curve agrees very well with the predicted curve of Figure 4.16.

Next a RF frequency sweep is performed with +0.5dBm LO power applied. The –20dBm RF signal is swept from 2.23GHz to 2.60GHz, resulting in an IF from 30MHz to 400MHz. Figure 4.22 shows the measured curve. A 3dB-bandwidth of ~250MHz is measured (50MHz in excess of the predicted value). Furthermore, the shape of the curve in Figure 4.22 agrees well with the predicted shape of Figure 4.18.

Finally the port-to-port isolations were measured using a spectrum analyzer and a power meter :

LO-to-IF Isolation : 41dB

RF-to-IF Isolation : 60dB

Both the LO-to-IF and RF-to-IF isolations are slightly less than their simulated values, but are still very satisfactory.

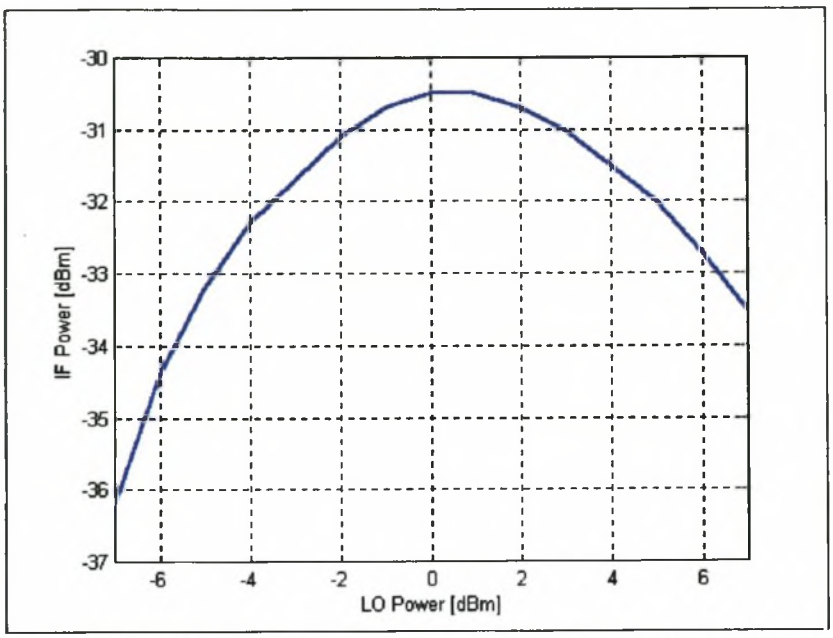

Figure 4.21 : Measured LO power vs IF power for S-band harmonic mixer

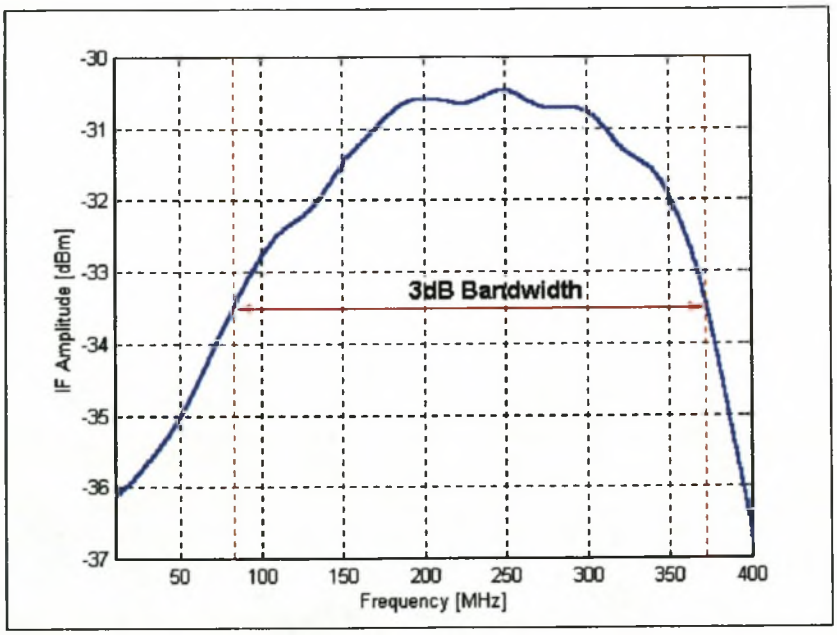

Figure 4.22 : Measured RF-sweep of S-band harmonic mixer, showing IF amplitude against IF Frequency for +0.5 dBm applied LO power and –20 dBm applied RF power

4.1.10 Comments

The S-band harmonic mixer performs very satisfactorily. Conversion loss is only slightly less than expected. This is most likely due to a slight mismatch or manufacturing tolerances. Isolation on the ports is satisfactory. The performance of the mixer could for the larger part be predicted adequately.

The IF low-pass filter could however be slightly improved. The filter has a shunt capacitor closest to the mixer. This capacitor shorts out the RF signal, necessitating the matching circuit. This problem could have been overcome by ensuring an inductor as the filter element closest to the mixer.

In an attempt to improve the conversion loss even more, a narrowband matching structure could have been used at the LO port instead of the low-pass filter. The low-pass filter does not isolate the RF port from the IF, undoubtedly resulting in some lost IF power.

Judging by Figure 4.13, the IF port is not as optimally matched to the antiparallel diode pair as one would have preferred. A second iteration for the design of the matching networks would have improved the match.

With these guidelines in mind, and with the experience gained, the design of the X-band mixer is taken on.

4.2) X-Band Mixer

The second design is for an X-band down-converting mixer. As with the S-band mixer, a number of specifications will be set for the mixer, setting out a basic approach for the design procedure. The design procedures for the filters implemented in the X-band mixer are given in Appendix C.

4.2.1 Specifications

A RF frequency of ω_{RF} = 11 GHz is chosen, making the mixer suitable for use in some satellite communication systems. A 6% bandwidth of ~700 MHz is chosen, half the bandwidth obtained with the S-band mixer, so that the option of reduced conversion loss with reduced bandwidth can be explored. The IF is chosen to be 1.1 GHz (a value of exactly 1GHz resulted in numerical instability of the software due to the harmonic relation between the integer values). For optimal

conversion loss in the frequency band, a 2nd order subharmonic mixer will be implemented instead of a 4th order mixer.

4.2.2 Choice of Frequencies

With the RF fixed on ω_{RF} = 11.0 GHz and the IF on ω_{IF} = 1.1GHz, the LO is automatically fixed on ω_{LO} = 4.95 GHz. Equation 4.2 verifies that the relation between the frequencies is correct :

$$\omega_{IF} = \omega_{RF} - 2\omega_{LO} = (11.0 - 2\times 4.95)GHz = 1.1GHz \quad \text{.....(4.2)}$$

The choice of frequencies can be summarized as follows :

$$\omega_{RF} = 11.0\ GHz$$
$$\omega_{LO} = 4.95\ GHz$$
$$\omega_{IF} = 1.1\ GHz$$

4.2.3 Topology

The topology chosen for the X-band mixer is very similar to that implemented on the S-band mixer. The popular series-topology is implemented, with the LO applied on one side of the antiparallel diode pair, and the RF and IF are respectively applied and extracted on the opposite side of the diodes. A shorted stub will be used on the side of the LO, while a open-ended stub will be used on the side of the RF and IF. Figure 4.23 shows the intended topology.

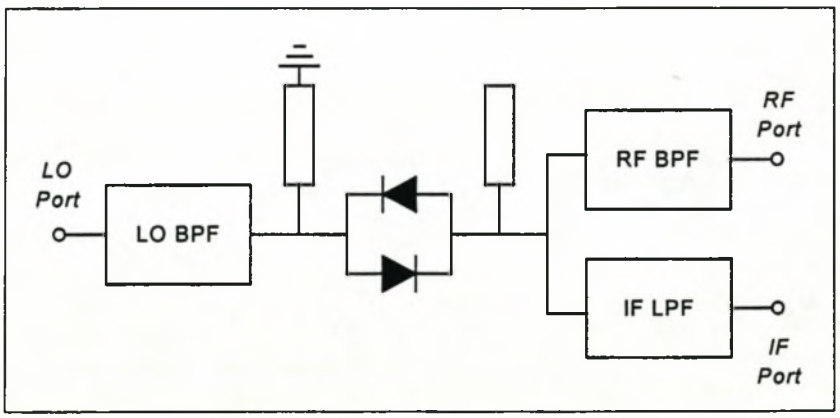

Figure 4.23 : Intended Topology intended for use with the X-band Harmonic Mixer

Filters will be used on all three of the ports. This choice led to satisfying results with the S-band mixer. Unlike the S-band mixer, the IF is high enough to use distributed element filters. Distributed element filters will therefore be used at all three ports.

A Taconic microstrip substrate intended for use at X-band is chosen to realize the circuit. It has the following characteristics :

$$\varepsilon_r = 2.48$$
$$h = 0.787$$
$$t = 0.05$$

4.2.4 Choice of Diodes

The HSMS-8202 diode in a SOT-23 package is again used for the design. The model extracted in Chapter 2 is still valid in X-band, and is used for the design of the mixer.

4.2.5 Basic Design

The basic design for the X-band harmonic mixer is similar to that shown in Figure 4.2 (Microwave Office schematic). It consists of the large-signal port *P1*, the antiparallel diode pair *S1*, a small-signal port *P2*, the open-ended stub *TL1*, and the short-circuited stub *TL2* (implemented as ideal transmission lines).

The port impedances for the two ports need to be found. The datasheets of the HSMS-8202 suggest an increase in LO power with an increase in frequency, and an initial value of +8dBm is chosen for the LO power. A nonlinear analysis is performed, and the port impedances are as follows :

$$Z_{in}\Big|_{\omega_{LO}}^{Port1} = (21.3 + j30.3)\Omega$$
$$Z_{in}\Big|_{\omega_{RF}}^{Port2} = (127 + j168)\Omega$$
$$Z_{in}\Big|_{\omega_{IF}}^{Port2} = (42.8 - j15)\Omega$$

Figure 4.24 shows the plot of the input impedances of the small signal port from 10 GHz to 12 GHz.

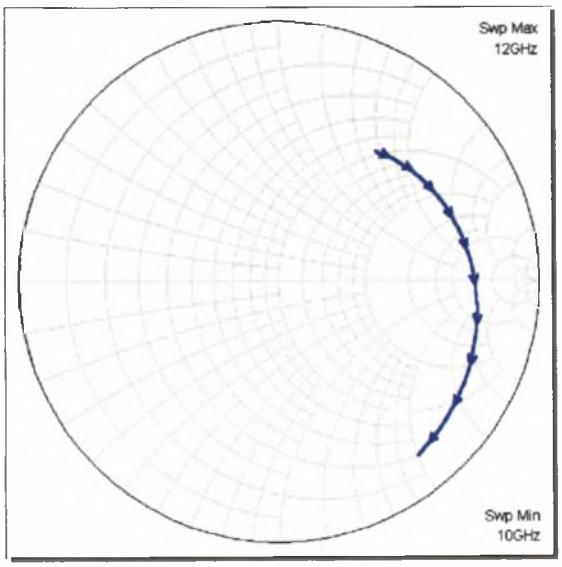

Figure 4.24 : Input Impedance on the Small-Signal port

Figure 4.25 displays the output spectrum for the small-signal port (Port 2 on Figure 4.2). The RF signal of about –20 dBm at 11GHz is clearly visible as the largest signal on the plot. The IF signal $\{\omega_{RF} - 2\omega_{LO}\}$ at 1.1 GHz is relatively strong (-30.5dBm) for an unmatched mixer, but since the real part of the input impedance of the IF frequency is once again close to 50Ω, this result is to be expected. Also visible on Figure 4.25 is the image frequency at $\{\omega_{RF} + 2\omega_{LO}\}$ = 20.8 GHz. The image is clearly not reactively terminated, and contains power that can possible be added to the IF, when terminated correctly [1]. Also note that neither the LO nor any of its harmonics is present in the output signal. This is due to the combination of the antiparallel diode pair and the open circuit stub.

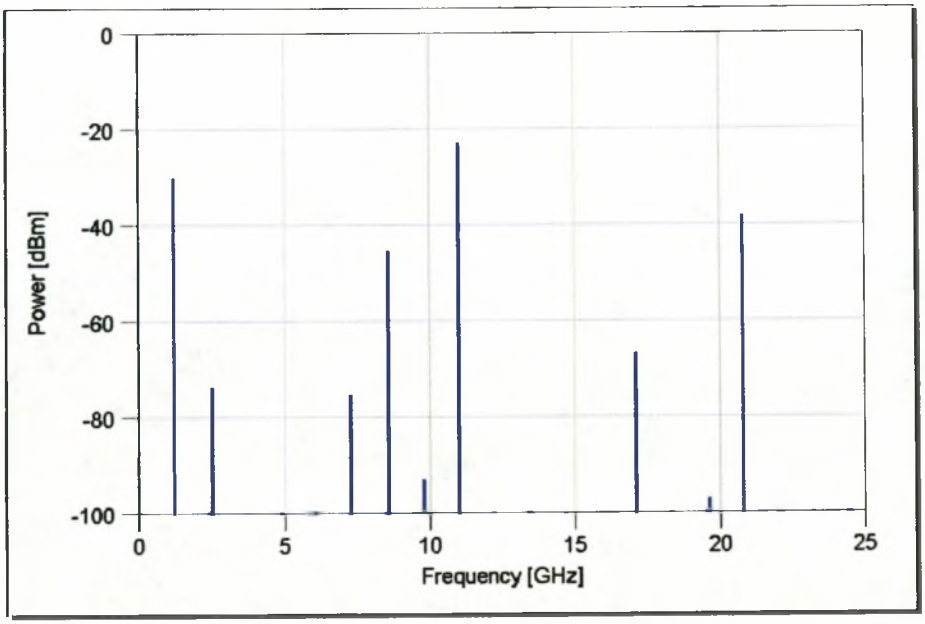

Figure 4.25 : Small-Signal Port Output Spectrum

This concludes the basic design for the X-band subharmonic mixer. As with the S-band mixer, a third port will now be added to the basic structure, whereafter the matching and filtering structures will be added.

4.2.6 Extended Design

The IF port is added to the small-signal side of the mixer in such a way that it lets through the frequencies around 1.1 GHz, while it presents an open circuit to the RF at 11GHz. The LO is already somewhat isolated from the IF port by the open-ended stub.

Once again matching networks will be needed to ensure optimum power transfer to and from the IF port and RF port respectively. The S-band mixer design has shown that networks consisting of stubs and lines perform adequately, and therefore this approach will again be implemented. The intended topology for the design is shown in Figure 4.5.

4.2.6.1 IF Low-pass Filter

From Figure 4.25 it is evident that the two large frequencies centered around 10MHz need to be removed from the IF port. This will be done using a stepped impedance low-pass filter [35]. The filter is designed to attenuate maximally at 11 GHz, while passing the IF at 1.1 GHz. When designing stepped impedance filters, a general compromise has to be made between bandwidth, ripple, attenuation and realizability. The designed 7-element filter provides 46dB isolation at the RF frequency, while the ripple in the IF-band is negligible. The simulated response is shown in Figure 4.26.

Ideally the low-pass filter provides the antiparallel diode pair with a 50Ω termination at ω_{IF}, while it becomes an open circuit for the higher frequencies. The next step is to design the band-pass filter for the RF.

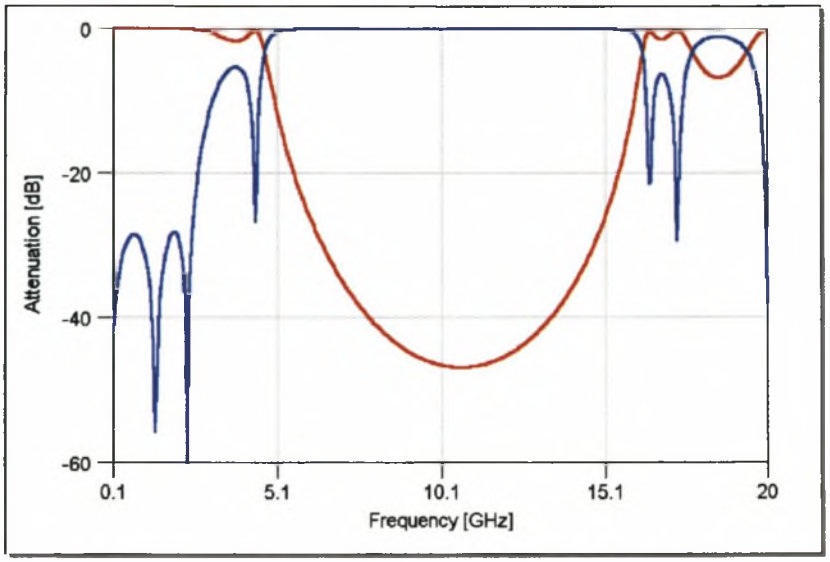

Figure 4.26 : Low-Pass Filter Frequency Response (s_{11} = blue, s_{21} = red)

4.2.6.2 RF Band-Pass Filter

The RF band-pass filter should ideally pass the band of frequencies around 11 GHz, while presenting an open circuit to the other frequencies. A 5^{th}-order coupled line filter provides ~3GHz RF bandwidth, while attenuating the IF signal by ~80dB [8, 34]. The response for the simulated filter (using microstrip) is shown in Figure 4.27.

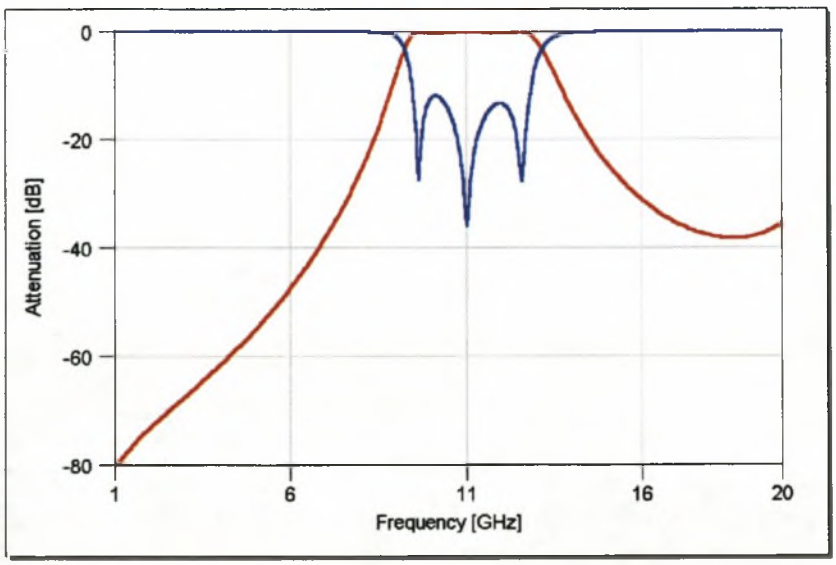

Figure 4.27 : Band-Pass Filter Frequency Response (s_{11} = blue, s_{21} = red) for realized microstrip filter

Once the filters have been implemented, the antiparallel diode pair needs to be matched to these filters in order to see a 50Ω termination at the 1.1GHz and 11GHz at the IF port and RF port respectively.

4.2.6.3 IF Matching Network

The purpose of the IF matching network is again twofold :

- Match the 50Ω IF port to the IF filter at 1.1GHz;
- Isolate the IF port from the antiparallel diode pair at 11GHz.

At 1.1GHz the input impedance of the antiparallel diode pair at the IF port is $\{42.8 - j15\}\Omega$. This impedance is matched to the 50Ω filter by a length of transmission line with an impedance of 90Ω, 25° long at the IF frequency. The match is completed by an open-ended stub with impedance 90Ω and length 35° at the IF frequency. This combination provides a very good match in the IF band from 0.7GHz to 1.5GHz, as is evident from Figure 4.28. However, the RF port still contains no matching network, and is completely unmatched to the antiparallel diode pair, as seen on Figure 4.29.

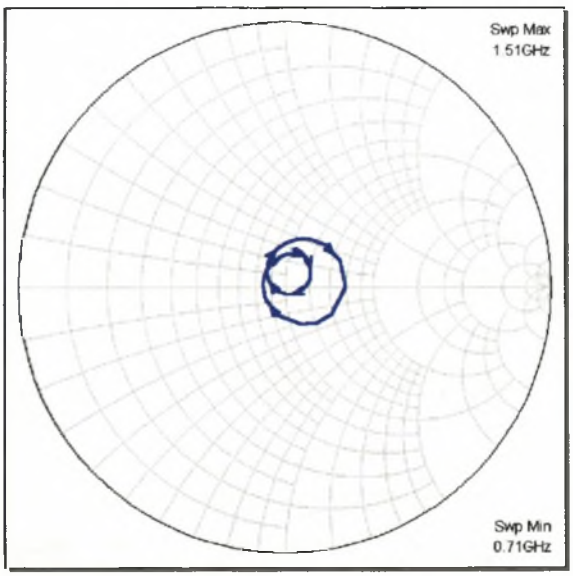

Figure 4.28 : IF port Input Impedance for 0.7 – 1.5GHz (after the addition of the IF matching network)

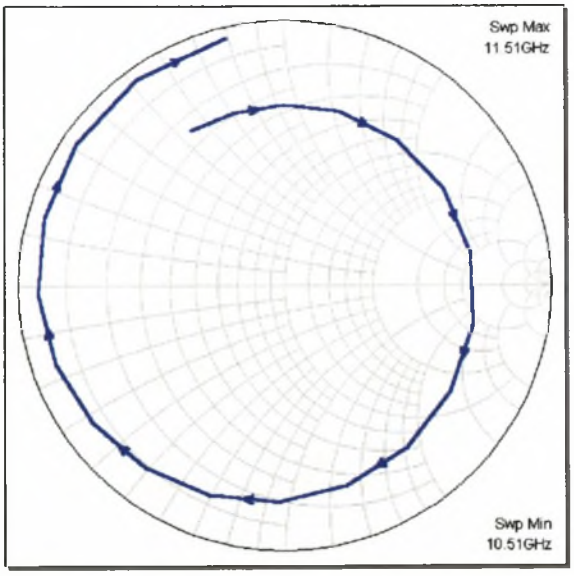

Figure 4.29 : RF port Input Impedance from 10.5GHz – 11.5GHz (after the addition of the IF matching network)

4.2.6.4 RF Matching Network

The only purpose of the RF matching network is to match the 50Ω RF band-pass filter to the antiparallel port at 11GHz. The RF band-pass filter already provides adequate isolation between the IF and RF ports at 11GHz.

The input impedance at the RF port is 127 – j168 Ω at 11GHz. This, together with the curve of Figure 4.29, suggests that the proposed 2-element stub match might not be adequate for the RF band. However, for the purpose of the illustration the 2-element match will be implemented.

The RF antiparallel diode pair is matched to the RF band-pass filter by first inserting a length of transmission line with impedance 70Ω and an electrical length of 63° at 11 GHz between the diodes and the band-pass filter (rotation on the Smith chart). A open-ended stub of 90Ω and of length 74.5° at 11GHz completes the match (movement towards the center of the Smith chart).

Figures 4.30 and 4.31 show the final input impedances of the RF port and the IF port respectively.

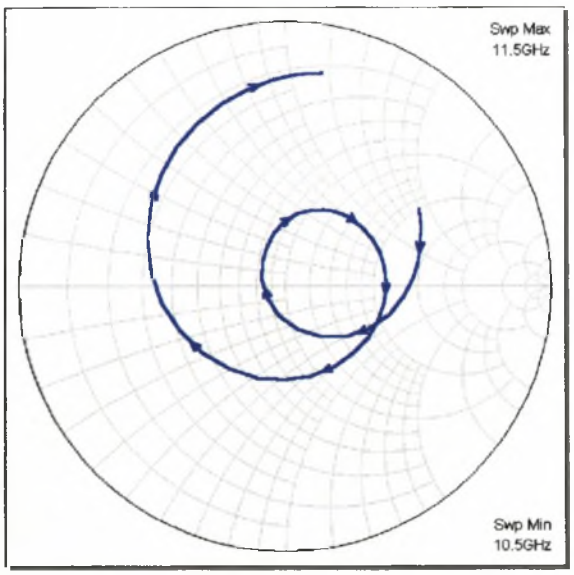

Figure 4.30 : Final RF port Input Impedance for 10.5 GHz to 11.5 GHz (after the addition of the IF and RF matching networks)

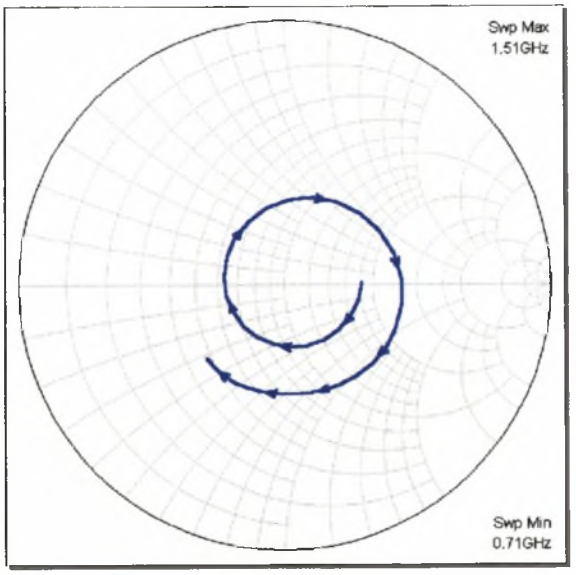

Figure 4.31 : Final IF port Input Impedance from 700 MHz to 1.5 GHz (after the addition of the IF and RF matching networks)

4.2.6.5 LO Isolation

Similar to the S-band mixer, a filter is used between the LO port and the antiparallel diode pair. The main objective of this filter is to reduce the real impedance seen by frequencies such as the RF and IF, leading to improved conversion loss.

Since the IF and RF is much further removed from the LO in the frequency spectrum than was the case with the S-band mixer (see Figure 4.32), it is possible to implement a band-pass filter

[14, 34]. The simulated frequency response of a 2nd-order band-pass filter providing ~40dB attenuation of the IF signal together with ~60dB attenuation of the RF is shown in Figure 4.33.

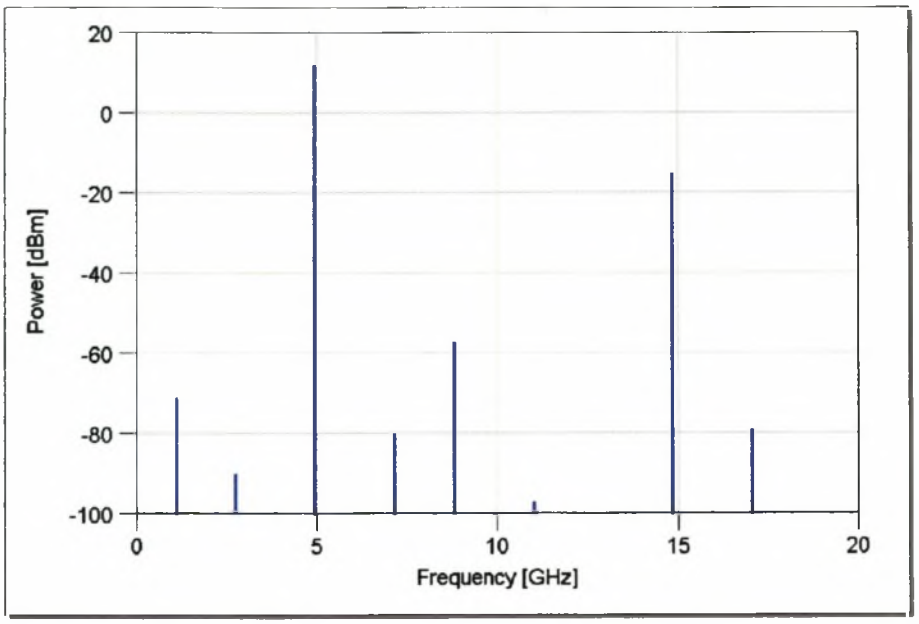

Figure 4.32 : Frequency Spectrum at LO port (before isolation)

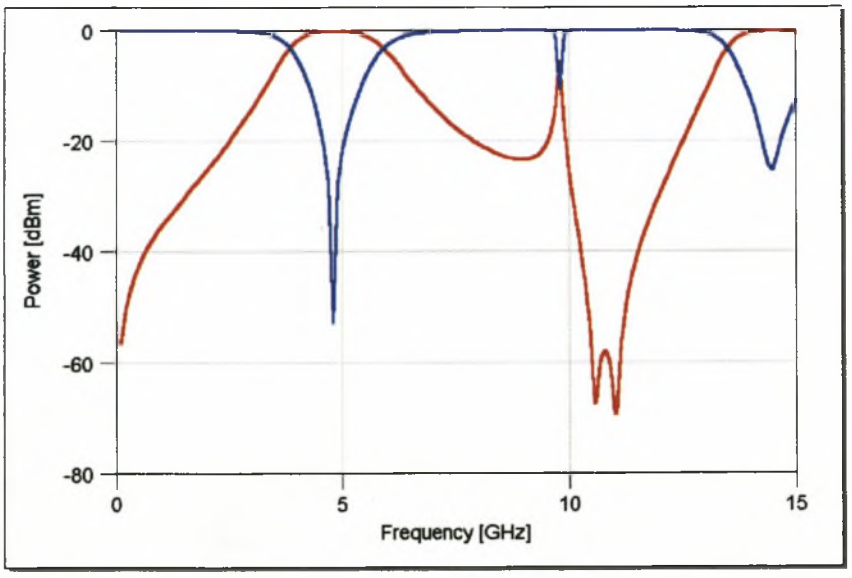

Figure 4.33 : Frequency Response of implemented LO BPF (s_{11} = blue, s_{21} = red)

4.2.7 Microstrip Simulation

The circuit is transformed to microstrip and its operation simulated. For the simulation all ideal transmission lines from the initial design are replaced with microstrip lines of the correct length and width, and are joined by the necessary T-junctions or cross-junctions. The shorted stub on the large-signal side is realized with a microstrip line connected to ground by a ground strap. The model used in Chapter 2 for the SMA-connectors [26] was used on the ports of the mixer.

After the circuit was simulated, it was noted that the RF and LO signals were not as optimally isolated from the IF port as it was intended. Therefore, the isolation was enhanced by adding to shunt open-ended stubs between the IF port and the IF low-pass filter. The stubs had an impedance of 90Ω, and were 90° long at the RF and LO frequencies respectively. Their addition improved the isolation, but did not alter the conversion loss or IF input impedance significantly.

The circuit was once again optimized for minimal conversion loss. The process of optimization was identical to that of the S-band mixer.

Figure 4.34 shows the simulated output spectrum at the IF port with an applied LO ranging between –5dBm and +15dBm, and an applied RF of –20dBm. The simulated mixer has an optimum conversion loss of 6.5dB, and this is achieved at an LO power of +9.5dBm.

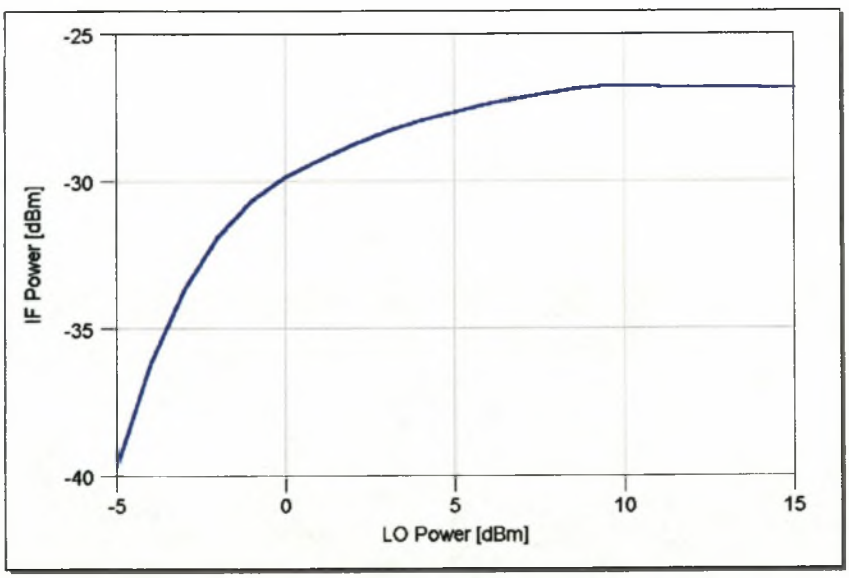

Figure 4.34 : Simulated LO power against IF Power of the X-band Harmonic Mixer

Figure 4.35 shows the simulated output spectrum at the IF port (with +9dBm applied LO power and –20dBm RF power). The IF (1.1 GHz), LO (4.95 GHz) and RF (11 GHz) signals are visible,

with the LO and RF well suppressed to below –80dBm. Also visible is the $\{2\omega_{RF} - \omega_{LO}\}$ mixing product at 16.6 GHz. This product is not suppressed by the IF low-pass filter (Figure 4.26), but is small enough (-77dBm) not to interfere with the IF signal.

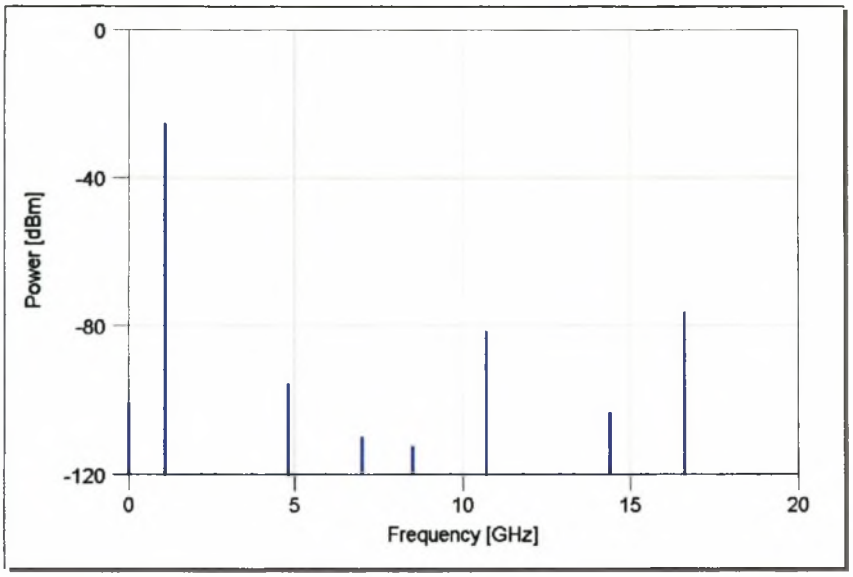

Figure 4.35 : Simulated Output Spectrum at the IF Port with +9dBm LO Power and –20dBm RF Power applied

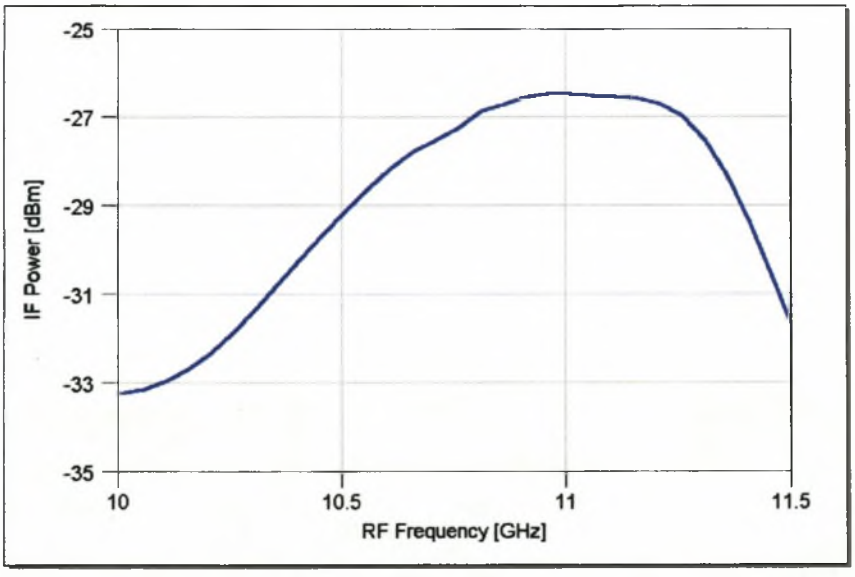

Figure 4.36 : Simulated plot of RF frequency against IF power for the X-band mixer with +9dBm LO Power and –20dBm RF Power applied

The bandwidth of the X-band mixer is measured by plotting RF frequency against IF power. Figure 4.36 shows the simulated response, with an optimal conversion loss of 6.5 dB achieved at

11 GHz. From the plot the bandwidth is estimated to be ~750 MHz, slightly more than the 6% bandwidth required by the specification

4.2.8 Realization

A layout of the realized mixer is shown in Figure 4.37. The SMA-connectors are connected to the ports via lengths of 50Ω line. A photograph of the manufactured mixer is shown in Figure 4.38.

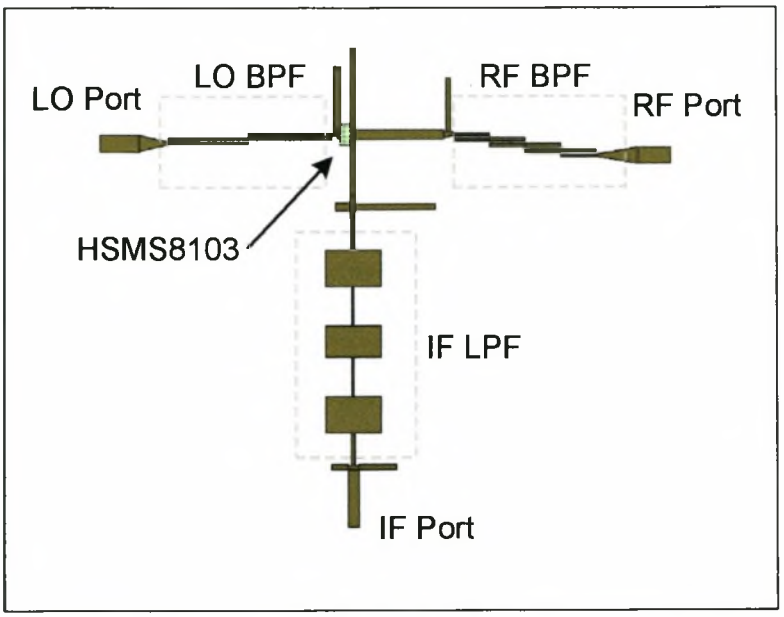

Figure 4.37 : Layout of finalized X-band mixer (Scale 1 : 1)

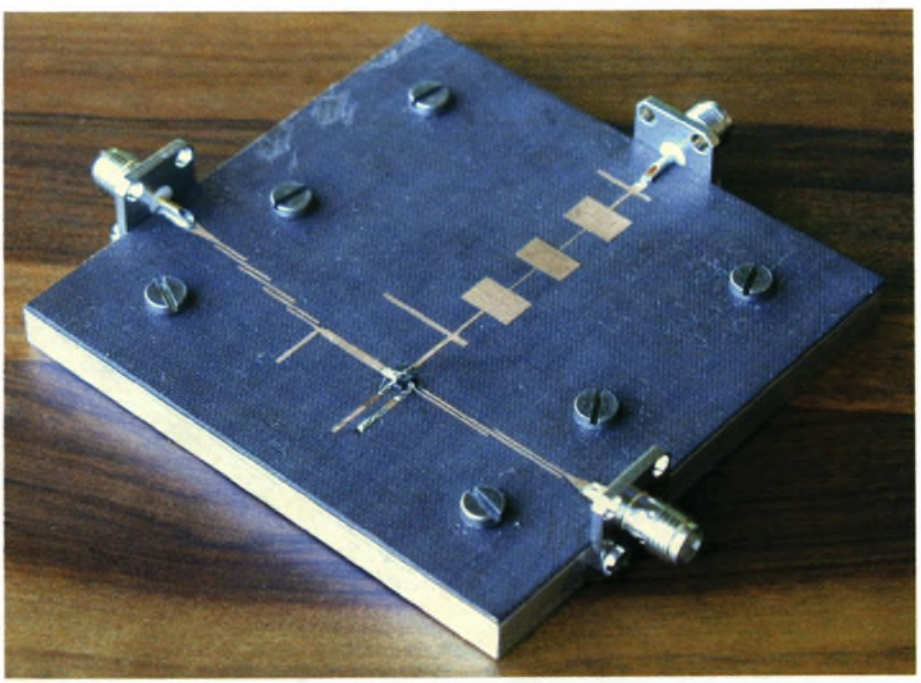

Figure 4.38 : The Manufactured X-band Mixer

4.2.9 Measurements

The X-band mixer was measured to determine conversion loss, isolation and bandwidth. Again the measurements generally agreed very well with the predicted results.

Figure 4.39 shows the mixer's measured conversion loss by plotting input LO power against output IF power. The minimum conversion loss is 7.8dB (1.3dB less than the value predicted in Figure 4.34). This optimum conversion loss is achieved with 8dBm – 10dBm LO power (similar to the predicted values of Figure 4.34). The shape of the measured curve agrees well with the predicted curve of Figure 4.34, although an unexpected resonance is experienced at lower LO levels. Curves very similar to that of Figure 4.39 (with specific reference to the resonance) have been recorded by [36].

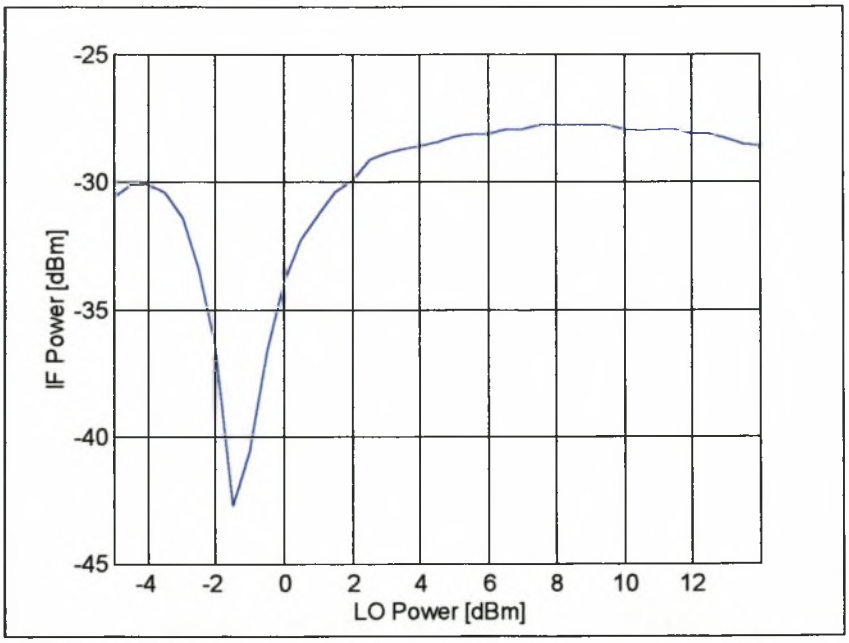

Figure 4.39 : Measured LO power vs IF power for X-band harmonic mixer

Next a RF frequency sweep is done with +9dBm LO power applied to the mixer. The –20dBm RF signal was swept from 10.5GHz to 11.5GHz, resulting in an IF from 600MHz to 1.6GHz. Figure 4.40 shows the measured curve. A 3dB-bandwidth of ~550MHz is measured, 200MHz less than the predicted value. The shape of the curve in Figure 4.40 agrees well with the predicted shape of Figure 4.36.

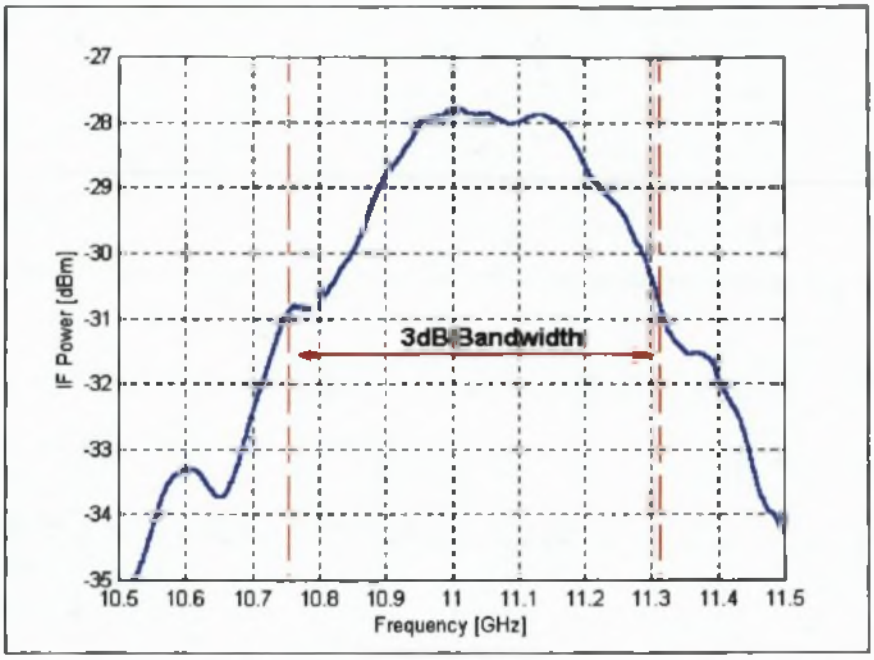

Figure 4.40 : Measured RF-sweep of X-band harmonic mixer with +9dBm LO Power and –20dBm RF Power applied

Finally the port-to-port isolations are measured using a spectrum analyzer and a power meter :

LO-to-IF Isolation : 37dB

RF-to-IF Isolation : 46dB

These values (especially the LO-to-IF isolation) are slightly less than the anticipated value. This is most likely due to the position of the antiparallel diode pair, which was soldered slightly off its intended position.

4.2.10 Comments

The design and realization of the X-band mixer is successful. The mixer achieves a very competitive conversion loss. For the larger part the mixer can again be modeled very adequately, while the design procedure facilitates a successful design.

In the previous section the aspect of diode position was mentioned. When the mixer was manufactured, the diodes were soldered 2mm off their intended position, in the direction of the stubs. This resulted in an initial measurement of 19dB conversion loss. The diodes were subsequently soldered on correctly, and the mixer performed according to specification. This demonstrates the mixer's sensitivity for the position of the diodes.

Conclusion

This thesis explored the analysis and synthesis of diode harmonic mixers. The aim of the analysis was to characterize the harmonic mixer sufficiently in order to set up a design procedure. This design procedure would then be used to synthesize and realize a harmonic mixer from a set of specifications.

A literature study was performed to investigate the implementation and performance of harmonic mixers. It soon became evident that there does not exist a general design method for harmonic mixers which considers all the possibilities of mixer design that are available to the designer. With this deficiency in mind, the process of characterizing the harmonic mixer was initiated. A study of the conventional diode mixer topologies was made, whereafter the performance of the harmonic mixer could be related to the performance of the conventional mixer topologies. The general mixer properties such as conversion loss, isolation, noise, input impedance and intermodulation were defined and discussed.

The operation of the harmonic mixer was then investigated. By starting with the Schottky mixer diode, equations describing the operation of the harmonic mixer were derived, and the operation of a fundamental building block of harmonic mixers, the antiparallel diode pair, was investigated. Properties inherent to the antiparallel diode pair (such as selected mixing product rejection, LO amplitude noise rejection, etc.) were investigated, and verified mathematically. The phenomenon of unbalance in the antiparallel diode pair was investigated, and observations of the mixer's sensitivity for diode unbalance were made.

Mixer analysis by means of a large-signal and small-signal analysis was explored. After the harmonic balance method was introduced as a popular tool for large-signal analysis, the adaptation of the method for a mixer containing an antiparallel diode pair was explored. The small-signal analysis was adapted for use with the harmonic mixer by describing the mixer as a multi-port, multi-frequency structure. Once the mixer analysis was complete, the input impedance, conversion loss and noise were related to the harmonic mixer by the small-signal parameters calculated in the small-signal analysis.

In order to gain a better intuitive understanding of the operation of the antiparallel diode pair, a number of simulations were done on selected mixer circuits containing the antiparallel diode pair. The junction conductance and capacitance waveforms were verified, and the variation of the input impedance with swept LO power was investigated. A measurement was done to extract the parameters of the HSMS-8202 diode pair, and the resulting model was used for later mixer designs.

Once the investigation of the operation of the harmonic mixer was complete, the synthesis of the mixer was considered. An extended literature study was performed on various examples of harmonic mixer designs and implementations. Once this was completed, the various criteria for mixer design were discussed. The design criteria were related to the mixer characteristics developed in Chapter 2. Suggestions were made for optimum mixer design, and a design topology was proposed. The design provided a step-by-step procedure to design a variety of harmonic mixers. Such a procedure has not been presented in literature.

Finally the presented design procedure was evaluated with the synthesis and manufacturing of two harmonic mixers, one at S-band and the other at X-band. The manufactured mixers were measured, and generally agreed well with the results predicted from the simulations. Satisfactory results were obtained for conversion loss (7.8 dB optimum), bandwidth (10% optimum) and port isolation (all in excess of 40 dB).

It was found that the proposed design topology gives good and repeatable results. Its success depends on the validity of the assumption of port isolation. This requirement can be met without difficulty when the IF, RF and LO frequencies are spaced far enough apart, as was the case with the implemented designs, and often harmonic mixers in general. When the spacing between the various frequencies becomes small, it becomes difficult to realize filters that present open circuits at the surrounding frequencies, and the design method might become less effective. It was also noted that the mixer is very sensitive to manufacturing tolerances. A study of sensitivity will therefore ensure optimum design methods.

The scenario lends itself to simultaneously matching the antiparallel diode pair to both ports on one of its sides. By utilizing an optimization routine to find an optimal match for both ports given an initial guess, a better match can be achieved faster. Although it was not done in the current text in order to facilitate the demonstration, the option of combining filtering and matching into one structure must definitely be considered. A well-defined technique for optimum

matching of all ports with minimal dependence on any assumptions will definitely add significantly to the success of the method.

The harmonic mixer was considered as a tool for frequency conversion. After an analysis of the mixer, a procedure for synthesis was proposed. Such a method has to date not been available in literature. The method was verified, and the results agreed well with the manufactured mixers. Further verification and optimization might be needed before a robust method for harmonic mixer design is presented.

Appendix A : The Reflection Algorithm

The Reflection Algorithm [143] is an alternative to the harmonic balance method for solving the large-signal mixer problem. Although the circuit is divided into linear and nonlinear parts and a solution is then found iteratively, as with the HB method, the main differences to the HB method are as follows :

1) The reflection algorithm uses propagating waves instead of currents and voltages, and
2) The method is self-initiating; it is not required to make an initial guess.

The reflection algorithm is a type of "splitting method" where a new estimate is defined as the point lying geometrically between the previous two estimates (as opposed to Newton's method which uses gradient information).

The linear circuit is separated from the nonlinear circuit by means of a length of transmission line with characteristic impedance Z_c, as shown in Figure A.1. The transmission line is assumed to be a integral number of wavelengths long at the LO, resulting in equal steady-state voltages and currents at the terminals of the diode and the linear circuit. Note that the series resistances R_s of the two diodes of the antiparallel diode pair is not included in the linear part of the circuit.

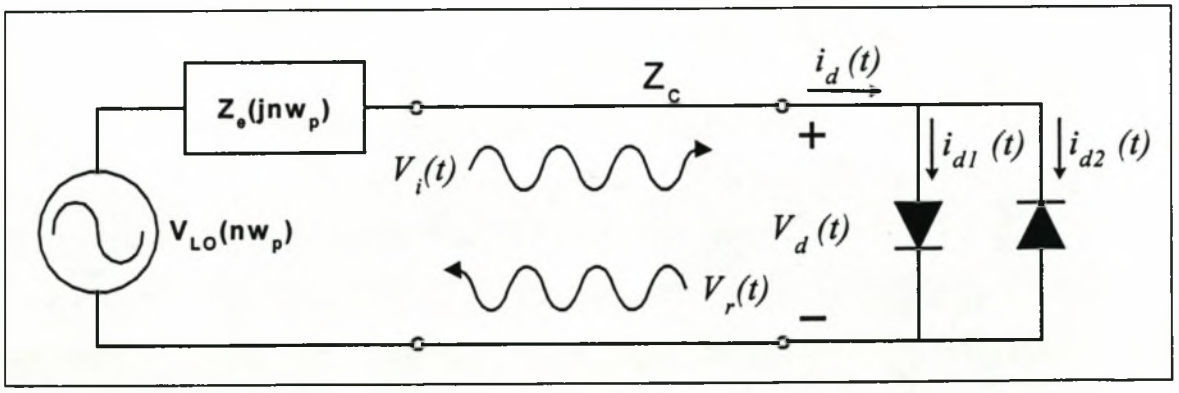

Figure A.1 : Large-Signal Circuit used for the Reflection Algorithm

As the LO is applied at the left of the transmission line, an incident wave $V_i(t)$ is excited. The incident wave $V_i(t)$ is obtained via elementary circuit analysis and given by

$$V_i(t) = \frac{V_{LO} Z_c}{\sqrt{Z_c^2 + \left|Z_e(j\omega_p)\right|^2}} \cos(\omega_p t + \theta) \qquad \text{..... (A.1)}$$

where

$$\theta = tan^{-1}\left(\frac{Im\left\{Z_e\left(j\omega_p\right)\right\}}{Re\left\{Z_e\left(j\omega_p\right)\right\}+Z_c}\right) \qquad \text{..... (A.2)}$$

The transmission line only provides a convenient way of dividing the diode circuit into two parts, as shown in Figure A.2. The terminating resistance of the circuit on the left-hand side of the transmission line becomes the source resistance of the circuit on the right hand side of the transmission line.

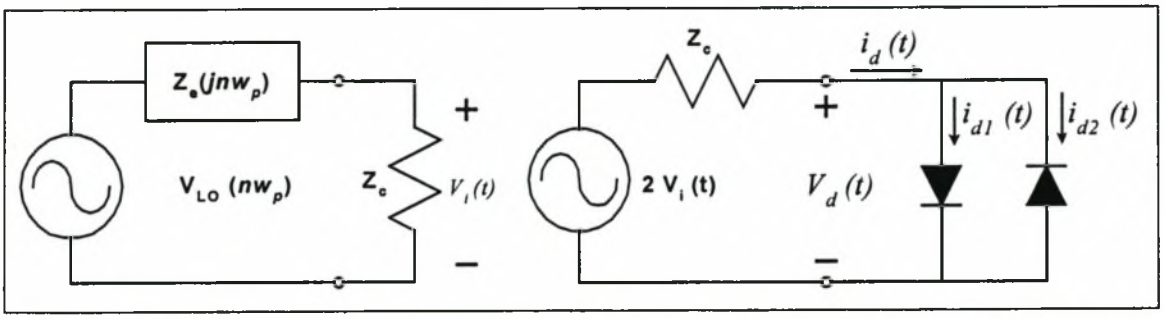

Figure A.2 : The division of the mixer circuit into equivalent circuits for use with the Reflection Algorithm

The incident wave $V_i(t)$ now propagates through the transmission line, reaching the pair of antiparallel diodes. The model for the antiparallel diode pair consists entirely of lumped elements (linear and nonlinear), and as was the case previously, a solution is most conveniently obtained in the time-domain. Using equations (A.1) – (A.2), the following differential equation is found by applying Kirchoff's voltage law :

$$-2V_i(t)+Z_cI_{apdp}+\frac{I_{apdp}R_s}{2}=0 \qquad \text{..... (A.3)}$$

where I_{apdp} is the current into the antiparallel diode pair, defined as follows (under the assumption of identical diodes *D1* and *D2*) :

$$\begin{aligned} I_{apdp}\Big|_{(D1=D2)} &= I_d\left(V_j(t)\right)+C_j\left(V_j(t)\right)\frac{d}{dt}\left\{V_j(t)\right\} \\ &+I_d\left(-V_j(t)\right)+C_j\left(-V_j(t)\right)\frac{d}{dt}\left\{-V_j(t)\right\} \end{aligned} \qquad \text{..... (A.4)}$$

The differential equation (A.3) is solved numerically, and the terminal voltage and current of the antiparallel diode pair, $V_p(t)$ and $I_{apdp}(t)$ are found. The reflected wave propagating from right to left towards the LO source is now given by

$$V_r(t) = \frac{V_p(t) - Z_c I_{apdp}(t)}{2} \qquad \text{..... (A.5)}$$

using transmission line theory. At the source $V_r(t)$ is first Fourier transformed to obtain $V_r(j\omega_p)$ at each harmonic of the LO, then $V_r(j\omega_p)$ is multiplied by the reflection coefficient $\Gamma(j\omega_p)$, and finally the inverse Fourier transform is taken. The new incident wave $V_i^2(t)$ is found by adding the reflected wave to the original wave (the "splitting" algorithm), or after p iterations

$$V_i^{p+1} = V_i(t) + IFFT\left[\Gamma(j\omega_p) FFT\left\{V_i^p(t)\right\}\right] \qquad \text{..... (A.6)}$$

where the reflection coefficient at the harmonics of the LO is given by its usual relation

$$\Gamma(j\omega_p) = \frac{Z_e(j\omega_p) - Z_c}{Z_e(j\omega_p) + Z_c} \qquad \text{..... (A.7)}$$

Conversion of the process is indicated by minimum variation in the terminal voltages and currents $V_p(t)$ and $I_{apdp}(t)$ of the antiparallel diode – as soon as this criteria is achieved, the values for $V_p(t)$ and $I_{apdp}(t)$ are the valid large-signal solutions.

Whether it is a single diode or antiparallel diode (or any other nonlinear circuit), the reflection algorithm provides a method of solving the unknown voltages and currents in the diode(s). On completion of the large-signal analysis, the set of harmonic voltages $V_j = V_j(n\omega_p)$ and harmonic currents $I_d = I_d(n\omega_p)$ for n = 0,1,2,... are known. Therefore the time-varying conductance waveform $g_T(t)$ and time-varying capacitance waveform $C_T(t)$ due to the LO are known quantities.

Appendix B : Filters implemented in the S-band Harmonic Mixer

Three filter structures were implemented in the S-band harmonic mixer :

- A low-pass filter on the IF port,
- A low-pass filter on the LO port,
- A band-pass filter on the RF port.

The details for the realized filters are given in the following sections. The layout for the mixer is shown in Figure B.1.

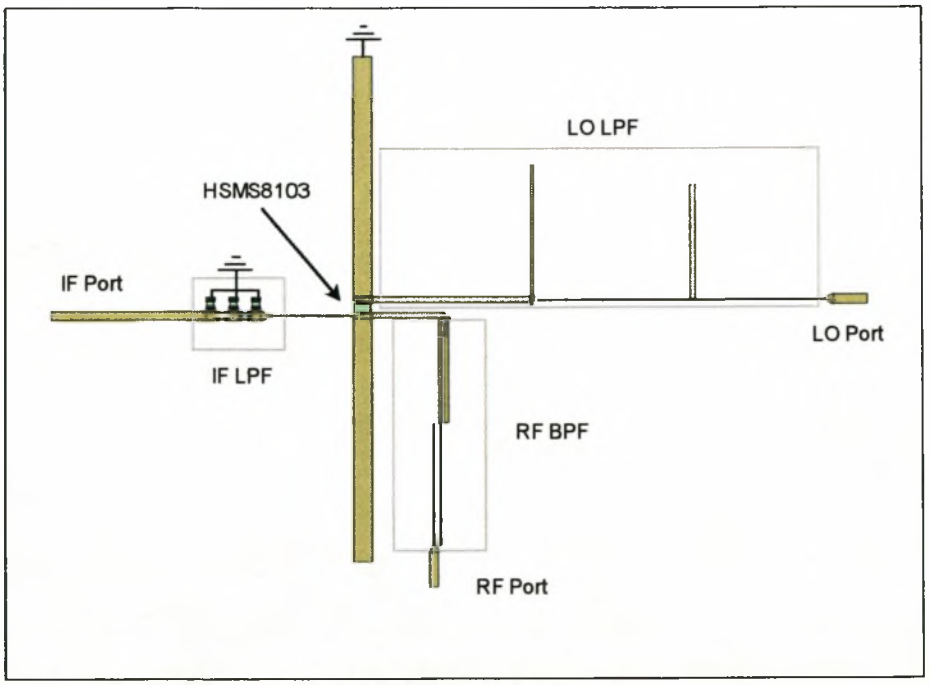

Figure B.1 : S-Band Harmonic Mixer Layout

B.1) The IF low-pass Filter

It was decided that the IF filter should cut off at 500 MHz, and attenuate as much as possible at 1.1 GHz and 2.45 GHz. The filter was realized using a 5-element LC-ladder [8]. After the initial design, the component values were optimized for realizable component values. Both the inductors and

capacitors are 0805-type surface mount components, while the inductors have Q = 50. Figure B.2 demonstrates the topology of the filter. Figure B.2 shows the simulated frequency response.

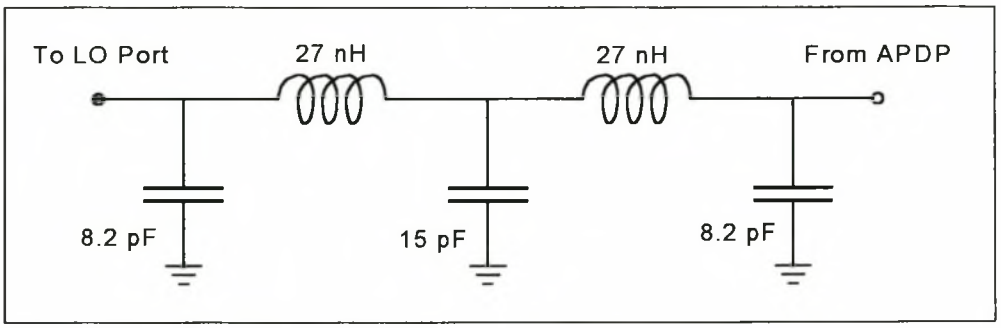

Figure B.2 : Lumped Topology for the IF low-pass filter

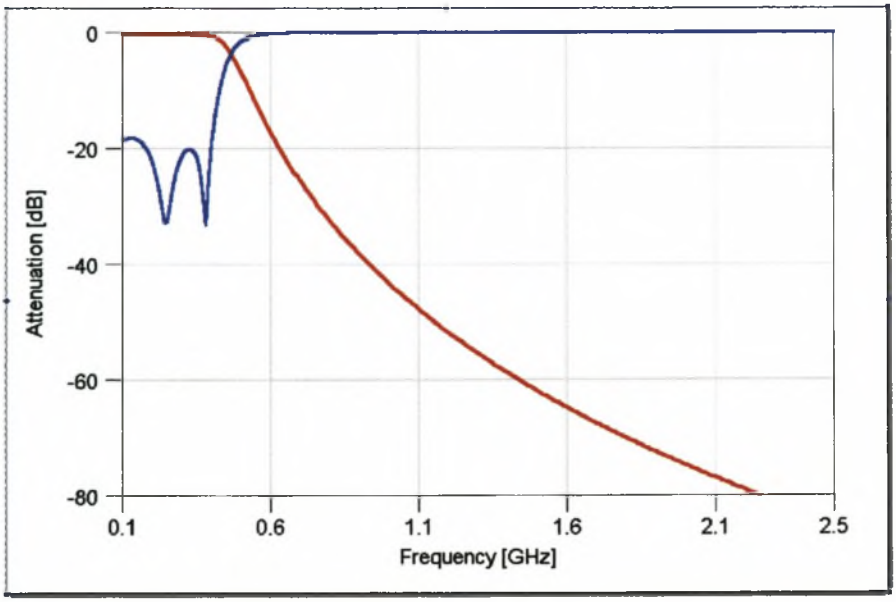

Figure B.3 : Response for the IF low-pass filter (s_{11} = blue, s_{21} = red)

B.2) The LO low-pass Filter

The LO low-pass filter implemented consisted of 4 quarter wave-stubs at the RF frequency. The low-pass filter should ideally be an open circuit to the RF. The topology of the filter, and the dimensions of the lengths of microstrip is given in Figure B.4. Figure B.5 shows the simulated characteristic of the low-pass filter.

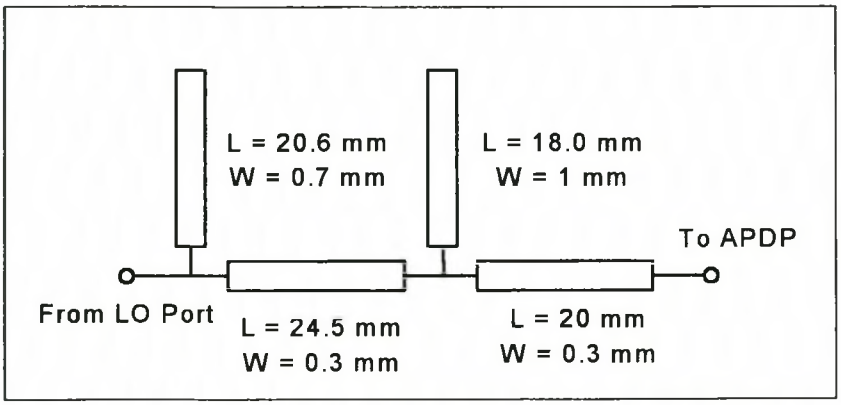

Figure B.4 : Microstrip Topology for LO low-pass filter

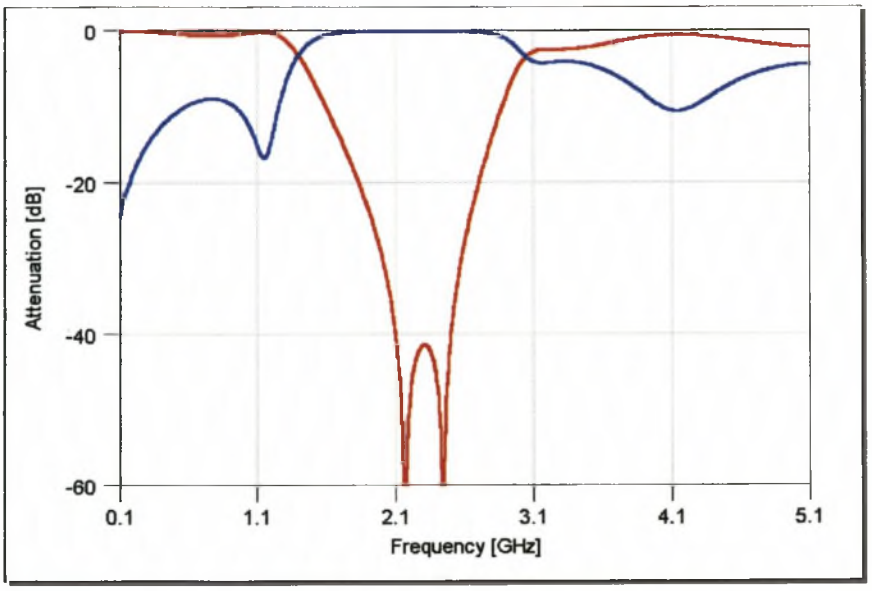

Figure B.5 : Response for the LO low-pass filter (s_{11} = blue, s_{21} = red)

B.3) The RF band-pass Filter

The RF band-pass filter is chosen to comprise two sections of coupled lines. Using [8] and [34], the usual design procedure is followed, and the filter is realized in microstrip. Figure B.6 shows the topology for the filter, as well as the measurements for the microstrip lines. Figure B.7 shows the simulated response of the band pass filter.

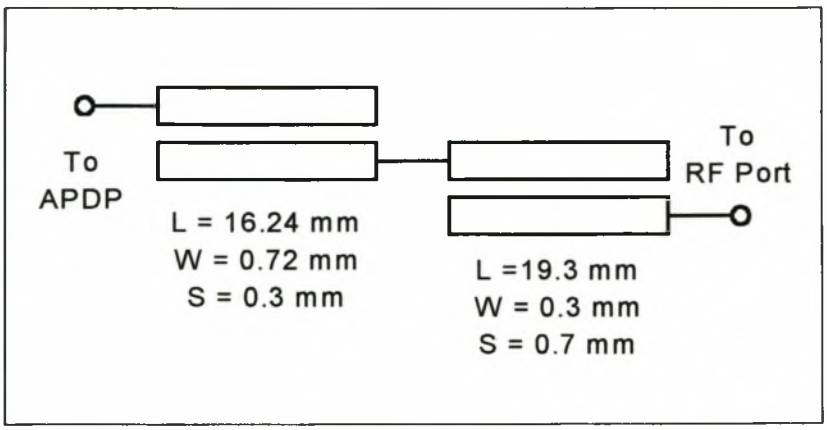

Figure B.6 : Microstrip Topology for RF band-pass filter

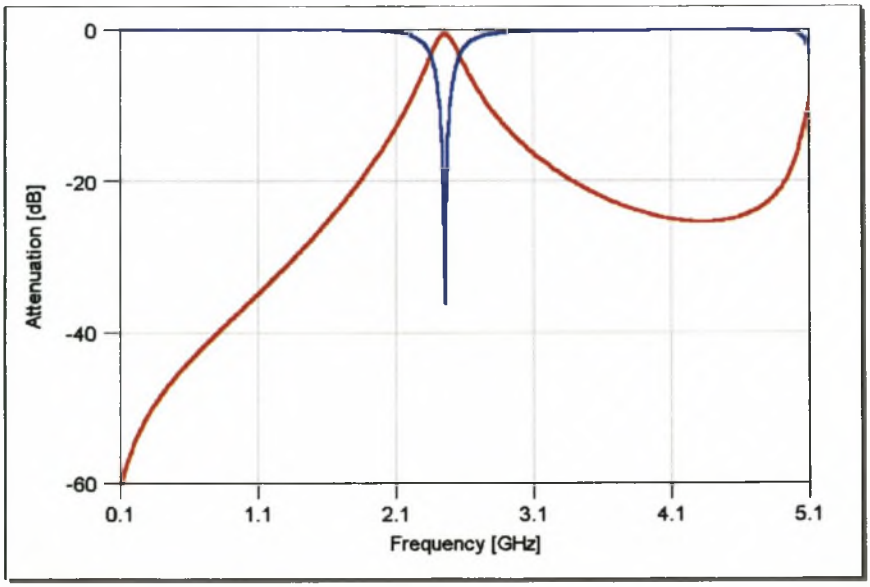

Figure B.7 : Response for the RF low-pass filter (s_{11} = blue, s_{21} = red)

This concludes the design for the filters implemented in the S-band harmonic mixer. All the planar structures were realized in microstrip with $\varepsilon_r = 3.86$ and h = 0.787.

Appendix C : Filters implemented in the X-band Harmonic Mixer

Three filter structures were implemented in the X-band harmonic mixer :

- A low-pass filter on the IF port,
- A band-pass filter on the LO port,
- A band-pass filter on the RF port.

All the filters were realized as planar structures. The details for the realized filters are given in the following sections. The layout for the mixer is shown in Figure C.1.

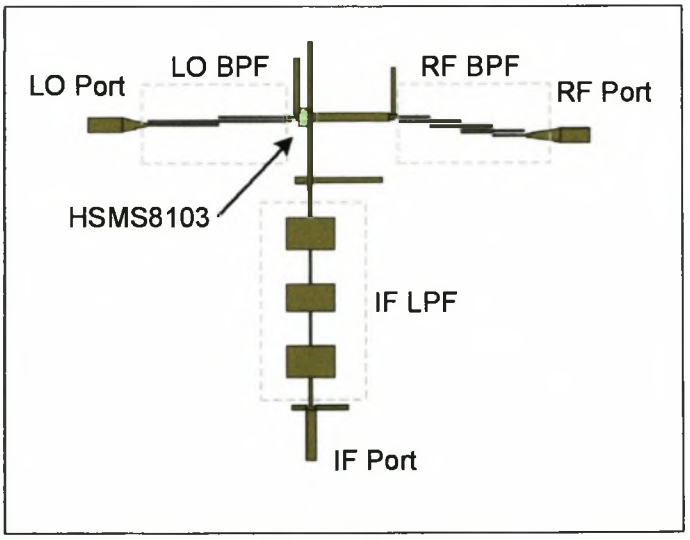

Figure C.1 : X-Band Harmonic Mixer Layout

C.1) The IF low-pass Filter

It was decided that the IF filter should cut off at 5 GHz, and attenuate as much as possible at 11 GHz. The filter was realized as a stepped impedance low-pass filter [35]. The design is chosen to have a larger ripple, but a steeper roll-off in return. Figure C.2 demonstrates the topology of the filter. Figure C.2 shows the simulated frequency response.

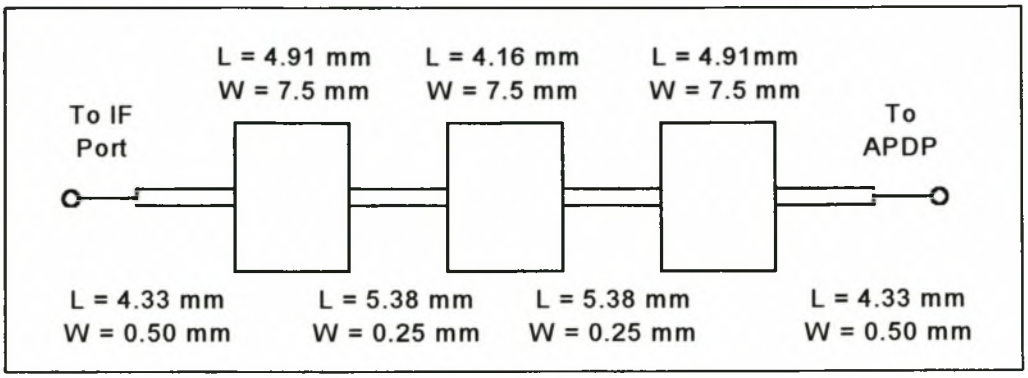

Figure C.2 : Topology for the IF low-pass filter

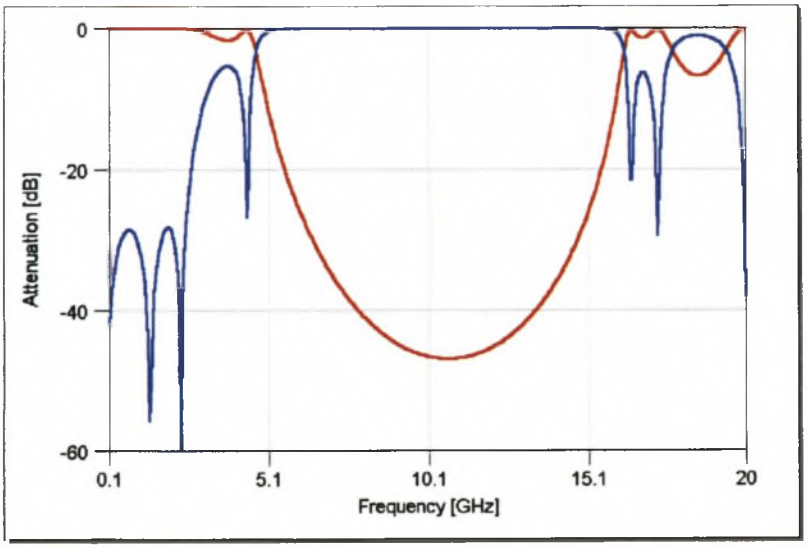

Figure C.3 : Response for the IF low-pass filter (s_{11} = blue, s_{21} = red)

C.2) The LO band-pass Filter

The LO filter requires minimum bandwidth, and therefore a topology with two coupled sections was decided upon [8] and [34]. The topology of the filter, and the dimensions of the lengths of microstrip is given in Figure C.4. Figure C.5 shows the simulated characteristic of the low-pass filter.

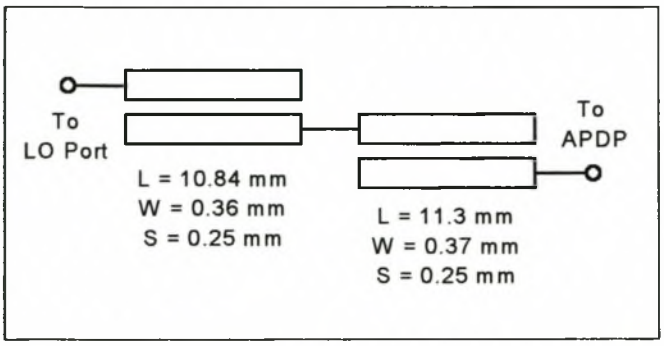

Figure C.4 : Microstrip Topology for LO band-pass filter

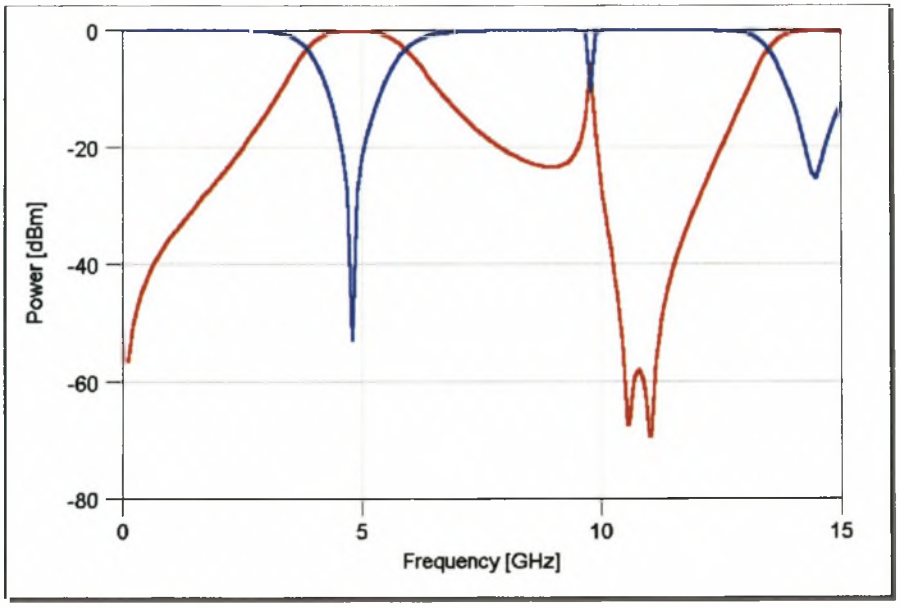

Figure C.5 : Response for the LO low-pass filter (s_{11} = blue, s_{21} = red)

C.3) The RF band-pass Filter

The RF band-pass filter is chosen to comprise four sections of coupled lines. Using [8] and [34], the usual design procedure is followed, and the filter is realized in microstrip. Figure C.6 shows the topology for the filter, as well as the measurements for the microstrip lines. Figure C.7 shows the simulated response of the band-pass filter.

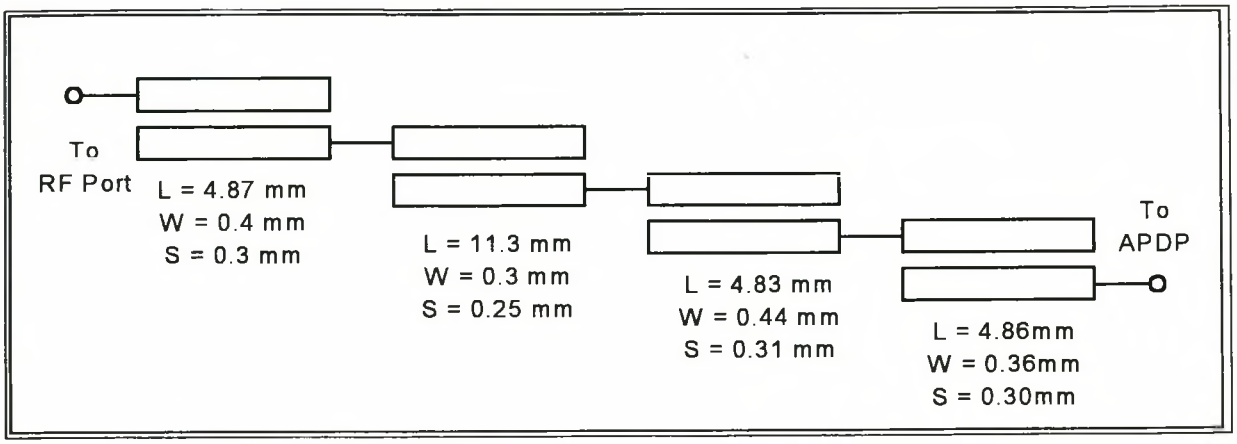

Figure C.6 : Microstrip Topology for RF band-pass filter

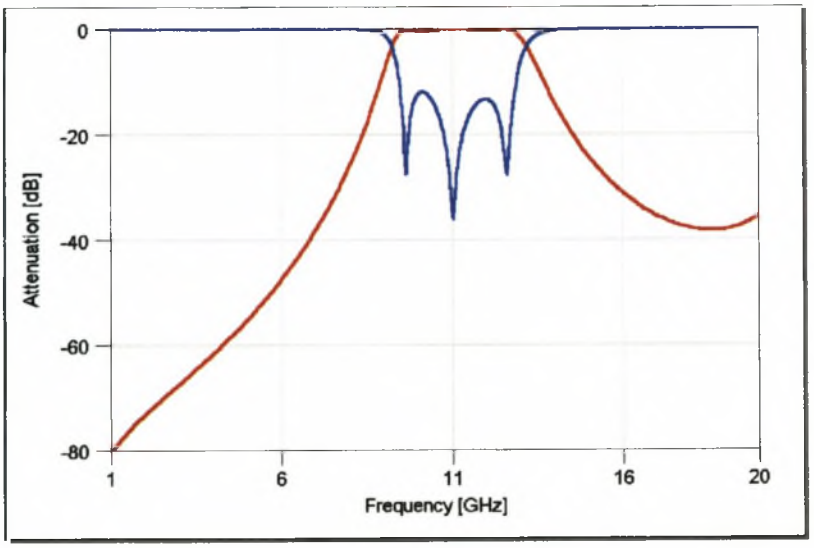

Figure C.7 : Response for the RF band-pass filter (s_{11} = blue, s_{21} = red)

This concludes the design for the filters implemented in the X-band harmonic mixer. All the structures were realized in microstrip with $\varepsilon_r = 2.48$ and h = 0.787.

References

[1] Martin V. Schneider, William W. Snell, Jr., "Harmonically Pumped Stripline Down-Converter", *IEEE Transactions on Microwave Theory and Techniques*, vol. MTT-23, no. 3, pp. 271-275, March 1975

[2] Marvin Cohn, James E. Degenford, Burton A. Newman, "Harmonic Mixing with an Antiparallel Diode Pair", *IEEE Transactions on Microwave Theory and Techniques*, vol. MTT-23, no. 8, pp. 667-673, August 1975

[3] Thomas F. McMaster, Martin V. Schneider, William W. Snell, Jr. "Millimeter-wave Receivers with Subharmonic Pump", *IEEE Transactions on Microwave Theory and Techniques*, vol. MTT-24, no. 12, pp. 948-952, December 1976

[4] Specifications: HP 11970 Series Harmonic Mixers, Hewlett Packard

[5] Ross L. Finney, George B. Thomas Jr., "Calculus", 2nd Edition, Addison-Wesley Publishing Company, 1994

[6] Stephen A. Maas, "Nonlinear Microwave Circuits", Artech House, 1988

[7] Bert C. Henderson, "Mixers in Microwave Systems (Part 1)", Watkins-Johnson Company, vol. 17, no. 1, 1990

[8] David M. Pozar, "Microwave Engineering", 2nd Edition, John Wiley and Sons, 1998

[9] Stephen A. Maas, "Microwave Mixers", 2nd Edition, Artech House, 1993

[10] Liam Devlin, "Mixers", Plextex Communications Technology Consultants

[11] Mark R. Barber, "Noise Figure and Conversion Loss of the Schottky Barrier Mixer Diode", *IEEE Transactions on Microwave Theory and Techniques*, vol. MTT-15, no. 11, pp. 629-635, November 1967

[12] Just-Dietrich Büchs, Günther Begemann, "Frequency conversion using harmonic mixers with resistive diodes",

[13] Shunichiro Egami, "Nonlinear, Linear Analysis and Computer-Aided Design of Resistive Mixers", *IEEE Transactions on Microwave Theory and Techniques*, vol. MTT-22, no. 3, pp. 270-275, March 1973

[14] Rick Poore, "Noise in Ring Topology Mixers", Agilent EEsof EDA, 2001

[15] Marek T. Faber, Jerzy Chramiec, Miroslaw E. Adamski, "Microwave and Millimeter-wave Diode and Frequency Multipliers", Artech House, 1995

[16] Daniel N. Held, Anthony R. Kerr, "Conversion Loss and Noise of Microwave and Millimeter-wave Mixers: Part 2 – Experiment", *IEEE Transactions on Microwave Theory and Techniques*, vol. MTT-26, no. 2, pp. 55-61, February 1978

[17] "Surface Mount Microwave Schottky Mixer Diodes", Technical Data, Agilent Technologies

[18] Dominic A. Fleri, Leonard D. Cohen, "Nonlinear Analysis of the Schottky-Barrier Mixer Diode", *IEEE Transactions on Microwave Theory and Techniques*, vol. MTT-21, no. 1, pp. 39-43, January 1973

[19] P.W. van der Walt, "Efficient Technique for Solving Nonlinear Mixer Pumping Problem", *Electronics Letters*, vol. 21, no. 20, pp. 899-900, September 1985

[20] A.R. Kerr, "A Technique for Determining the Local Oscillator Waveforms in a Microwave Mixer", *IEEE Transactions on Microwave Theory and Techniques*, vol. 23, no. 10, pp. 828-831, October 1975

[21] Anthony R. Kerr, "Noise and Loss in Balanced and Subharmonically Pumped Mixers: Part II – Application", *IEEE Transactions on Microwave Theory and Techniques*, vol. MTT-27, no. 12, pp. 944-950, December 1979

[22] Anthony R. Kerr, "Noise and Loss in Balanced and Subharmonically Pumped Mixers: Part I – Theory", *IEEE Transactions on Microwave Theory and Techniques*, vol. MTT-27, no. 12, pp. 938-943, December 1979

[23] Daniel N. Held, Anthony R. Kerr, "Conversion Loss and Noise of Microwave and Millimeter-wave Mixers: Part 1 – Theory", *IEEE Transactions on Microwave Theory and Techniques*, vol. MTT-26, no. 2, pp. 49-55, February 1978

[24] Mitsuhiro Shimozawa, Kenji Kawakami, Kenji Itoh, Akio Iida, Osami Ishida, "A novel sub-harmonic pumping direct conversion receiver with high instantaneous dynamic range", *IEEE MTT-S Digest*, pp. 819-822, 1996

[25] Kenji Itoh, Kenji Kawakami, Osami Ishida, Koji Mizuno, "Unbalance effects of an antiparallel diode pair on the virtual local leakage in an even harmonic mixer", *IEEE MTT Symposium*, 1998

[26] Marian L. Majewski, Robert W. Rose, James R. Scott, "Modeling and Characterization of Microstrip-to-Coaxial Transitions", *IEEE Transactions on Microwave Theory and Techniques*, vol. MTT-29, no. 8, pp. 799-805, August 1981

[27] Specifications: Surface Mount Low Barrier X-band Schottky Diodes, MA4E2054 Series, M/A-Com

[28] T.H. Oxley, "Introduction – Mixer Background", *Advanced microwave mixer technology*, MEPL Reprint Series, 1989

[29] Kenji Itoh, Akio Iida, Yoshinobu Sasaki, Shuji Urasaki, "A 40 GHz Band Monolithic Even Harmonic Mixer With An Antiparallel Diode Pair", *IEEE MTT-S Digest*, pp. 879-882, 1991

[30] Ryoji Kawasaki, Masami Akaike, "A Broad-Band Second-Harmonic Mixer Covering 76-106 GHz", *IEEE Transactions on Microwave Theory and Techniques*, vol. MTT-26, no. 6, pp. 425-427, June 1978

[31] R.G. Hicks, "High sensitivity full waveguide Ku-band harmonic mixer", *Advanced microwave mixer technology*, T.H. Oxley, Editor, MEPL Reprint Series, 1989

[32] D. Weiner, J. Griffin, L. McCarty, "The Image Rejection Harmonic Mixer", *IEEE MTT-S Digest*, pp. 36-38, 1982

[33] J.L. Merenda, D.Neuf, P. Piro, "4 to 40 GHz even Harmonic Schottky Mixer", IEEE MTT-S Digest, pp.695-698, 1988

[34] Seymour B. Cohn, "Parallel-Coupled Transmission-Line-Resonator Filters", *IRE Transactions on Microwave Theory and Techniques*, vol. MTT-6, no. 2, pp. 223-231, April 1958

[35] Ralph Levy, "Tables of Element Values for the Distributed Low-Pass Prototype Filter", *IEEE Transactions on Microwave Theory and Techniques*, vol. MTT-13, no. 5, pp. 514-525, September 1965

[36] R. Katz, S. Maas, A. Sharma, D. Smith, "A Novel Monolithic HEMT Harmonic Mixer at Q-Band", *IEEE Microwave and Millimeter-wave Monolithic Circuits Symposium Digest*, pp. 39-42, 1995

[37] Bert C. Henderson, "Mixers in Microwave Systems (Part 2)", Watkins-Johnson Company, vol. 17, no. 2, 1990

[38] Antti V. Räisänen, Robert J. Dengler, Imran Mehdi, John E. Oswald, Debabani Choudhury, Peter H. Siegel, "Subharmonic mixer with planar Schottky diodes in a novel split-block at 200-240 GHz", *IEEE MTT-S Digest*, pp. 775-777, 1994

[39] Stephen A. Maas, "The RF and Microwave Circuit Design Cookbook", Artech House, 1998

[40] Stephen A. Maas, "Two-tone Intermodulation in Diode Mixers", *IEEE Transactions on Microwave Theory and Techniques*, vol. MTT-35, no. 2, pp. 307-314, March 1987

[41] Thomas J. Ellis, "A planar circuit design for high order sub-harmonic mixers", *IEEE MTT Symposium*, 1997

[42] Ulrich Güttich, Karl M. Strohm, Friedrich Schäffler, "D-Band Subharmonic Mixer with Silicon Planar Doped Barrier Diodes", *IEEE Transactions on Microwave Theory and Techniques*, vol. 39, no. 2, pp. 366-368, February 1991

[43] B.K. Kormanyos, G.M. Rebeiz, "A 30-180 GHz Harmonic Mixer-Receiver", *IEEE MTT-S Digest*, pp. 341-344, 1992